

# MÁSTERES de la UAM

Facultad de Ciencias /12-13

Máster en Química  
Teórica y Modelización  
Computacional



**Theoretical study  
of the stability and  
fragmentation dy-  
namics of neutral  
and ionized glycine,  
 $\beta$ -alanine and clus-  
ters of  $\beta$ -alanine in  
gas phase.**

*Dariusz Grzegorz  
Piekarski*



# ACKNOWLEDGEMENTS

July 8, 2013

---

This master thesis was written in the Departamento de Química at the Universidad Autónoma de Madrid (UAM) under the supervision of Dr. Sergio Díaz–Tendero in the framework of The European Master in Theoretical Chemistry and Computational Modelling (TCCM).

I feel glad to thank professor Manuel Yáñez, the coordinator of Theoretical Chemistry and Computational Modelling and professor Otilia Mó for selecting me in that European Master Project.

I am extremely thankful to Dr. Sergio Díaz–Tendero for supervising this thesis, for his advices, dedicating a lot of his time, in spite of busy schedule, helping to find solutions for any problems. I am extremely grateful to him for showing his confidence in me and giving extra motivation which allow me to finish master thesis on time. I feel lucky to be supervised by him and extremely pleasure of that.

I would like to assert my honest gratitude to professors Fernando Martín and Manuel Alcamí whose are creators of some of the ideas of the project and gave me opportunity to work with this group.

I would like to thank also to the experimental group of professor Lamri Adoui in Caen (France) : Sylvain Maclot, Dr. Patrick Rousseau, Dr. Alicja Domaracka, Dr. Michael Capron and Prof. Bern Huber for full cooperation, which allow us to work together in a nice project. Private communications with Sylvain gave me new ideas to perform calculations and better understanding the experiment details.

It is also my pleasure to thank professor Maria João Ramos who perfectly introduced me to her group in Porto and shared her knowledge and experienced with me. During the three months stay I got many valuable tips for which I should thanks to: Dr. Natércia Brás and João Coimbra.

Finally, I am grateful to the group managers Dr. Beatriz Martín and Wilson Rodríguez for introducing me to the life of the department and arranging many nasty paperwork issues. Also all PhDs students of Universidad Autónoma de Madrid mainly Alberto “Pei” and Etienne for valuable tips and hints that make my science life easier and happier. I owe a lot my friends from all the world that I met during the master courses. Thank you all, not only for discussion how to “bite” a special scientific problem, but mostly for my personal development and enjoying time.

At the end I would like to thank again to professors Manuel Alcamí, Fernando Martín, Manuel Yáñez and Otilia Mó for giving me the opportunity to work with their group in the next years. ¡Muchas Gracias!



---

## Portfolio

I finished master studies in Poland at the University of Technology in Kielce (M.Sci. Eng.) and at the Jagiellonian University in Cracow (M.Sci. in Chemistry). Just after studies I started work as operative agent at TNT Express Worldwide Poland and at Kiel-Inox as programmer (sinumerik) and operator of Computer Numerical Control (CNC) machine. After a few years I decided to change my profession to do something more demanding—science and I applied for Erasmus Mundus Master Program. During two years of doing European Master in Theoretical Chemistry and Computational Modeling (EMTCCM), apart of this manuscript, I attended two intensive courses:

- M1 Intensive Course held in Oviedo, Spain, 23.01-17.02.2012
- 7<sup>th</sup> International Intensive Course of the European Master in Theoretical Chemistry and Computational Modelling (IIC-EMTCCM) held in Perugia, Italia, 03-28 September, 2012;

Moreover, I took part in two congresses, where I presented posters entitled:

- “Stability and fragmentation of neutral and positively charged glycine and  $\beta$ -alanine: a density functional theory study” at the 8<sup>th</sup> Congress on Electronic Structure: Principles and Applications ESPA 2012, held in Barcelona, Spain, 26-29 June 2012;
- “Fragmentation dynamics of excited amino acids in gas phase: glycine and  $\beta$ -alanine” at the conference V Jornadas de Jóvenes Investigadores en Física Atómica y Molecular (J2IFAM2013) held in Madrid, Spain, 13-15 February 2013 ;

I attended two workshops:

- European School on Molecular Excited States held in ZCAM (Zaragoza Scientific Center for Advanced Modeling) Zaragoza, Spain, and co-organized by the Erasmus Mundus Master in Theoretical Chemistry and Computational Modelling (TCCM), 4-8 June, 2012;
- QSMC 2012 NANO-IBCT Workshop (Quantum Scattering codes and Monte Carlo simulations to model dynamical processes in biosystems) held in Madrid, Spain, 7-9 November, 2012

Additionally, I participate the attendance of the seminars at Universidad Autónoma de Madrid: “Attoscience and Ultrafast Optics at ICFO” by Prof. Jens Biegert (30/09/2011), “Visualizing, training and controlling ultrafast molecule dynamics of singly and doubly excited states of  $H_2$ ” by Prof. Geert-Jan Kroes (27/09/2011), “Quantum Chemistry in Leuven” by Minh Nguyen (26/09/2011), “Photoionization of the hydrogen molecule using attosecond laser pulses” by Dr. Jhon Fredy Pérez-Torres, “Interferences in vibrationally resolved molecular photoelectron spectroscopy” by Etienne Plésiat (23/05/2012), “Electron and nuclear dynamics of  $H_2^+$  induced by intense ultrashort laser pulses” by Rui Silva (5/11/2012), The RABITT technique to study strong field effects and continuum-continuum transitions in Helium” by Alvaro Jimenez (10/12/2012), “Control of molecular dynamics under strong laser fields” by Dr. Jesús González (04/02/2013), “Theoretical Study on the Fragmentation Dynamics of L-Alanine<sup>2+</sup>” by Estefania Rossich (20/05/2013), “GridTDSE: A parallel code for Cartesian coordinate-based wave packet propagations in QMD. The case of hydrogen confined in SWCNTs” by Dr. Jaime Suárez (06/06/2013), “Infrared Spectra of Alkyl Mercury Compounds” by Dr. Merche Montero (18/02/2013).

More than that, I did a stay at a foreign institution in the group of professor Maria João Ramos from University of Porto in Portugal, where I learned the classical molecular dynamics simulations in AMBER package and QMMM methods (ONIOM) and practiced them on the clusters of  $\beta$ -alanine.

The detail informations about all the courses during that two years are in the table 1:

Assignment	Mark over 10	Year	ETCS point	Average/year
MODELIZACIÓN DE PROCESOS DE INTERÉS EN QUÍMICA DE LA ATMÓSFERA Y ASTROQUÍMICA	8.2	2011/2012	5.0	8.55
LENGUA EUROPEA (ESPAÑOL)	9.2	2011/2012	5.0	
FUNDAMENTOS MATEMÁTICOS DE LA QUÍMICA TEÓRICA	9.1	2011/2012	5.0	
MÉTODOS DE LA QUÍMICA CUÁNTICA Y MECÁNICA ESTADÍSTICA	9.0	2011/2012	10.0	
TÉCNICAS COMPUTACIONALES Y CÁLCULO NUMÉRICO	9.0	2011/2012	6.0	
SIMETRÍA EN ÁTOMOS, MOLÉCULAS Y SÓLIDOS Y MECÁNICA CUÁNTICA	9.8	2011/2012	9.0	
FORMACIÓN EN UNIX Y UNIX DE GESTIÓN	6.4	2011/2012	5.0	
DINÁMICA	8.0	2011/2012	5.0	
ESTADOS EXCITADOS	9.0	2011/2012	5.0	
MÉTODOS AVANZADOS DE LA QUÍMICA CUÁNTICA	7.8	2011/2012	5.0	
TEORÍA AVANZADA DE LA ESTRUCTURA ELECTRÓNICA Y LA MATERIA CONDENSADA	9.8	2012/2013	9.0	9.63
TÉCNICAS COMPUTACIONALES AVANZADAS	9.9	2012/2013	6.0	
DINÁMICA QUÍMICA Y MOLECULAR Y SIMULACIÓN Y MODELIZACIÓN POR ORDENADOR	9.8	2012/2013	9.0	
APLICACIONES	9.0	2012/2013	6.0	
AVERAGE of 2 YEARS				9.09

**Table 1:** Detailed information about all the courses attended during European Master in Theoretical Chemistry and Computational Modelling (EMTCCM).



# Contents

<b>I</b>	<b>Introduction</b>	<b>15</b>
1	Introduction	19
<b>II</b>	<b>Theoretical Methods</b>	<b>23</b>
2	Density functional theory	25
2.1	The Hohenberg–Kohn theorems . . . . .	27
2.2	The Kohn and Sham method . . . . .	29
2.3	Exchange–correlation potential . . . . .	32
2.3.1	Local density approximation (LDA) . . . . .	32
2.3.2	Local spin density approximation (LSDA) . . . . .	33
2.3.3	Non–local corrections or Generalized Gradient Approximations (GGA) . . . . .	33
2.3.4	Meta–GGA . . . . .	33
2.3.5	Hybrid exchange functionals . . . . .	34
2.4	Basis sets . . . . .	35
3	Molecular Dynamics	37
3.1	Atom–Center Density Matrix Propagation (ADMP) . . . . .	38
3.2	Classical molecular dynamics in AMBER. . . . .	39
3.3	QMMM . . . . .	40
4	Computational details	43
4.1	Optimization details . . . . .	43
4.2	Molecular Dynamics details (ADMP) . . . . .	43
4.3	Molecular Dynamic (classical) and QMMM details. . . . .	47
<b>III</b>	<b>Results and Discussion</b>	<b>51</b>
5	Glycine	53
5.1	Conformational study . . . . .	53
5.2	Unimolecular decomposition . . . . .	58
5.2.1	Experimental results . . . . .	58
5.2.2	Cation . . . . .	61
5.2.3	Dication . . . . .	63
6	$\beta$ -Alanine	69
6.1	Conformational study– neutrals . . . . .	69
6.2	Experimental results . . . . .	70
6.3	Fragmentation dynamics (with ADMP) . . . . .	72

---

6.4	Conformational study- dications . . . . .	81
6.5	Unimolecular decomposition . . . . .	83
6.6	Reactions between two singly charged fragments . . . . .	90
<b>7</b>	<b>Clusters of <math>\beta</math>-alanine</b>	<b>93</b>
<b>IV</b>	<b>Conclusions</b>	<b>109</b>

# List of Figures

1.1	Glycine, $\alpha$ and $\beta$ conformers of alanine. . . . .	20
4.1	Total energy as a function of time for different time steps and fictitious mass. . . . .	45
4.2	Electronic kinetic energy as a function of time for different time steps and fictitious mass. . . . .	46
4.3	Nuclear kinetic energy as a function of time for different time steps and fictitious mass. . . . .	47
4.4	Optimized geometries for the three conformers: dim1, dim2 and dim3 of $\beta$ -Ala at the B3LYP/6-311++G(d,p) level of theory. . . . .	49
5.1	Optimized geometries for the neutral isomers of glycine at the B3LYP/6-311++G(d,p) level of theory. Relative energies ( $\Delta E$ ) in kcal mol <sup>-1</sup> with respect to most stable neutral (g1). . . . .	54
5.2	Optimized geometries for the cation isomers of glycine at the B3LYP/6-311++G(d,p) level of theory. Relative energies ( $\Delta E$ ) in kcal mol <sup>-1</sup> with respect to most stable cation (g9 <sup>+</sup> ). . . . .	55
5.3	Stationary points on the isomerization part of the PES corresponding to the minima and transitions states of glycine radical cation. Relative energies ( $\Delta E$ ) in eV with respect to most stable neutral glycine (g1). . . . .	56
5.4	Optimized geometries for the dication isomers of glycine at the B3LYP/6-311++G(d,p) level of theory. Relative energies ( $\Delta E$ ) in kcal mol <sup>-1</sup> with respect to most stable dication (g9 <sup>2+</sup> ). . . . .	57
5.5	Stationary points on the isomerization part of the PES corresponding to the minima and transitions states of glycine dication. Relative energies ( $\Delta E$ ) in eV with respect to most stable neutral glycine (g1). . . . .	58
5.6	Mass spectrum of the cationic products obtained by fragmentation of the glycine cation in two charged fragments after the interaction of neutral glycine with Xe <sup>25+</sup> ions at the energy of 387.5 keV. . . . .	59
5.7	Mass spectrum of the cationic products obtained by fragmentation of the glycine dication in two charged fragments after the interaction of neutral glycine with Xe <sup>25+</sup> ions at the energy of 387.5 keV. . . . .	60
5.8	Coincidence map for the fragmentation of the glycine dication in two charged fragments after the interaction of neutral glycine with Xe <sup>25+</sup> ions at the energy of 387.5 keV. The time-of-flight (in ns) of the heavier fragment (TOF2) is plotted as a function of the time-of-flight of the lighter one (TOF1). . . . .	60
5.9	Fragmentation from glycine cation (g3 <sup>+</sup> ). 1 <sup>st</sup> VIP from g1 is given as entrance channel. Relative energies ( $\Delta E$ ) in eV with respect to most stable neutral glycine (g1). . . . .	61
5.10	Fragmentation of NH <sub>2</sub> CH <sub>2</sub> <sup>+</sup> . Relative energies ( $\Delta E$ ) in eV. . . . .	62
5.11	Additional fragmentation path of glycine cation. 1 <sup>st</sup> VIP from g1 is given as entrance channel. Relative energies ( $\Delta E$ ) in eV with respect to most stable neutral glycine (g1). . . . .	63
5.12	Fragmentations of dication of glycine in the wake of Coulomb explosion. Relative energies ( $\Delta E$ ) in eV with respect to most stable neutral glycine (g1). . . . .	64
5.13	Fragmentations of dication of glycine: Coulomb explosion versus “enol” fragmentation paths. Relative energies ( $\Delta E$ ) in eV with respect to most stable neutral glycine (g1). Inset (1): Isomerization of C(OH) <sub>2</sub> <sup>+</sup> . Relative energies ( $\Delta E$ ) in eV. . . . .	65
5.14	Fragmentations of dication of glycine: Coulomb explosion versus “dicationic forms” paths. Relative energies ( $\Delta E$ ) in eV with respect to most stable neutral glycine (g1). . . . .	67

5.15	Snapshots of molecular dynamics simulations of a glycine dication with (a) 2.18 eV of internal energy giving a fission process leading to fragments $\text{NH}_2\text{CH}_2^+/\text{COOH}^+$ , b) 2.45 eV and c) 2.72 eV leading the isomerization by H-transfer in diol $\text{NH}_2\text{CH}(\text{OH})^{2+}$ and $\text{NH}_3\text{CHCOOH}^{2+}$ , respectively. . . . .	68
6.1	Optimizing geometries for the neutral isomers of $\beta$ -Alanine at the B3LYP/6-311++G(d,p) level of theory. Relative energies ( $\Delta E$ ) in $\text{kcal mol}^{-1}$ with respect to most stable neutral (a1). . . . .	70
6.2	Mass spectrum of the cationic products obtained by fragmentation of $\beta$ -alanine dication in two charged fragments after the interaction of neutral glycine with $\text{Xe}^{25+}$ ions at the energy of 387.5 keV. . . . .	71
6.3	Coincidence map for the fragmentation of the $\beta$ -alanine dication in two charged fragments after the interaction of neutral $\beta$ -alanine with $\text{Xe}^{25+}$ ions at the energy of 387.5 keV. The time-of-flight (in ns) of the heavier fragment (TOF2) is plotted as a function of the time-of-flight of the lighter one (TOF1). . . . .	71
6.4	Snapshots of molecular dynamics simulations of a $\beta$ -alanine dication giving a fission processes and leading to fragments with a) $\text{C}_\alpha$ - $\text{C}_{\text{carboxylic}}$ bond breaking: (1) $\text{NH}_2\text{CHCH}_3^+/\text{COOH}^+$ , (2) $\text{NH}_3\text{CHCH}_2^+/\text{COOH}^+$ , (3) $\text{NH}_2\text{CH}_2\text{CH}_2^+/\text{COOH}^+$ ; b) $\text{C}_\alpha$ - $\text{C}_\beta$ bond breaking: (4) $\text{NH}_2\text{CH}_2^+/\text{CH}_2\text{COOH}^+$ . . . . .	73
6.5	Snapshots of molecular dynamics simulations of a $\beta$ -alanine dication leading to the isomerization by H-transfer in (5) Diol $^{2+}$ , (6) 5-membered ring dication, (7) linear $\text{NH}_3\text{CH}_3\text{CHCOOH}^{2+}$ and (8) 4-membered ring dication. . . . .	74
6.6	Snapshots of molecular dynamics simulations of a $\beta$ -alanine dication giving a combined processes and leading to a) Coulomb explosion+isomerization+fragmentation: (9); b) Coulomb explosion+fragmentation: (10), (17); c) fragmentation+isomerization: (11); d) isomerization+Coulomb explosion+fragmentation: (12); e) isomerization+dehydration: (13), (14), (15); f) isomerization+Coulomb explosion: (16). . . . .	76
6.7	Ab initio molecular dynamics statistics for each neutral conformer of $\beta$ -alanine with relative energy $\approx 2 \text{ kcal/mol}^{-1}$ . . . . .	79
6.8	Ab initio molecular dynamics statistic for all neutral conformers of $\beta$ -alanine; percentage of the most important fragmentation channels as a function of energy ( in Hartree). . . . .	80
6.9	Ab initio molecular dynamics statistic for all neutral conformers of $\beta$ -alanine; percentage of the most important fragmentation channels as a function of energy ( in Hartree) for all studied of $\beta$ -alanine with relative energy $\approx 2 \text{ kcal/mol}^{-1}$ . . . . .	81
6.10	Optimizing geometries for the dication isomers of $\beta$ -Alanine at the B3LYP/6-311++G(d,p) level of theory. Relative energies ( $\Delta E$ ) in $\text{kcal mol}^{-1}$ with respect to most stable isomer (a20 $^{2+}$ ). . . . .	82
6.11	Stationary points on the PES corresponding to the minima and transitions states of $\beta$ -Alanine dications. Relative energies ( $\Delta E$ ) in eV with respect to most stable neutral $\beta$ -alanine (a1). . . . .	83
6.12	Fragmentations of dication of $\beta$ -alanine: Coulomb $\text{C}_\alpha$ - $\text{C}_\beta$ bond cleavage in competition with combined process $\text{NH}_2\text{CH}_2^+ + \text{CH}_2\text{OH}^+ + \text{CO}$ (9). Relative energies ( $\Delta E$ ) in eV with respect to most stable neutral $\beta$ -alanine (a1). . . . .	84
6.13	Fragmentations of dication of $\beta$ -alanine: Coulomb explosion additional channels. Relative energies ( $\Delta E$ ) in eV with respect to most stable neutral $\beta$ -alanine (a1). . . . .	85
6.14	Fragmentations of dication of $\beta$ -alanine: “enol” versus “cyclic” versus “linear” fragmentation paths. Relative energies ( $\Delta E$ ) in eV with respect to most stable neutral glycine (g1). . . . .	87
6.15	Fragmentations of dication of $\beta$ -alanine: “enol” versus “cyclic” fragmentation paths. Relative energies ( $\Delta E$ ) in eV with respect to most stable neutral glycine (g1). . . . .	89
6.16	Fragmentations of dication of $\beta$ -alanine: summary of combined fragmentation paths. Relative energies ( $\Delta E$ ) in eV with respect to most stable neutral glycine (g1). . . . .	90
6.17	Chemical reactions between two cation in the PES of dication of $\beta$ -alanine. Relative energies ( $\Delta E$ ) in eV with respect to most stable neutral $\beta$ -alanine (a1). . . . .	91

7.1	Average geometries of the six neutral conformers ( $\beta$ -Ala) <sub>2</sub> taken from classical molecular dynamics calculations for different temperature: 300K, 423K, 443K, 463K, 498K and optimized geometries for each structure at the M06/6-311++G(d,p) level of theory. . . . .	95
7.2	Average geometries of the six neutral conformers ( $\beta$ -Ala) <sub>3</sub> taken from classical molecular dynamics calculations for different temperature: 300K, 423K, 443K, 463K, 498K and optimized geometries for each structure at the M06/6-311++G(d,p) level of theory. . . . .	96
7.3	Average geometries of the six neutral conformers ( $\beta$ -Ala) <sub>4</sub> taken from classical molecular dynamics calculations for different temperature: 300K, 423K, 443K, 463K, 498K and optimized geometries for each structure at the M06/6-311++G(d,p) level of theory. . . . .	97
7.4	Average geometries of the six neutral conformers ( $\beta$ -Ala) <sub>5</sub> taken from classical molecular dynamics calculations for different temperature: 300K, 423K, 443K, 463K, 498K and optimized geometries for each structure at the M06/6-311++G(d,p) level of theory. . . . .	98
7.5	Average geometries of the six neutral conformers ( $\beta$ -Ala) <sub>6</sub> taken from classical molecular dynamics calculations for different temperature: 300K, 423K, 443K, 463K, 498K. . . . .	99
7.6	Average geometries of the six neutral conformers ( $\beta$ -Ala) <sub>7</sub> taken from classical molecular dynamics calculations for different temperature: 300K, 423K, 443K, 463K, 498K. . . . .	100
7.7	Average geometries of the six neutral conformers ( $\beta$ -Ala) <sub>8</sub> taken from classical molecular dynamics calculations for different temperature: 300K, 423K, 443K, 463K, 498K. . . . .	101
7.8	Average geometries of the six neutral conformers ( $\beta$ -Ala) <sub>9</sub> taken from classical molecular dynamics calculations for different temperature: 300K, 423K, 443K, 463K, 498K. . . . .	102
7.9	Average geometries of the six neutral conformers ( $\beta$ -Ala) <sub>10</sub> taken from classical molecular dynamics calculations for different temperature: 300K, 423K, 443K, 463K, 498K. . . . .	103
7.10	Average geometries of the six neutral conformers ( $\beta$ -Ala) <sub>20</sub> taken from classical molecular dynamics calculations for different temperature: 300K, 423K, 443K, 463K, 498K. . . . .	104
7.11	Binding energies as a function of clusters sizes. . . . .	107
7.12	Schematic hypothetic formation of the peptide bond. . . . .	108



# List of Tables

1	Detailed information about all the courses attended during European Master in Theoretical Chemistry and Computational Modelling (EMTCCM).	5
4.1	Combination of parameters $\Delta t$ (fs) and $\mu$ (amu).	44
4.2	Relative Energies ( $\Delta E$ ) in kcal mol <sup>-1</sup> at different levels of theory.	50
5.1	Nomenclature	53
5.2	Assignment of the peaks corresponding to the regions of interest in the mass spectrum for glycine cation (see figure 5.6).	59
5.3	Assignment of the correlation islands corresponding to the regions of interest in the coincidence map for glycine dication. Relative intensities are given in percentage of the total intensity of the map.	61
6.1	Assignment of the correlation islands corresponding to the regions of interest in the coincidence map for $\beta$ -alanine dication (see Fig. 2 in the main article). Relative intensities are given in percentage of the total intensity of the map.	72
7.1	Relative Energies ( $\Delta E$ ) in kcal mol <sup>-1</sup> at different levels of theory in respect to the most stable conformer. RMS of atomic displacement in respect to average structure in Å at different levels of theory. Binding energies in eV at different levels of theory.	105



## Part I

# Introduction



---

Nowadays theoretical chemistry together with computational modeling made use of the supercomputer power and have become an integral part of research and development in many fields. Molecular dynamics methods describe the motions at the atomic level in molecules and simulates chemical reactions. In addition, optimization methods permit an accurate exploration of the Potential Energy Surface (PES). Both methodologies allow a better understanding of the stability and fragmentation of multiply charged molecular ions in the gas phase. In this work we employ optimization methods together with molecular dynamics simulations to perform a complex study of the two simplest amino acids, glycine and  $\beta$ -alanine, in gas phase: neutral and positively charged species are considered. The structure of the neutral clusters of  $\beta$ -alanine is also evaluated within classical molecular dynamics simulations. We present accurate results for a better understanding of mass spectrometry experiments via computer simulation models.

“If perchance there should be foolish speakers who, together with those ignorant of all mathematics, will take it upon themselves to decide concerning these things, and because of some place in the Scriptures wickedly distorted to their purpose, should dare to assail this my work, they are of no importance to me, to such an extent do I despise their judgment as rash.”

Mikołaj Kopernik, polish astronomer, mathematician, lawyer, economist, priest, strategist, doctor and precursor of *Scientific Revolution*



# Chapter 1

## Introduction

### Aminoacids

For all practical purposes every property that describes life-forms is affected by amino acids. They are essential for life to encode genetic information; they are mainly the “fingerprint” of the structure of proteins and the expression of that information depends almost entirely on them. Proteins are a relatively homogeneous class of molecules with the same type of linear polymer, built of different combinations of the same 20 amino acids. The difference between them lies in the sequences in which the amino acids are implemented into the peptide chain. The essential of their functional variety is mainly included in differences between their chemical properties and also in the diversity of the three-dimensional structures that they can form. Because of that, we are interested in the structural varieties and in the chemical processes that can occur in amino acids and in the clusters of amino acids when they are excited and ionized.

Living organisms can use many chemical reactions to supply themselves continuously with chemical energy and use it without difficulty, but by themselves these reactions could not occur fast enough under physiological conditions to maintain life. The rates of these reaction will increase by the presence of enzymes, which are proteins and the former are built of amino acids. We are going to make life easier and start investigation of the simplest amino acid at the timescale, at which normally those molecules allow reaction to occur at living organisms. After ionization in gas phase we can observe fragmentation, proton migrations and other interest reactions taking place at the femtosecond scale. These are much easier to understand and can be explained at a quantum level with a reasonable simulation time than under physiological conditions.

In solution and in crystalline state amino acids exist as zwitterions, where synergies with the environment stabilized them by electrostatic, polarization, and H-bonding interactions. On the other hand, isolated amino acids in the gas phase, where these intermolecular interactions have no effect, they exist as non-ionized species. Although  $\beta$ -amino acids are less plentiful than their  $\alpha$  conformers, they are also observed in peptides, and in free form. They can form cyclic structures leading to  $\beta$ -lactams which have potential biological activity.<sup>1;2</sup>

The structures of the side chain of each amino acid is different. In this work, we are interested in two simple amino acids: glycine and  $\beta$ -alanine. In glycine, the amino group can be connected only to the alpha carbon atom  $C_\alpha$  (first atom connected to -COOH group) and in alanine, the amino group can be in both positions:  $C_\alpha$  or  $C_\beta$  (first or second atom connected to -COOH group); in this study we have considered the second case (see figure 1.1).

### Glycine

This amino acid is an exception, where the side chain is only one hydrogen atom; the central carbon atom is thus asymmetric and it is always found as L isomer in the nature. The frequency of occurrence in proteins place this amino acid on the 3<sup>rd</sup> position with 7.2 %. Only alanine and leucine present higher probability to be found in proteins with 8.3% and 9.0% of frequency, respectively.<sup>3</sup>

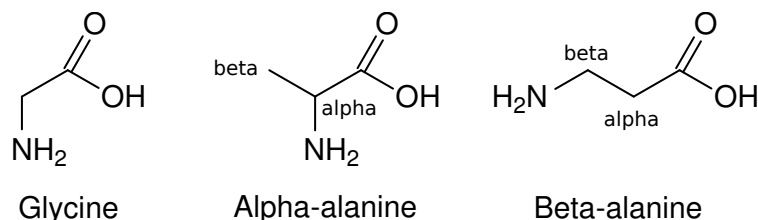


Figure 1.1: Glycine,  $\alpha$  and  $\beta$  conformers of alanine.

## $\beta$ -Alanine

$\beta$ -Alanine (beta-alanine) is a naturally occurring nonessential amino acid. For example  $\beta$ -Alanine is a component of co-enzyme A (in pantothenic acid) and carnosine, which has been proven to possess antioxidant properties, it can inhibit the action of free radicals<sup>4-6</sup> and also retard cancer growth in animal models.<sup>7</sup>  $\beta$ -Alanine can be used to increase intra-muscular carnosine, which is important in the contraction of muscle tissues and nowadays it is becoming a popular ergogenic aid to sports performance.<sup>8</sup> Increasing the concentration of carnosine in muscles leads to advantages in training adaptations and competition performance arising from its antioxidant properties. Making exercises, hydrogen-ion buildup stimulate muscle's fatigue, and carnosine has been shown to act as a hydrogen-ion buffer<sup>9</sup> in muscle fibers. Muscle carnosine content is higher for those, whose diet is rich of the best sources of  $\beta$ -Alanine.<sup>10</sup> In addition, the presence of this amino acid was found in plants and fruits, as well as in animal brain and insect cuticles.<sup>11</sup>

Scientists are interested in amino acids since they understood the important role that they play. Detailed information about them can be found in many books and hundreds of papers. The first theoretical studies about glycine in gas phase were started in earlies '80<sup>12;13</sup>. They firstly observed the stable enols of radical cation of glycine. Glycine has been studied by many theoreticians and experimentalists<sup>14-25</sup>, because it is the simplest amino acid and an important model compound.  $\beta$ -alanine is the simplest  $\beta$ -amino acid which in gas phase have been investigated as well by many scientists.<sup>26-29</sup> Moreover many theoreticians and experimentalists showed the important role played by organic radical cations in various chemical reactions,<sup>5;30-32</sup> where the first step is the ionization of the molecule. A large number of biologic and biochemical problems involving functional radical cations were studied by electron paramagnetic resonance (EPR) spectroscopy.<sup>33</sup> In the case of mono functional radical ionization it normally occurs at the functional group. In the case of two functional groups, we can make a look to the review of Symons et al.<sup>34</sup>, where linear and cyclic radical cations were investigated. On the other hand, more recent studies about radical cations were performed on vinyl ethers,<sup>35</sup> acrylates,<sup>36</sup> cycles,<sup>32</sup> lactones,<sup>37</sup> delocalized methoxyacetone<sup>38</sup> diketone,<sup>39</sup> and cyclopropylacetylene.<sup>40</sup>

On the other hand, ion-biomolecule collisions has become a fundamental technique to study radiation damage of biological tissues. With the advent of the hadrontherapy,<sup>41</sup> an ion beam based cancer treatment, it is necessary to better understand the radiation damage at the molecular level.<sup>42</sup> The changes in the biomolecules are not caused directly by ion-beam radiations but by radicals and ions created after fragmentation of amino acids along the ionization path.<sup>43;44</sup> The  $C_\alpha$  atoms of amino acids can form stable radicals, stabilized by capto-dative effect.<sup>45</sup> For example amyloid- $\beta$  (*Abeta*42) peptide is central to the pathology of Alzheimer disease and includes information about radical on  $C_\alpha$  of glycine<sup>29</sup> and glycine<sup>33</sup>.<sup>46</sup> Moreover, it has been shown that oxidative reactions of proteins are catalyzed by free radicals<sup>47</sup> and also occurred in amino acids, where could damage their structure and in consequence develop diseases like Alzheimer.<sup>48</sup> More than that,  $\beta$ -alanine can work as a neurotransmitter in the central nervous system, binding the receptor sides to glycine and  $\gamma$ -aminobutyric acid (GABA)<sup>49</sup> and also plays an important role in the visual system.<sup>50</sup>

Therefore, it is very important to get a deep knowledge of their structures, stability and fragmentation when two or more electrons have been removed.<sup>51-54</sup> In general, a multiply ionized molecule becomes less stable than its neutral parent due to the extraction of electrons from the bonding regions and the charge-charge repulsion forces acting inside the molecule. The breaking of the molecule into charged fragments, often referred as Coulomb explosion, leads in many occasions to more stable structures. Therefore only a limited number of molecules are

thermo-chemically stable as dications in the gas phase. Moreover, it is important to understand the fragmentation mechanisms and the role of transient species. Since multiply charged molecular ions play an important role in the gas phase chemistry.<sup>55-58</sup> Additionally, the study of the conformational behavior of ionized and non-ionized amino acids is important for understanding the dynamics of the peptide and protein backbones. We expect that the exhaustive conformational study as well as the fragmentation analysis presented here, will help to explain the role of the length in oxidative processes of amino acids and to interpret recent mass spectrometry experiments. Moreover, we would like to find the dependencies between the ionization energy and energy deposited on the molecule after ionization.

The “cherry” on the cake would be understanding and explaining the formation of relevant new species in interstellar space<sup>59</sup> and planet atmospheres.<sup>60</sup> In the gas phase, after ionization we can observe ultrafast reactions that can lead to species existing in the meteorites. After a meteorite crash in 1969 in Australia a group of scientists, performing a careful analysis of its residues, found that it was rich in organic compounds including amino acids. Besides that, there were found diamino monocarboxylic acids.<sup>61</sup> In CI chondrites (a type of carbonaceous meteorite)  $\beta$ -alanine was confirmed as the most abundant amino acid and its concentration was  $\sim 10$  times higher than for  $\alpha$ -alanine.<sup>62</sup> If they can play a key role in space chemistry and can be delivered to the early Earth by asteroids, comets, and interplanetary dust particles, thus would they be considered as the origin of life on the Earth?<sup>63</sup> The question is how these compounds can appear in the interstellar space?<sup>64-67</sup> The search of prebiotic molecules, as glycine and  $\beta$ -alanine, due to the significant astrobiological implications that suppose its detection in the interstellar media, meteorites, and comets has been a hot topic in the last decades centering much experimental<sup>68-70</sup> and theoretical efforts.<sup>71-73</sup>

In this work we present a theoretical study on neutral and ionized glycine and  $\beta$ -alanine in the gas phase. Our aim is to understand the stability and fragmentation of these two amino acids and interpret recent experimental results. To this we performed density theory calculations (DFT) and ab initio molecular dynamic (AIMD) simulations. Additionally, we also carried out classical molecular dynamics simulations on neutral clusters of  $(\beta\text{-alanine})_n$ , ( $2 \leq n \leq 10$  and  $n = 20$ ). For the smallest clusters ( $n \leq 5$ ) we also analyzed the structures of different isomers at the DFT level of theory.

The manuscript is divided into four parts. The first part is the *Introduction*, where we summarized basic information about glycine and  $\beta$ -alanine, relevant previous works, the importance of this work and a general overview of the thesis structure. *Part II* presents a background information on the methods that we used: DFT and Molecular Dynamics. In *Part III* we present three chapters with the obtained results and the analysis of them. *Chapter five* discuss the conformational study of neutrals, cations and dications, as well as the potential energy surface (PES) for decomposition of cations and dications of glycine; *Chapter six* focuses on the stability and fragmentation dynamics of doubly-charged  $\beta$ -alanine. *Chapter 7* gives an overview of the results obtained for neutral clusters of  $\beta$ -alanine. *Part IV* is a summary of this thesis, including the conclusions we have drawn from our research, suggestions for a future work, and tips for the experimental groups. Finally, at the end of the thesis we present the bibliography.



## Part II

# Theoretical Methods



## Chapter 2

# Density functional theory

### Introduction to the methodology

A very important question that should be answered before performing any molecular modeling simulation is which are our computational limitations. They depend mainly on the size of our system and the methodology which we are able to use. This reasoning can make our study efficient and effective. A reasonable choice is a key step to have a detailed knowledge about the fragmentation reactions and stability of molecular ions in the gas phase (the main objective of this work).

In the last years many scientists make their own battles with the advent of experimental and financial limitations; due to the fast development of computational science we can use powerful and less expensive computers, and new computational methods, which allow us to do more sophisticated calculations on bigger and bigger systems. Chemists and physicists combined their knowledge about chemical and physical properties of the molecules with computational science and express fundamental chemical and physical laws into computationally based methods called levels of theory. These methods can be separated into two kinds:

- Molecular Mechanics (MM) - based on the laws of classical mechanics for prediction of the structure and properties of molecular systems. MM is characterized by a force field, which describes only interactions between nuclei; and electrons are absolutely negligible. Because of that the electronic effects are included in the energy function. Despite of these limitations there is a wide field of use with this level of theory due to its computational efficiency, which allow modeling of extremely big systems. MM can not be applied to the problems strictly depended on the electronic structure, like fragmentation reactions. Other disadvantages at this level of theory are the force field limitations to describe the typical classes of molecule, mainly neutral one.
- Quantum mechanics (QM) - based on the laws of quantum mechanics for prediction of the structure and properties of the molecular systems. These methods represent the most fundamental level of theory at which molecules can be treated. The manner in which the methods approximate the wave function and solve the Schrödinger equation is known as level of theory.

The combination of MM with QM gives hybrid methods, which overcome the CPU limitations of QM and the limitation appears in the electronic region (like bond cleavage or hydrogen transfer) of MM. By combining both methods we have the so-called Quantum Mechanics/Molecular Mechanics (QMMM) approach.

In this manuscript we used the two first type of methods mentioned above, in particular:

- The density functional theory method (DFT) is a QM method and is briefly described in this chapter;
- MM methods for big systems (clusters of  $\beta$ -alanine);
- Results implying the traditional wave function ab initio methods with a large variety of computational schemes to deal with the electron correlation problem for cluster of  $\beta$ -alanine are also shown in chapter 7.

In particular second order perturbation theory due to Møller and Plesset (MP2) and couple-cluster with single and double excitations, where triple excitations were also included through a perturbative treatment (CCSD(T)). These two methods are the most accurate among the mentioned above, but also, computationally, the most expensive. Moreover, the exact wave functions and energies of all states of the system could be reached by these levels of theory.

The Density Functional Theory (DFT)<sup>74</sup> represents an alternative to the conventional high level ab initio methods to introduce the effects of electron correlation. The concept of the DFT method is to express the energy of the ground state of a many-electron system  $E$ , through the electron density  $\rho$ , which replace the wave function:  $E = E[\rho]$ . The main problem appears when we want to find the precise algorithm that relates energy to the electron density. This formula is not known, so we have to use approximate expressions, which usually provide very good results but, if the functional give wrong results, there is no systematic way to improve it. Despite that problems, using DFT methods are very popular to treat medium and large systems because require less CPU time compared to ab initio methods, and the obtained results are similar to those calculated by the MP2 method.

For molecules we have to simplify the Schrödinger equation using the Born–Oppenheimer approximation,<sup>75</sup> which allows to decouple the electrons and nuclei movement. We can thus write an electronic Hamiltonian:

$$\hat{H}_{el} = \sum_i \hat{h}_i + \sum_i \sum_{j>i} \frac{1}{r_{ij}} \quad (2.1)$$

where,  $\hat{h}_i = -\frac{1}{2}\nabla_i^2 - \sum_A \frac{Z_A}{r_{iA}}$

The Hamiltonian form equation 2.1 is a sum of the kinetic energy of electrons  $T_{el}$ , the electron–electron repulsion  $U_{ee}$  and external potential  $v$ :

$$\hat{H}_{el} = T_{el} + U_{ee} + v \quad (2.2)$$

Then, we are able to solve the time independent Schrödinger equation obtaining the electronic energy  $E_{el}$  and the electronic wave function  $\Psi_{el}$ . The latter depends on the electron coordinates which depend parametrically only on the nuclear coordinates:

$$\hat{H}_{el}\Psi_{el} = E_{el}\Psi_{el} \quad (2.3)$$

and thus the total energy is given by the sum of the electronic energy and the constant nuclear repulsion term:

$$E_{tot} = E_{elec} + E_{nuc} \quad (2.4)$$

$$E_{nuc} = \sum_{A=1}^M \sum_{B>A}^M \frac{Z_A Z_B}{r_{AB}} \quad (2.5)$$

There exist many different implementations to solve equation 2.3 using some approximations which are different in complexity and in accuracy, often in an impractical way. The basic idea lying in the Hartree–Fock<sup>76;77</sup> (HF) method is that the exact N–body ground state wave function of a system can be expressed approximately by a single Slater determinant (in other words, the wave function consists of all antisymmetric products composed of N spin orbitals):

$$\Theta_{SD} = \frac{1}{\sqrt{N!}} \begin{vmatrix} \varphi_1(\vec{x}_1) & \varphi_2(\vec{x}_1) & \cdots & \varphi_N(\vec{x}_1) \\ \varphi_1(\vec{x}_2) & \varphi_2(\vec{x}_2) & & \varphi_N(\vec{x}_2) \\ \vdots & \vdots & \ddots & \vdots \\ \varphi_1(\vec{x}_N) & \varphi_2(\vec{x}_N) & \cdots & \varphi_N(\vec{x}_N) \end{vmatrix} \quad (2.6)$$

which is built up from one–electron wave functions. The Pauli exclusion principle is satisfied for a total antisymmetric wave function as the one given by a Slater determinant. The one–electron wave functions are constructed as a linear combination of atomic functions. To solve a set of  $N$ –coupled equations for the  $N$  electrons we apply the variational principle (equation 2.8). The result in the form of the ground state wave function and the energy obtained are approximately the exact ones. We have to remember that a single Slater determinant representation excludes Coulomb correlation for electrons with different spins. The electron correlation<sup>78</sup> can be included in a perturbation method, adding electron correlation through an addition of a small correlation potential to the Hamiltonian of the Hartree–Fock approach. The latter is computationally expensive and the HF does not give accurate enough results. The alternative method proposed is the density functional theory (DFT), which includes electron correlation at a low computational cost.

## 2.1 The Hohenberg–Kohn theorems

### The first theorem

In 1964 Hohenberg and Kohn published a paper in *Physical Review* called *Inhomogeneous Electron Gas*,<sup>79</sup> which is considered the origin of the Density Functional Theory (DFT); going further they show that:

“Any observable of a stationary non–degenerated ground state can be calculated, exactly in theory, from the electron density of the ground state. In other words, any observable can be written as a functional of the electron density of the ground state ”

Proof of existence based on the demonstration that given a density  $\rho(r)$ , the external potential  $v(r)$  (usually Coulomb potential of the nuclei) is determined except in an additive constant. This was based on *reductio ad absurdum*, supposing that the form of the theorem is erroneous and leading to conflict.

The exact electronic density  $\rho(r)$  is given by:

$$\rho(r) = N \int |\Psi(r, r_2, r_3, \dots, r_N)|^2 dr_2 \dots dr_N \quad (2.7)$$

It is associated with the corresponding non–degenerate ground state of  $N$  particles (with just one wave function with energy of this state), we can assume that the same electron density can be obtained from two external potentials  $v_1(r)$  and  $v_2(r)$ . The potentials differ each other in more than a constant (when we add a constant to the potential, the wave function and therefore the charge density is unchanged so we have to require that two external potentials are different not only by a constant), what automatically requires generating two different many–electron Hamiltonians  $\hat{H}_1 = T + U + v_1(r)$  and  $\hat{H}_2 = T + U + v_2(r)$ , with ground state wave functions  $\Psi_1$  and  $\Psi_2$ .  $T$  in the latter equation is the kinetic energy and  $U$  is the electron–electron interaction. Thus the two distinct energies are  $E_1 = \langle \Psi_1 | \hat{H}_1 | \Psi_1 \rangle$  and  $E_2 = \langle \Psi_2 | \hat{H}_2 | \Psi_2 \rangle$  respectively.

The variational principle states that the expectation value of the Hamiltonian ( $\hat{H}$ ) on the trial wave function  $|\Psi\rangle$  is always equal or greater than the energy of the ground state  $E_0$ :

$$\langle \Psi | \hat{H} | \Psi \rangle = E \geq E_0 = \langle \Psi_0 | \hat{H} | \Psi_0 \rangle \quad (2.8)$$

The minimum value of  $\langle \Psi | \hat{H} | \Psi \rangle$  is thus an estimation of the variational value of the exact ground state energy. In this way we can calculate the expected value of the energy of  $\Psi_1$  with  $\hat{H}_2$  :

$$E_2 = \langle \Psi_1 | \hat{H}_2 | \Psi_1 \rangle = \langle \Psi_1 | \hat{H}_1 | \Psi_1 \rangle + \langle \Psi_1 | \hat{H}_2 - \hat{H}_1 | \Psi_1 \rangle = E_1 + \int \rho(r)[v_2(r) - v_1(r)]dr \quad (2.9)$$

Similarly we can also calculate the expected value of the energy of  $\Psi_2$  with  $\hat{H}_1$ :

$$E_1 = \langle \Psi_2 | \hat{H}_1 | \Psi_2 \rangle = \langle \Psi_2 | \hat{H}_2 | \Psi_2 \rangle + \langle \Psi_2 | \hat{H}_1 - \hat{H}_2 | \Psi_2 \rangle = E_2 + \int \rho(r)[v_1(r) - v_2(r)]dr \quad (2.10)$$

When we summarize equations 2.9 and 2.10 we get the inequality:

$$E_1 + E_2 < E_2 + E_1 \quad (2.11)$$

The equation 2.11 proves that the initial assumption was incorrect:  $\Psi_1$  and  $\Psi_2$  are eigenstates of different Hamiltonians so they are different and because of that the inequality is strict. This demonstrates that it does not exist two different potentials that can have the same ground state electron density associated with an external potential. In other words, the ground state electron density can uniquely specifies the  $v(r)$ . Determining the total number of electrons and according the Hohenberg–Kohn theorem (establishing  $v(r)$  by  $\rho(r)$ ), we can say that both the Hamiltonian and the wave function of the ground state are determined by the electron density. In the same way we can also get the expectation value of every ground state variable like, particularly  $E = E[\rho]$  or kinetic energy, Coulomb repulsion, etc. We can write the general relation between density and wave function as:

$$\rho(r) \implies v(r) \implies \hat{H} \implies \Psi \quad (2.12)$$

It is worth to say that the first Hohenberg–Kohn theorem is valid only for non-degenerated ground states, where  $\rho(r)$  is N-representable and  $v$ -representable. N-representable means that the ground state electron density has to be a positive function, defined in all space, and its integral has to be equal to the total number of electrons of the system:

$$\rho(r) \geq 0 \quad \wedge \quad \int \rho(r)dr = N \quad (2.13)$$

$v$ -representable refers to the existence of the external potential from which we can derive the electron density. In the case of the trial densities for which we can not find a suitable external potential, for degenerated and for excited states, inequalities 2.9 and 2.10 can not be achieved. In other cases, the energy is a functional of density:

$$E[\rho] = T[\rho] + U_{Ne}[\rho] + U_{ee}[\rho] \quad (+V_{NN}) \quad (2.14)$$

, where  $T[\rho]$  and  $U_{ee}$  are universal functionals, independent on the external potential.

Introducing the Hohenberg–Kohn functional  $F_{HK}[\rho]$ , which usually contains  $T[\rho]$  and  $U_{ee}$  we can rewrite the equation 2.14 in terms of the energy, which is a functional of the density for a specific external potential  $v(r)$ . Thus, the result from the first Hohenberg–Kohn theorem is:

$$E_v[\rho] = \int \rho(r)v(r)dr + F_{HK}[\rho] \quad (2.15)$$

## The second theorem

The second theorem supplies the variational principle for  $E[\rho]$  and is formulated as follows:

*“The electron density of a non-degenerate ground state can be calculated, exactly in theory, determining the density that minimizes the energy of the ground state”*

For a  $N$ -representable and  $v$ -representable trial density  $\tilde{\rho}(r)$  we can write:

$$E_0 \leq E_v[\tilde{\rho}(r)] \quad (2.16)$$

Applying the first Hohenberg–Kohn theorem into the exact and trial densities we will demonstrate the validity of the equation 2.16. The exact and trial densities define different Hamiltonians and thus, different wave functions:

For the exact density:

$$\rho(r) \rightarrow v_n(r) \rightarrow \hat{H} \rightarrow \Psi \quad (2.17)$$

and for the trial density:

$$\tilde{\rho}(r) \rightarrow \tilde{v}_n(r) \rightarrow \tilde{\hat{H}} \rightarrow \tilde{\Psi} \quad (2.18)$$

Calculating the energy for the trial density, using the Hamiltonian defined by the exact density, we get:

$$E_v[\tilde{\rho}(r)] = \langle \tilde{\Psi} | \hat{H} | \tilde{\Psi} \rangle \geq \langle \Psi | \hat{H} | \Psi \rangle = E_0 \quad (2.19)$$

Equation 2.19 is a consequence of the variational principle (equation 2.8) and is nonequivalent. Moreover, it certifies that for any trial density the resulting energy will be always equal or higher than the exact ground state energy. Looking for a density that minimizes the energy, we will find the exact density of the ground state:

$$\frac{\delta E_v[\rho]}{\delta \rho} = 0 \quad (2.20)$$

## 2.2 The Kohn and Sham method

Kohn and Sham proposed a method to calculate the energy from the density by introducing orbitals; strictly it is an expansion of the kinetic energy  $T[\Psi]$  for a single determinant function. They discovered that because of the problem that appears due to the fact that the density relation with  $F_{HK}$ ,  $T[\rho]$  is not known. They proposed a fictitious system for  $N$  non-interacting electrons moving under an external potential  $v_s(r)$  and providing a wave function  $\Psi_s$ , which has the same density as the real system. One can reproduce the density of the ground state of the real systems by means of studying fictitious systems in which we modified the interaction of the particles. All the quantities related to the fictitious systems will be with index “ $s$ ”. For such a system, excluding electron–electron interactions the orbital approximation provides to the exact HF method, the exact result. For a single–electron term the Hamiltonian is:

$$\hat{H}_s = \sum_{i=1}^N \hat{h}(i) = \sum_{i=1}^N -\frac{1}{2} \nabla^2(i) + \sum_{i=1}^N v_s(i) \quad (2.21)$$

and the exact wave function is:

$$\Psi_s = \frac{1}{\sqrt{N!}} |\chi_1(1)\chi_2(2)\chi_3(3) \cdots \chi_N(N)| \quad (2.22)$$

Solving the HF equations we can obtain the molecular orbitals:

$$\left[ -\frac{1}{2} \nabla^2 + v_s(r) \right] \chi_i = \epsilon_i \chi_i \quad (2.23)$$

where,  $\langle \chi_i | \chi_j \rangle = \delta_{ij}$

The exact density (equation 2.24) and the exact kinetic energy for that system are:

$$\rho(r) = \sum_{i=1}^{N_{occ}} |\chi_i(r)|^2 \quad (2.24)$$

$$T_s[\rho] = \sum_{i=1}^{N_{occ}} \left\langle \chi_i \left| -\frac{1}{2} \nabla^2 \right| \chi_i \right\rangle \quad (2.25)$$

We will get the density by solving the equation:

$$\mu = v_s(r) + \frac{\delta T_s[\rho]}{\delta \rho(r)} = \frac{\rho E_v[\rho]}{\delta \rho(r)} \quad (2.26)$$

where

$$E_v[\rho] = \sum_{i=1}^{N_{occ}} \epsilon_i = T_s[\rho] + \int \rho(r) v_s(r) dr \quad (2.27)$$

Introducing the term  $v_{ee}$  into equation 2.27 we will get the real system, in which all N electrons interact:

$$E_v[\rho] = \sum_{i=1}^{N_{occ}} \epsilon_i = T[\rho] + \int \rho(r) v(r) dr + v_{ee} \quad (2.28)$$

Introducing the Coulomb repulsion in terms of the electron density:

$$J[\rho] = \frac{1}{2} \iint \frac{\rho(r_1)\rho(r_2)}{|r_1 - r_2|} dr_1 dr_2 \quad (2.29)$$

we can write the total exchange–correlation energy  $E_{XC}[\rho]$  as:

$$E_{XC}[\rho] = (T[\rho] - T_s[\rho]) + (v_{ee}[\rho] - J[\rho]) = T_C[\rho] + W_{XC}[\rho] \quad (2.30)$$

where,  $T_C[\rho] = T[\rho] - T_s[\rho]$  and  $W_{XC}[\rho] = v_{ee}[\rho] - J[\rho]$

$T_C[\rho]$  is the kinetic correlation energy and  $W_{XC}[\rho]$  is the exchange–correlation energy.  $E_{XC}[\rho]$  contains all the contributions to the energy that we need to obtain it as a function of the density. We can write it as:

$$E_{XC}[\rho] = \int \rho(r)v_{XC}(r)dr \quad (2.31)$$

Including equation 2.29 and  $E_{XC}[\rho]$  into equation 2.28 we will get:

$$E_v[\rho] = T[\rho] + \int \rho(r)v(r)dr + \frac{1}{2} \iint \frac{\rho(r_1)\rho(r_2)}{|r_1 - r_2|} dr_1 dr_2 + E_{XC}[\rho] \quad (2.32)$$

Applying in the same way as for equation 2.26 we have:

$$\mu = \frac{\delta T_s[\rho]}{\delta \rho(r)} + v(r) + \int \frac{\rho(r_2)}{|r_1 - r_2|} dr_2 + \frac{\delta E_{XC}[\rho]}{\delta \rho(r)} = \frac{\rho E_v[\rho]}{\delta \rho(r)} \quad (2.33)$$

If we define the exchange–correlation potential as:

$$v_{XC}(r) = \frac{\delta E_{XC}[\rho]}{\delta \rho(r)} \quad (2.34)$$

and the Coulomb potential as:

$$\phi(r) = v(r) + \int \frac{\rho(r_2)}{|r_1 - r_2|} dr_2 \quad (2.35)$$

we get finally:

$$\mu = \frac{\delta T_s[\rho]}{\delta \rho(r)} + (\phi(r) + v_{XC}(r)) \quad (2.36)$$

or else:

$$\mu = \frac{\delta T_s[\rho]}{\delta \rho(r)} + v_{eff}(r) \quad (2.37)$$

When we compare equations 2.37 with 2.26 we can see that they are the same, when we change  $v_s(r)$  for  $v_{eff}(r)$ . This means that the only difference between the real system and the fictitious one lies in the different effective potential  $v_{eff}(r)$ , which can be defined as:

$$v_{eff}(r) = v_n(r) + \int \frac{\rho(r_2)}{|r_1 - r_2|} dr_2 + v_{XC}(r) \quad (2.38)$$

Therefore we need to solve the coupled equations:

$$\hat{h}_{KS}\chi_i = \epsilon_i\chi_i \quad (2.39)$$

with

$$\hat{h}_{KS} = -\frac{1}{2}\nabla^2 + v_{eff}(r) \quad (2.40)$$

where,  $\langle \chi_i | \chi_j \rangle = \delta_{ij}$

We obtain a set of equations similar like in the HF case. The orbitals in equations 2.39 are called KS orbitals and in terms of them we can calculate the electron density of the ground state:

$$\rho(r) = \sum_{i=1}^{N_{oc}} |\chi_i(r)|^2 \quad (2.41)$$

Using equation 2.41 we can similarly to HF apply a procedure for a set of trial molecular orbitals  $\{\chi_i(r)\}$  to obtain the electron density.  $\{\chi_i(r)\}$  are defined as a set of trial wave functions (linear combination of atomic orbitals–LCAO,  $|\Psi\rangle = C_1 |\psi_1\rangle + C_2 |\psi_2\rangle$ ) and are normalized  $\int \dots \int |\Psi(r_1, r_2, r_3, \dots, r_N)|^2 dr_1 dr_2 \dots dr_N = 1$ . From this density we can get  $v_{eff}(r)$  and finally obtain the eigenvalues of equations 2.39. This process must be iterative until the convergence criteria will be fulfilled.

## 2.3 Exchange–correlation potential

A good choice of the exchange–correlation potential ( $v_{XC}$ ) is a fundamental aspect of DFT. This functional have to be found using some approximations. The most widely used are: local density approximation (LDA), non–local or so–called generalized gradient approximation (GGA), meta–GGA, and hybrid functionals, where B3LYP is commonly known and was mostly used in this work.

### 2.3.1 Local density approximation (LDA)

$E_{XC}[\rho]$  depends particularly on the density. The contribution to the correlation energy is treated independently of the exchange one:

$$E_{XC}^{LDA}[\rho] = E_X^{LDA}[\rho] + E_C^{LDA}[\rho] \quad (2.42)$$

Then exchange energy per particle with  $\alpha = 2/3$  is given as:

$$E_X^{LDA}[\rho] = -\frac{9}{4}\alpha \left(\frac{3}{8\pi}\right)^{\frac{1}{3}} \int \rho^{\frac{4}{3}} dr \quad (2.43)$$

and

$$v_X^{LDA}(r) = \frac{\delta(\rho(r)E_X[\rho])}{\delta\rho(r)} = -\frac{3}{2}\alpha \left(\frac{3}{\pi}\right)^{\frac{1}{3}} \rho^{\frac{1}{3}} \quad (2.44)$$

This functional works fine for systems with density which is keep up approximately constant.

### 2.3.2 Local spin density approximation (LSDA)

Two densities are different in open shell systems. Because of that for this functional we minimized separately equations for  $\alpha$  and  $\beta$  densities. Thus, we can write:

$$E_{XC}^{LSDA}[\rho^\alpha] = E_X^{LSDA}[\rho^\alpha] + E_C^{LSDA}[\rho^\alpha, \rho^\beta] \quad (2.45)$$

then:

$$E_X^{LSDA}[\rho^\alpha] = -\frac{9}{4}\alpha \left(\frac{3}{8\pi}\right)^{\frac{1}{3}} \int (\rho^\alpha)^{\frac{4}{3}} dr \quad (2.46)$$

and

$$E_C^{LSDA}[\rho^\alpha, \rho^\beta] = \int \rho^\alpha(r) E_C[\rho^\alpha, \rho^\beta] dr \quad (2.47)$$

As we can see, the energy of  $\alpha$  and  $\beta$  are not treated independently, so we have to solve the system of two equations:

$$\delta \left[ E_v[\rho^\alpha] - \mu^\alpha \left( \int \rho^\alpha(r) dr - N_\alpha \right) \right] = 0 \quad (2.48)$$

$$\delta \left[ E_v[\rho^\beta] - \mu^\beta \left( \int \rho^\beta(r) dr - N_\beta \right) \right] = 0 \quad (2.49)$$

### 2.3.3 Non-local corrections or Generalized Gradient Approximations (GGA)

LDA approximation is based only on the electron density. For GGA we introduce density gradients into the description of exchange and correlation effects. This contributes to an energy functional that depends not only on the density but also on its gradient. The form for a GGA functional becomes:

$$E_{XC}^{GGA}[\rho] = \int f(\rho, \nabla\rho) dr \quad (2.50)$$

One of the main advantages of GGA, in comparison with LDA, is the significantly better description of the binding energy obtained for molecules. Because of that, DFT-GGA methods gain acceptance in the quantum chemistry community during the early 90's and they are nowadays widely employed.

### 2.3.4 Meta-GGA

Meta-GGA in comparison with the previous energy functionals, goes even further, including into the description of exchange and correlation the effects of the kinetic energy density  $\tau(r)$ :

$$\tau(r) = \frac{1}{2} \sum_{i=1}^{N_{occ}} |\nabla \chi_i(r)|^2 \quad (2.51)$$

and/or the Laplacian of the density,  $\nabla^2 \rho(r)$ :

$$E_{XC}^{meta-GGA}[\rho] = \int f(\rho, \nabla \rho, \tau, \nabla^2 \rho) dr \quad (2.52)$$

The presence of the Laplacian requires performing calculations of the second derivatives of the basis functions; larger quadrature grid must therefore be used in calculations.

### 2.3.5 Hybrid exchange functionals

The existence of the exact connection between the non-interacting density functional system and the fully interacting many body system allows to formulate the exact functional as:

$$E_{XC}[\rho] = \frac{1}{2} \int dr dr' \int_{\lambda=0}^1 d\lambda \frac{\lambda e^2}{|r-r'|} [\langle \rho(r)\rho(r') \rangle_{\rho,\lambda} - \rho(r)\delta(r-r')] \quad (2.53)$$

where the  $\langle ee' \rangle_{\rho,\lambda}$  is the expectation value of the density-density correlation function and is computed at density  $\rho(r)$  for the system described by an effective potential:

$$v_{eff} = v_{en} + \frac{1}{2} \sum_{i \neq j} \frac{\lambda e^2}{|r_i - r_j|} \quad (2.54)$$

Having that and knowing the variation of the density-density correlation function with the coupling constant  $\lambda$ , we can compute the exact energy. When  $\lambda = 0$  the non-interacting system corresponds identically to the HF system although the LDA and GGA functionals are constructed to be excellent approximations for the fully interacting system with  $\lambda = 1$  (homogeneous electron gas). Then, it is logical to approximate the integral over the coupling constant as a weighted sum of the end points:

$$E_{XC} \approx aE_{FOCK} + bE_{XC}^{GGA} \quad (2.55)$$

, where the  $a$  and  $b$  coefficients have to be determined typically by fitting procedures adjusting to reference values. The most often used energy functional was proposed by Beck, adopted to equation 2.55 is the Beck three parameters method:<sup>80</sup>

$$E_{XC} = E_{XC}^{LSDA} + a_0 (E_X^{EXACT} - E_X^{LSDA}) + a_x \Delta E_X^{B88} + a_c \Delta E_C^{PW91} \quad (2.56)$$

where,  $a_0 = 0.20$ ,  $a_x = 0.72$ ,  $a_c = 0.81$ .  $E_X^{EXACT}$  is the exact exchange energy,  $\Delta E_X^{B88}$  is Becke's 1988 gradient correction (to the LSDA) for exchange,<sup>81</sup> and  $\Delta E_C^{PW91}$  is the 1991 gradient correction for correlation of Perdew and Wang.<sup>74</sup>

Nowadays, hybrid functionals are commonly used in many quantum chemistry calculations and mostly notable the B3LYP functional is called by someone as the "magical" one. Binding energies, geometries, frequencies etc.

obtained with hybrid functionals are much reliable than those given by most of the GGA functionals.

## 2.4 Basis sets

In the last years a big collection of basis sets was generated in the context of wave function based approaches. The orbitals  $\chi_i$  expressed through the set of  $L$  predefined basis functions  $\{\eta_\mu\}$  are used to build the approximate wave function. If our aim is to construct a high quality wave function, taking into account electron correlation as well, very large basis sets are necessary. Particularly, basis functions with quite complex nodal structures (polarization function) are needed, thus in highly correlated calculations the basis set requirements leads to the computationally demanding processes.<sup>82</sup>

### Gaussian Type Orbitals (GTO)

Via wave function based approaches (i.e. HF), the set of  $\{\eta_\mu\}$  is conventionally chosen as a one consisting of so-called Cartesian Gaussian type orbitals (GTO). Its general form is:

$$\eta^{GTO} = N x^l y^m z^n \exp^{-\alpha r^2} \quad (2.57)$$

$N$  is a normalization factor ( $\langle \eta_\mu | \eta_\mu \rangle = 1$ , but  $\eta_\mu$  is not orthogonal;  $\langle \eta_\mu | \eta_\nu \rangle \neq 0$  for  $\mu \neq \nu$ ).  $\alpha$  acts as the orbital exponent and reproduces the compact (large  $\alpha$ ) or diffuse (small  $\alpha$ ) behavior of the function.  $L = l + m + n$  is used to classify the GTO as type of functions: s ( $L = 0$ ), p ( $L = 1$ ), d ( $L = 2$ ), etc.  $\exp(r^2)$  is an exponential dependence, which allows to solve analytically the four-center-two-electrons integrals in the Coulomb and HF exchange terms with a GTO basis set. Because of that GTO basis functions are commonly used and we more preferable than the Slater type orbitals basis functions.

### Slater Type Orbitals (STO)

Slater type orbitals basis functions are simply exponentials  $\exp^{-\zeta r}$ , which mimic the exact eigenfunctions of the hydrogen atom. Unlike the GTO functions, Slater type orbitals represent the correct cusp behavior near the nuclei ( $r \rightarrow 0$ ) and the the tail regions of wave function ( $r \rightarrow \infty$ ) is properly described (GTO fall off too rapidly). A typically expressed STO is:

$$\eta^{STO} = N r^{n-l} \exp^{-\zeta r} Y_{lm}(\Theta, \phi) \quad (2.58)$$

$n$  is a principal quantum number,  $\zeta$  correspond to the orbital exponent and  $Y_{lm}$  are the usual spherical harmonics describing the angular part of the function. Despite that STO usually needs three times less functions than GTO to achieve a certain accuracy of describing wave function, there is no analytical methods to compute the two-electron integrals with a STO basis sets. This is the reason why GTO basis function are in common use. Another type of basis functions are so-called contracted GTO basis sets.

### Contracted Gaussian Function (CGF)

Contracted Gaussian functions are functions (usually between three and six; and not bigger than ten) combined by several primitive Gaussian functions, as the one in equation 2.57 into a fixed linear combination. In that manner constructed function is called contracted Gaussian function (CGF) and can be written as:

$$\eta_{\tau}^{GTO} = \sum_a^A d_{a\tau} \eta_a^{GTO} \quad (2.59)$$

We have used in that work the density functional theory in contribution with CGF basis sets. This seems the natural choice in Kohn–Sham methods to expand the molecular orbitals such as Gaussian calculation. The simplest but also the less accurate expansion of the molecular orbitals uses only one basis functions or one contracted functions for each atomic orbital up to including only the valence orbitals. This type of basis set is called minimal basis set.

### Minimal basis set

The most common representation of this kind of basis set is the STO–3G basis set. It combines three primitive GTO functions into one CGF. For hydrogen only 1s function is included. For carbon there are five functions: two describing the 1s and 2s atomic orbitals and one set of 2p functions ( $p_x$ ,  $p_y$  and  $p_z$ ), etc. Nowadays this basis set are not in use anymore. The next improvement appears in the double zeta basis sets.

### Double zeta basis set

The name comes from Greek letter  $\zeta$ , which is in the exponent of the STO functions because the set of functions is doubled. For hydrogen two 1s functions are included (1s and 1s') etc.

### Split valence basis set

Taking into account only the valence space, as the space of changes in the electronic wave function, we can limit the doubled set of functions to the valence orbitals. Therefore, the inner core electrons are treated in a minimal set. The typical examples are the 3-21G or 6-31G Gaussian basis sets developed by Pople and coworkers. Adding p functions to the hydrogen atoms and d functions to the chemical elements from the second and third row of the periodic table will augmented the basis set by the polarization functions. Polarization functions have more angular nodal planes than the occupied atomic orbitals. Therefore, the orbitals can distort from their original atomic symmetry and better adapt to the molecular environment. Polarized double zeta or split valence basis sets are necessary to obtain a better description of the long weakly bounded systems (e.g. van der Waals or hydrogen bonds). Adding extra diffuse functions (sp functions with small exponent  $\alpha$ ; it means that electrons are kept far away from nuclei) we can enlarge our basis set into one used in this thesis–6-311++G(d,p).

### 6-311++G(d,p)

This basis set use six primitive Gaussians for core atomic orbitals, and a split valence pair of three triple zeta basis functions for each valence atomic orbital. Diffuse functions are added to the heavy atoms and hydrogen as well. Polarization functions on p set on each hydrogen and d set of each heavy atom are also included.

When we increase the basis set we can obtain triple or quadruple zeta basis sets which are augmented by several sets of polarization functions including functions (possible higher angular momentum). The cc-pVTZ (for correlation-consistent polarized valence triple zeta) basis sets are typical, modern representatives of this approach in terms of Gaussian functions and as well as the 6-311++G(d,p) it is used in this master thesis.

## Chapter 3

# Molecular Dynamics

The two main families of simulation techniques in dynamics are molecular dynamics (MD) and Monte Carlo (MC) methods. Classical molecular dynamics and electronic structure methods were combined given the family of techniques called ab initio molecular dynamics (AIMD). In this work we have employed ab initio molecular dynamics methods for studying the mechanism of fragmentation of glycine and  $\beta$ -alanine and also to evaluate other properties of these molecules. The dynamics is a useful computational tool that complements the reaction paths to visualize the connections between saddle points and minima obtained during the constructions of the potential energy surface (PES). The dynamics also can help to understand something that cannot be found during building the PES and finally, confirms the experimental mass spectra. In this thesis we have used ab initio molecular dynamics to investigate single amino acids and classical dynamics to analyze clusters of  $\beta$ -alanine. The obvious advantage of ab initio MD over classical MD is that it gives a better description to dynamical properties of the system: it allows to observe breaking or creating bonds, hydrogen transfer, etc. Classical molecular dynamics use “predefined potentials”, either based on empirical data or on independent electronic structure calculations. It is a powerful tool to investigate interaction of big many-body systems, like clusters of  $\beta$ -alanine.

The basic idea of ab initio molecular dynamics methods is based on computing the forces acting on the nuclei from electronic structure calculations, that are performed “on-the-fly” during the generation of the molecular dynamics trajectory. In this way, the electronic variables are not integrated ahead, but are considered as active degrees of freedom. This means that, molecular dynamics can control complex systems and give an approximate solution of the many-electron problem. On the other hand, it implies that the accuracy of our calculations depends strictly on how far the selected model potential is shifted to the level of selecting a particular approximation for solving the Schrödinger equation.

Molecular dynamics simulations are solved numerically; the classical equations of motions are integrated step-by-step; they can be defined for a molecular systems as:

$$m_i \ddot{r}_i = f_i \qquad f_i = -\frac{\partial}{\partial r_i} U(r^N) \qquad (3.1)$$

where we consider a system of  $N$  particles moving under the influence of a potential function  $U$ ;  $f_i$  are the forces acting on the atoms, derived from a potential energy  $U(r^N)$ , and  $r^N = (r_1, r_2, \dots, r^N)$  represents the complete set of  $3N$  atomic coordinates.

According to the Hamiltonian:

$$\hat{H}(r^N, p^N) = \sum_{i=1}^N \frac{p_i^2}{2m_i} + U(r^N) \qquad (3.2)$$

we can write equations 3.1 in the form:

$$\dot{r}_i = \frac{\partial \hat{H}}{\partial p_i} = \frac{p_i}{m_i} \qquad \dot{p}_i = -\frac{\partial \hat{H}}{\partial r_i} = -\frac{\partial U}{\partial r_i} = f_i(r^N) \quad (3.3)$$

where  $r$  is the position of the particles with momenta  $p = mU(r^N)$ .

The molecular dynamics algorithm can be solved considering Newton’s mechanics for the nuclei movement. Using  $p_i = m_i \dot{r}_i$  we can write the Newton’s second law:

$$m_i \ddot{r}_i = f_i r^N \quad (3.4)$$

Nuclei movement can be also described using the Lagrangian formalism:

$$\mathcal{L}(r^N, \dot{r}^N) = \sum_{i=1}^N \frac{1}{2} m_i \dot{r}_i^2 - U(r^N) \quad (3.5)$$

and solving the Euler–Lagrange equations of motion:

$$\frac{d}{dt} \frac{\partial \mathcal{L}}{\partial \dot{r}_i} = \frac{\partial \mathcal{L}}{\partial r_i} \quad (3.6)$$

Both formalisms are equivalent, where the second one is more commonly used in ab initio molecular dynamics. The Lagrangian technique is used in the Atom-Center Density Matrix Propagation Molecular Dynamics method employed in this work.

### 3.1 Atom–Center Density Matrix Propagation (ADMP)

ADMP together with the well known Born–Oppenheimer (BO) and Carr–Parrinello (CP) molecular dynamics (MD) belong to the family of ab initio MD methods (AIMD), where calculations of the electronic potential energy surface are crossed over the classical nuclei movement “on-the-fly”. They differ in the treatment of the wave function propagation. In the CPMD approach the wave function is propagated together with the classical nuclear degrees of freedom using an extended Lagrangian. In other words, in the Lagrangian scheme, the electronic degrees of freedom are not iterated to the convergence at each step but are simply adjusted of the time scales. In that way energy surface reproduce a converged energy electronic surface quite well. That approach allow to save a lot of CPU time and give accurate efficiency. The Lagrangian for BOMD and CPMD for electronic ground state can be written as:

$$\mathcal{L}_{BOMD} = \sum_i \frac{1}{2} m_i \dot{r}_i^2 - \min_{\Psi_0} \langle \Psi | \hat{H}_{el} | \Psi \rangle \quad (3.7)$$

$$\mathcal{L}_{CPMD} = \sum_i \frac{1}{2} m_i \dot{r}_i^2 + \sum_i \frac{1}{2} \mu_i \langle \dot{\psi}_i | \dot{\psi}_i \rangle - \langle \Psi | \hat{H}_{el} | \Psi \rangle + constraints \quad (3.8)$$

The *dots* indicates time derivative,  $m$  are the physical ionic masses,  $r$  the nuclear coordinates,  $\mu$  are arbitrary parameters of appropriate units (fictitious masses or inertia parameters assigned to the orbital degrees of freedom),  $\min_{\Psi_0} \langle \Psi | \hat{H}_{el} | \Psi \rangle$  means that the electronic subsystem is close to its minimum energy i.e. to the exact Born–Oppenheimer surface and *constraints* might be a function of both the set of orbitals  $\{\psi_i\}$  and the nuclear positions  $\{r_i\}$ . The equations of motion resulting for CPMD approach are then:

$$m_i \ddot{r}_i(t) = -\nabla_i \langle \Psi_0 | \hat{H}_{el}^{HF} | \Psi_0 \rangle \quad (3.9)$$

$$\mu_i \ddot{\psi}_i(t) = -\hat{H}_{el}^{HF} \psi_i + \sum_j \Lambda_{ij} \psi_j \quad (3.10)$$

Schlegel et al.<sup>83</sup> proposed an alternative AIMD method. In the ADMP formalism, as a dynamic variables they apply the Gaussian basis sets and the one–particle density matrix ( $P$ ) within the extended Lagrangian, instead of plane–waves and Kohn–Sham molecular orbitals ( $\chi$ ) as in the CPMD scheme. Thus propagation of electronic variables along with the nuclei is possible through introduction of fictitious masses into each density matrix element, what leads to the simple adjustment of relative time scales. The most important advantages of using this dynamic scheme are:

- linear scale of computational time with system size  $\mathcal{O}(\mathcal{N})$  and small limit system;<sup>84;85</sup>
- compact and localized wave function for a molecular system are quite well described via electronic structure calculations;
- small number of basis function effectively describe the state of molecular system with a desire degree of accuracy;
- freedom of using fictitious masses for density matrix elements  $\Rightarrow$  desire separation in the time scale between motions of electrons and nuclei;

The Lagrangian for the combined nuclear–density matrix system can be written as:

$$\mathcal{L}_{ADMP} = \frac{1}{2} Tr (V^T M V) + \frac{1}{2} \mu Tr (\dot{P} \dot{P}) - E(R, P) - Tr [\Lambda (PP - P)] \quad (3.11)$$

$P$  is a single–particle density matrix,  $M$ ,  $R$  and  $V$  are nuclear masses, positions and velocities, respectively. The Lagrangian multiplier,  $\Lambda$  is introduced as a constraint on the total number of electrons,  $N_e$  and the idempotency of the density matrix.

The equations of motion are defined with respect to the principle of stationary action for the Lagrangian (3.11); the propagation of the nuclei and the density in the orthonormal basis (3.6) is given by:

$$\mu \frac{d^2 P}{dt^2} = - \left[ \frac{\partial E(R, P)}{\partial P} \right]_R + \Lambda P + P \Lambda - \Lambda \quad (3.12)$$

$$M \frac{d^2 R}{dt^2} = - \frac{\partial E(R, P)}{\partial R} \Big|_P \quad (3.13)$$

### 3.2 Classical molecular dynamics in AMBER.

Classical molecular dynamics simulations were performed using the AMBER<sup>86–89</sup> package. This is the collective name of a bunch of programs created mainly to perform molecular dynamics calculations on biomolecules. AMBER

posses a substructure database, force field parameters files and many useful programs as antechamber, leap, ptraj, etc. (the three listed were used in this work). These subprograms work together with reasonably good efficiency and became a powerful framework for running calculations of the dynamics at the pico or nano–timescale and even at the microsecond timescale, on big systems.

### General Amber Force Field (GAFF)

Force fields are the foundations of molecular mechanics; it is therefore important to choose the one that correctly describe our system without any missing force field parameters. The Antechamber program, introduced into AMBER was written by Junmei Wang, and it was provided to work good with the general AMBER force field (GAFF).<sup>90</sup> GAFF was created mainly to investigate rational drug design but works fine with almost all the organic molecules build of C, N, O, H, S, P, F, Cl, Br, so it should be the right choice for clusters of  $\beta$ -alanine as well. The energy function used in GAFF is a simple function of the form:

$$E_{pair} = \sum_{bonds} K_r(r - r_{eq})^2 + \sum_{angles} K_\theta(\theta - \theta_{eq})^2 + \sum_{dihedrals} \frac{V_n}{2}[1 + \cos(n\phi - \gamma)] + \sum_{i < j} \left[ \frac{A_{ij}}{R_{ij}^{12}} - \frac{B_{ij}}{R_{ij}^6} + \frac{q_i q_j}{\epsilon R_{ij}} \right] \quad (3.14)$$

Where  $r_{eq}$  and  $q_{eq}$  are equilibration structural parameters,  $K_r$ ,  $K_\theta$ ,  $V_n$  are force constants,  $n$  is the multiplicity and  $\gamma$  is the phase angle for torsional angle parameters. The  $A$ ,  $B$ , and  $q$  parameters characterize the non-bonded potentials. The charge method used in GAFF is HF/6-31G(d,p) RESP charge.<sup>91</sup> Detailed information about algorithms used to classify atoms, bond types and charges assignation to estimate the force field parameters can be found in the paper of Wang et al.<sup>90</sup>

### 3.3 QMMM

As it was mentioned previously, the proper choose of the level of theory is very important to correctly describe the physical phenomenon and achieve a reasonable CPU time. In this section we focus on the QMMM methods, in which part of the macromolecule undergoing the chemical reaction is treated at a quantum mechanics (QM) level and the rest at a mechanical mechanics (MM) level. In that methodology we can write the total Hamiltonian of the system in the form:

$$\hat{H} = \hat{H}^{QM} + \hat{H}^{QM/MM} + \hat{H}^{MM} \quad (3.15)$$

$\hat{H}^{QM} = \hat{H}_{elec}^{QM} + \hat{H}_{nucl}^{QM}$  and  $\hat{H}^{MM}$  are the QM and MM Hamiltonians.  $\hat{H}^{QM/MM}$  corresponds to the QM/MM interactions between QM and MM part and can be written as:

$$\hat{H}^{QM/MM} = v_{elec}^{QM/MM} + v_{nucl}^{QM/MM} + v_{vdw}^{QM/MM} \quad (3.16)$$

where,  $v_{elec}^{QM/MM}$ ,  $v_{nucl}^{QM/MM}$  and  $v_{vdw}^{QM/MM}$  are electron–charge, nuclei–charge and van der Waals interaction between QM and MM atoms.

Adding equation 3.17 to the core Hamiltonian of QM part allows explicitly to polarize the QM wave function by the classical point charges of the MM force field<sup>92</sup>:

$$v_{elec}^{QM/MM} = - \sum_i^n \sum_{B \in MM} \frac{q_B}{|R_B - r_i|} \quad (3.17)$$

$v_{nucl}^{QM/MM}$  is the electrostatic interaction between the QM and the MM atoms, which can be defined by many approximations. The most widely used is electrostatic embedding (EE), which polarized the QM wave function:

$$v_{nucl}^{QM/MM} = \sum_A^M \sum_{B \in MM} \frac{Z_A q_B}{|R_B - R_A|} \quad (3.18)$$

The vdW interaction can be expressed as:

$$v_{vdw}^{QM/MM} = \sum_{A>B} 4\epsilon_{AB} \left[ \left( \frac{\sigma_{AB}}{R_{AB}} \right)^{12} - \left( \frac{\sigma_{AB}}{R_{AB}} \right)^6 \right] \quad (3.19)$$

The parameters  $\{\epsilon_A, \sigma_A\}_{A \in QM}$  for QM atoms have to be known and the most common case is to use parameters of the corresponding force field for the QM atoms.

Using equations 3.15 and 3.16 with Hamiltonians decomposition allow us to define the total energy of a QM/MM approach ( $E_{total}$ ) as a sum of QM energy ( $E^{QM}$ ), MM energy ( $E^{MM}$ ) and the interaction energy ( $E^{QM/MM}$ ) between both part as:

$$E_{total} = E^{QM} + E^{MM} + E^{QM/MM} = E_{elec}^{QM} + E_{nucl}^{QM} + E^{MM} + E_{elec}^{QM/MM} + E_{nucl}^{QM/MM} + E_{vdw}^{QM/MM} \quad (3.20)$$

where,  $E^{QM/MM}$  is define as:

$$E^{QM/MM} = \left\langle \Psi \left| - \sum_i^n \sum_{B \in MM} \frac{q_B}{|R_B - r_i|} \right| \Psi \right\rangle + v_{nucl}^{QM/MM} + v_{vdw}^{QM/MM} \quad (3.21)$$

where, the first term of the equation 3.21 is to calculate the electrostatic interaction with EE scheme.



# Chapter 4

## Computational details

### 4.1 Optimization details

Quantum chemistry calculations were carried out using the density functional theory (DFT) for the lowest spin state for each charge: singlet (spin equal zero) or doublet (spin equal 1/2). In particular, geometry optimizations were performed using the B3LYP functional, which combines the Becke's three parameter nonlocal hybrid exchange potential<sup>80</sup> with the nonlocal correlation functional of Lee, Yang and Parr.<sup>93</sup> This functional has been used in combination with the 6-311++G(d,p) basis set. This basis set was optimized with Hartree-Fock method by enriching it from 3-21G till 6-311++G(d,p). The latter basis gives much better energy stability order in comparison with 6-31G(d,p) basis.<sup>94;95</sup> Moreover polarization functions should be included for the correct description of the bonding.<sup>96</sup> The diffuse functions present in a bigger basis set are used to describe properly the electronic density of ionic forms of amino acids and were applied to all conformational study in this work for consistency. In addition, the presence of diffuse functions together with polarization functions has been shown to provide a better description of the PES of glycine.<sup>97</sup> This level of theory also has been shown to give accurate results for similar systems.<sup>30</sup> Harmonic vibrational frequencies have been also evaluated at the same level to characterize minima and transition states in the potential energy surface (PES) and to compute the Zero Point Energy (ZPE) correction. The absence of "imaginary" frequencies in the calculated IR spectra was interpreted as standard condition to define the point on the potential energy surface as a minimum. On the other hand, the existence of just one "imaginary" frequency was used as a criteria of the transition state geometry achievement. For the obtained transition states, intrinsic reaction coordinate (IRC) calculations have been also carried out to verify the minima they connect.<sup>98</sup> To find the transition states we used the Synchronous Transit-Guided Quasi-Newton (STQN) method with two variations, QST2 and QST3. The QST2 method uses the optimized structures for the reactants and products to generate the transition state. The QST3 variation requires the optimized structures for the reactants and products and also the input of a guess for the transition state.<sup>99;100</sup> Using this methodology allowed us to describe and understand many challenging reaction transitions. The transition states obtained with QST2 and QST3 methods were confirmed by IRC calculations. Ab initio molecular dynamics (AIMD) were performed using the Atom-centered Density Matrix Propagation method (ADMP),<sup>83;101-103</sup> with the same functional B3LYP but with basis set a slightly reduced to 6-31++G(d,p). All these calculations were performed using the Gaussian09 program.<sup>104</sup> The methodology that we have proposed to our systems seems to be adequate to obtain a compromise between CPU time and accuracy and gave us a good agreement with the experimental results, allowing us to propose the fragmentations paths to interpret the mass spectrum products after collisions.

### 4.2 Molecular Dynamics details (ADMP)

Atom-Centered Density Matrix Propagation (ADMP) dynamics were used with DFT framework, in principle B3LYP functional with a basis set 6-31G++(d,p) (slightly reduced to compare to the PES study for glycine and

$\beta$ -alanine). This method allows to describe the state of molecular system with suitable accuracy using smaller number of basis functions.<sup>101</sup>

The main disadvantage of using ADMP molecular dynamics, as it has been showed previously for the generalized valence bond (GVB) and HF framework, could be the existence of a problems with energy conservations.<sup>105</sup> Due that problem we decided to carefully investigate our system in terms of energy conservation. For fixing this problem we decided to choose the right set of parameters. To do this, we performed molecular dynamics simulations starting from the geometry of the most stable neutral isomer of glycine with different values of the time step  $\Delta t$  (fs) and fictitious mass  $\mu$ (amu). We run all our simulations up to  $t=200$  fs and with nuclear kinetic energy NKE=0.005 amu. (table 4.1).

		Fictitious mass $\mu$ (amu)					
		0.1	0.2	0.15	0.11	0.09	0.05
Time step $\Delta t$ (fs)	0.1	0.1fs0.1amu	0.1fs0.2amu	0.1fs0.15amu	0.1fs0.11amu	0.1fs0.09amu	0.1fs0.05amu
	0.2	0.2fs0.1amu	0.2fs0.2amu	0.2fs0.15amu	0.2fs0.11amu	0.2fs0.09amu	0.2fs0.05amu
	0.15	0.15fs0.1amu	0.15fs0.2amu	0.15fs0.15amu	0.15fs0.11amu	0.15fs0.09amu	0.15fs0.05amu
	0.11	0.11fs0.1amu	0.11fs0.2amu	0.11fs0.15amu	0.11fs0.11amu	0.11fs0.09amu	0.11fs0.05amu
	0.09	0.09fs0.1amu	0.09fs0.2amu	0.09fs0.15amu	0.09fs0.11amu	0.09fs0.09amu	0.09fs0.05amu
	0.05	0.05fs0.1amu	0.05fs0.2amu	0.05fs0.15amu	0.05fs0.11amu	0.05fs0.09amu	0.05fs0.05amu

**Table 4.1:** Combination of parameters  $\Delta t$  (fs) and  $\mu$  (amu).

This study allowed us to choose the optimal set of parameters ( $\Delta=0.1$  and  $\mu=0.1$  as well) for this kind of systems. We shown the energies (in eV) versus trajectory time (in fs) that allow us to choose the best parameters combination ( $\Delta t$  and  $\mu$ ) and keep the constancy in total energy (figure 4.1), electronic kinetic energy (figure 4.2) and nuclear kinetic energy (figure 4.3).

The nuclear and electron kinetic energy increases rapidly over the first 40 fs of simulation suggesting that a large structural changes occur. These changes, as we can observe in the dynamics, are due to the Coulomb explosion leading to two separated fragments. The big step at 40 fs for both nuclear and electronic kinetic energy is very similar in all cases. As we expected, changing the fictitious mass and time step does not affect on nuclear energies at all. In case of electronic kinetic energies we can see that, as smaller fictitious mass as better, but  $\mu = 0.05$  amu together with  $\Delta t = 0.2$  fs caused explosion of the system in the first fs of simulation. Electron kinetic energy is stable as we could expect, since the temperature is directly proportional to the kinetic energy, should be also stable. For  $\Delta t = 0.1$  and  $\mu = 0.1$  amu conservation of energy is acceptable and we do not need the better accuracy, saving computational time. Increasing kinetic energy is observed together with decreasing potential energy of the system (now shown in the manuscript). This could be explained due to the electrostatic energies changes, which are potentials, depending on localization of the charges. When we start the simulations from the neutral conformer and change the spin and charge, the system changes the geometry and/or undergo fragmentation. The charge is distributing all over the molecule or into two separated fragments, which makes the electrostatic interaction lower. Because of that the system is more stable and the potential energy decreases together with increasing the kinetic energy. In the plots of the total energy conservation in the first 200 fs, changing the time step for all chosen values of fictitious mass, we can see, that the choice of the previous values of the parameters looks reasonably. The black curves, parallel to x-axes represent the highest and the lowest energy value for  $\mu = 0.1$  amu with different value of time step. Small differences allowed us to choose both parameters.

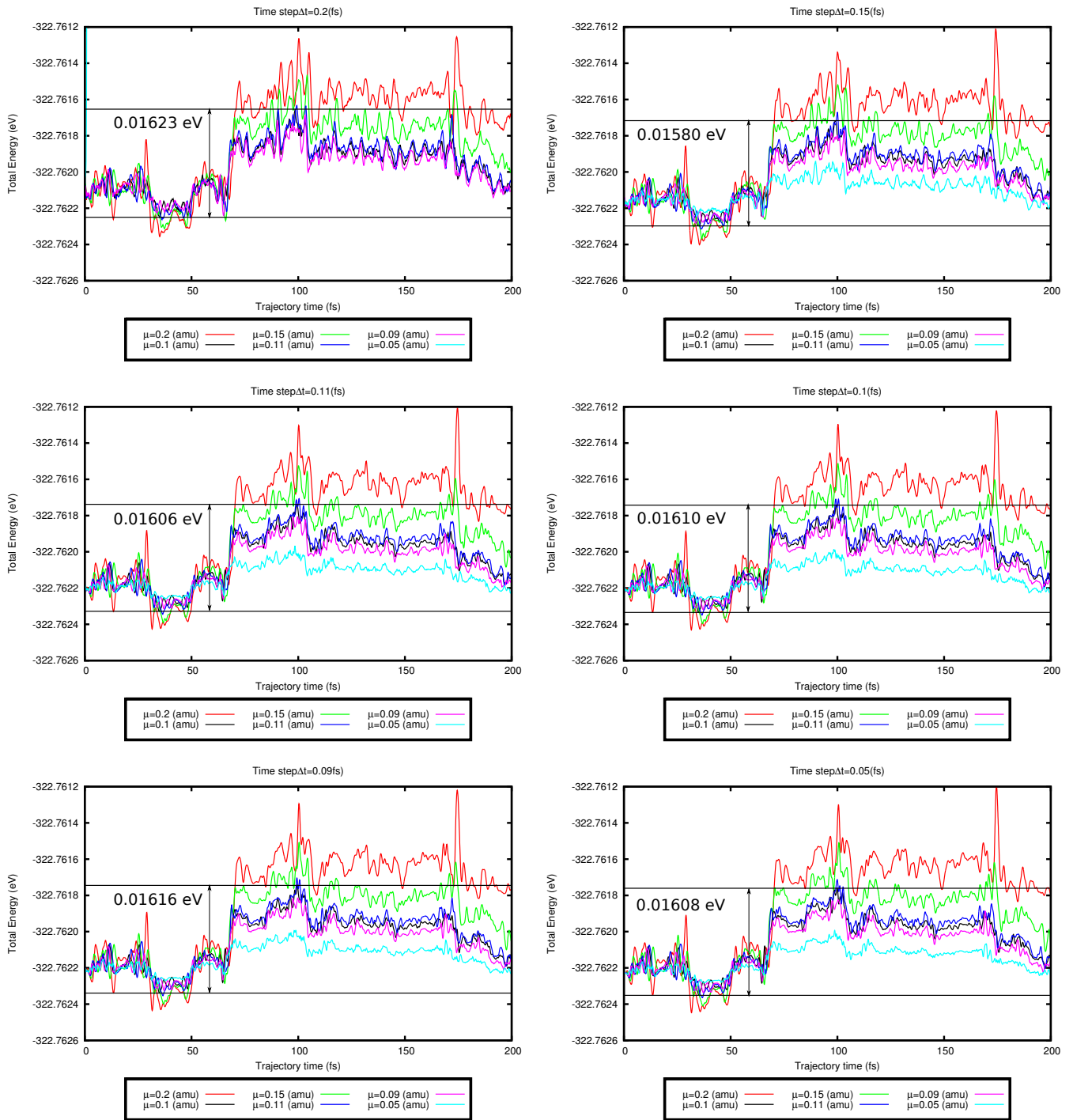
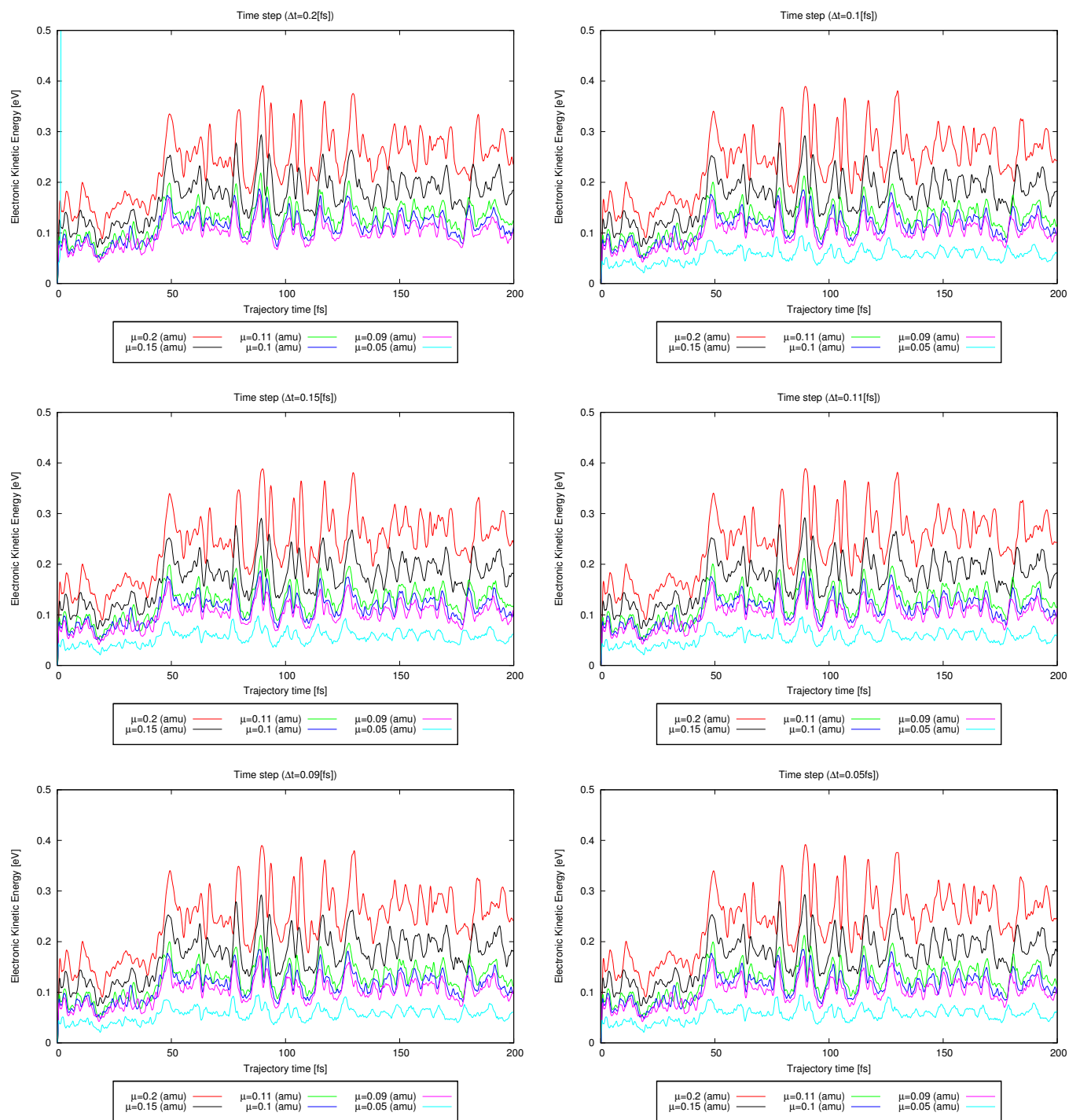


Figure 4.1: Total energy as a function of time for different time steps and fictitious mass.



**Figure 4.2:** Electronic kinetic energy as a function of time for different time steps and fictitious mass.

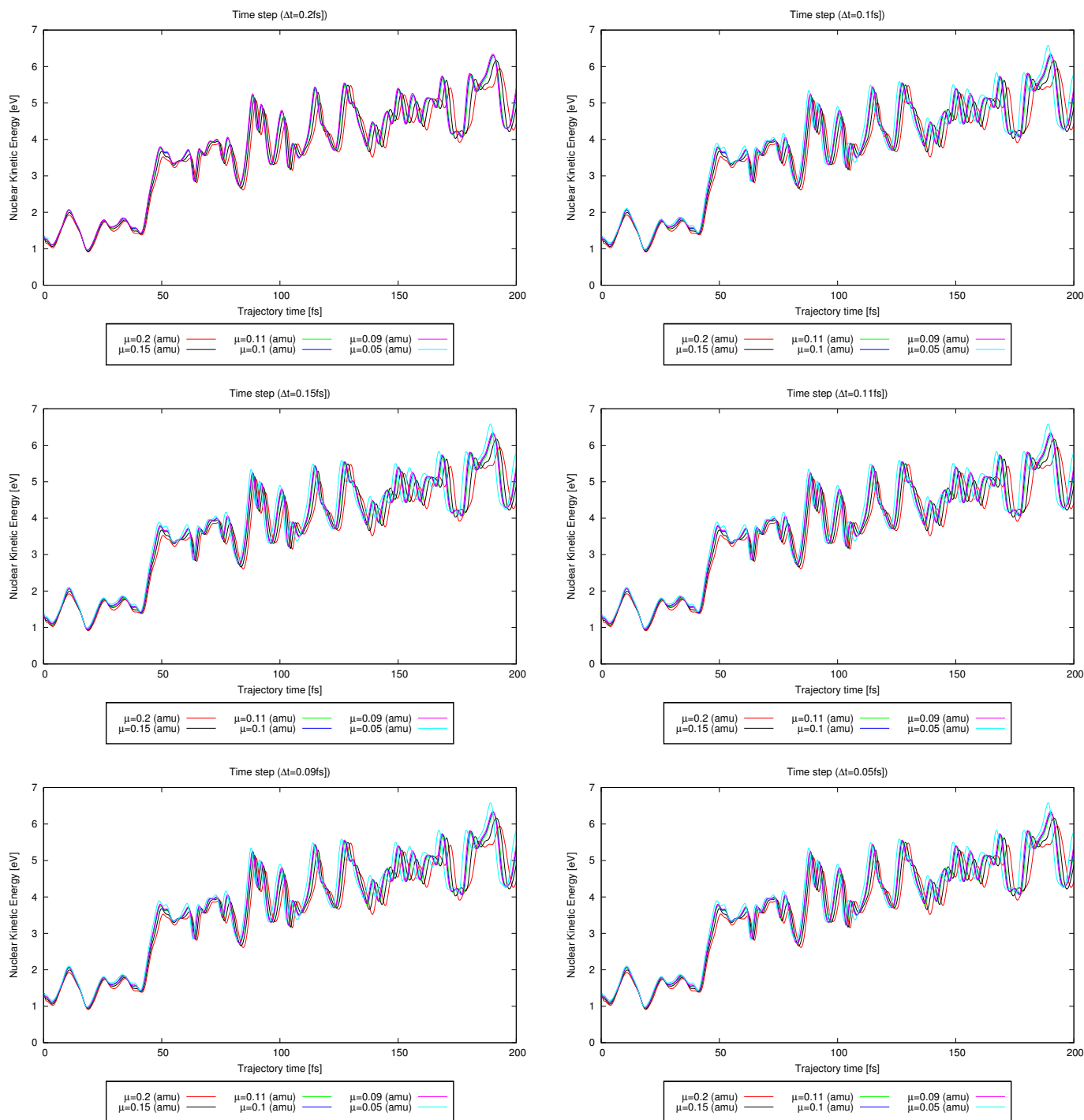


Figure 4.3: Nuclear kinetic energy as a function of time for different time steps and fictitious mass.

### 4.3 Molecular Dynamic (classical) and QMMM<sup>1</sup> details.

During the European Master in Theoretical and Computational Chemistry I had an opportunity to be part of the group of professor Maria João Ramos. During 3 months stay, using the knowledge and the experience of professor Maria João Ramos in Molecular Modelling, I learned how to work with big systems, like clusters of  $\beta$ -alanine, which can not be treated at a quantum level. To study that field of research we decided to use classical molecular dynamic and Quantum Mechanics/Molecular Mechanics (QMMM) approaches. We wanted to simulate the experiment in which the clusters of  $\beta$ -alanine are produced at a given temperature. Later they are ionized and different reactions

<sup>1</sup>In this thesis we do not present the results of calculations at this level of theory. This method will be consistently applied to investigate the clusters of  $\beta$ -alanine in the future study.

are observed, where the most abundant is emission of neutral moiety with  $m=18$  amu.

We used the general amber force field (gaff)<sup>90</sup> with the RESP charge<sup>91</sup> for the most stable neutral  $\beta$ -alanine conformer taken from the conformational study (chapter 5.1).  $\beta$ -alanine is not a standard amino acid, because of that we had to create the topology files. The topology files have to be created in a specific way allowing AMBER package to recognize it. Via that fact we have to define the atom numbers in the proper arrays which describe bonds, angles, dihedrals and parameters, in other words creating prmtop and inpcrd files:

- prmtop: the parameter/topology file, which defines the connectivity and parameters for a molecule. This informations are static and do not depend on the changes occurring during the MD simulations.
- inpcrd: the coordinates file (optionally contain informations about box coordinates and velocities). This informations are dynamic and change during the simulations.

The procedure to obtain this two files preformed with antechamber tools for the general amber force field (gaff) is as follow:

1. Build *BAL.pdb* file from optimized the most stable neutral  $\beta$ -alanine conformer *a1*.
2. Create *BAL.mol2* file.
3. Generate gaussian input file: *BAL.gcrt* using antechamber tools:
  - (a) `antechamber -fi mol2 -fo gcrt -i BAL.mol2 -o BAL.gau`
  - (b) `reoptimize the  $\beta$ -alanine conformer at HF/6-31G* SCF=tight Test Pop=MK iop(6/33=2) iop(6/42=6) opt level of theory to get gaussian output BAL.out`
4. Generate residue topology file *BAL.prepi* using gaussian output after reoptimization if we want to use RESP charge and amber atom types:
  - (a) `antechamber -fi gout -fo prepi -i BAL.out -o BAL_resp.prepi -j both -at amber -rn BAL`
5. Generate an ac file *BAL\_resp.ac* from gaussian output file *BAL.out*:
  - (a) `antechamber -fi gout -fo ac -i BAL.out -o BAL_resp.ac`
6. Extract resp charge to a charge file *BAL.crg* from *BAL\_resp.ac*
  - (a) `antechamber -fi ac -i BAL_reap.ac -c wc -cf BAL.crg`
7. Read in *BAL.crg* and *BAL.mol2* and generate an ac file *BAL.ac*:
  - (a) `antechamber -fi mol2 -i BAL.mol2 -c rc -cf BAL.crg -fo ac -o BAL.ac`
8. Determine the atom type for gaff *BAL\_gaff.ac*
  - (a) `atomtype -i BAL.ac -o BAL_gaff.ac -p gaff`
9. Generate residue topology file *BAL.prepc* with format tag (-f) of "car" in the cartesian prep input file:
  - (a) `prepgen -i BAL_gaff.ac -o BAL.prepc -f car`
10. Checking the missing force field parameters and generate additional force field file *BAL.frcmod*
  - (a) `parmchk -i BAL.prepc -o BAL.frcmod -f prepc`
11. Having *BAL.prepc* and *BAL.frcmod* we can use `xleap`<sup>106</sup> to generate the topology files for sander (*BAL.prmtop* and *BAL.inpcrd*):

- (a) `source leaprc.gaff`
- (b) `loadamberparams BAL.frcmod`
- (c) `loadamberprep BAL.prepc`
- (d) `bal = loadpdb BAL.pdb`
- (e) `solvatebox bal BAL 8.0`
- (f) `saveamberparm BAL BAL.prmtop BAL.inpcrd`

After having the topology files with the general amber force field parameters we run classical MD in gas phase for neutral cluster of  $\beta$ -alanine with size 2,3,4,5,6,7,8,9,10 and 20 at different temperatures: 300K, 373K, 423K, 443K, 463K, 498K. Classical Molecular Dynamics were used to determine the average structure of the neutral clusters as a function of temperature. To perform these simulations we used Assisted Model Building and Energy Refinement<sup>86-89</sup> (AMBER9) program. Later we took the geometry of average structures from the classical molecular dynamics with the smallest RMS of atomic displacement for each cluster size for each temperature. That procedure was successfully applied with the ptraj tool. At first we generated the average structure with translation and rotation aspects, which *de facto* is just the average of the coordinates during the trajectory. Averaging coordinates does not give physically meaningful structure. Because of that we generated average structure with mass weighted RMS fit of every frame to previously calculated average structure. That treatment is commonly used and allow to remove the rotation and translation aspects. In that manner we generate the average structures for 2,3,4,5,6,7,8,9,10 and 20 neutral cluster of  $\beta$ -alanine (chapter 7).

Later we performed optimization at quantum level for structures of  $(\beta\text{-Ala})_n$ , for  $n \leq 5$ . Before the optimization at DFT level we have to decide which functional we are going to use. For molecular structures containing strong intramolecular and intermolecular hydrogen bonds like in case of clusters of  $\beta$ -alanine deviations in their energetic ordering occur, which are traced back to different treatments of spatial non-locality in the exchange-correlation functional.<sup>107</sup> Because of that we did extensive study of the suitable functionals choosing dimer of  $\beta$ -alanine as a representative system. First of all, using gaussview program we create 3 very different in geometry dimers and we performed geometry and harmonic vibrational frequencies calculations using the most popular B3LYP functional with the 6-311G++(d,p) basis set as a starting point to further calculations. The final structure and nomenclature is shown in figure 4.4:

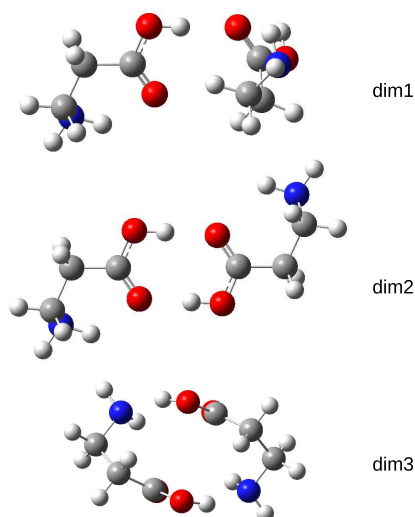


**Figure 4.4:** Optimized geometries for the three conformers: dim1, dim2 and dim3 of  $\beta$ -Ala at the B3LYP/6-311++G(d,p) level of theory.

In the calculations of the total energies and structural optimizations we employed other functionals with the same 6-311G++(d,p) basis set:

- hybrid: B3LYP,<sup>80;93;108</sup> B3LYP with Grimme's D3 dispersion,<sup>109</sup> M06 and its variation M062X,<sup>110</sup>

- hybrid-meta: MPWB1K;<sup>111</sup>
- dispersion: B97D;<sup>112</sup>

Geometry optimizations and harmonic vibrational frequencies calculations at the MP2/6-311++G(d,p) level of theory were also performed, as well as single-point energy calculations at the CCSD(T)/6-311++G(d,p) level over the geometry optimized at the MP2/6-311++G(d,p) level. All valence electrons were correlated at the MP2 and CCSD(T) levels of theory. The relative energy of the used functionals as well as MP2 with respect to CCSD(T) with the 6-311++G(d,p) show that for dimers of  $\beta$ -alanine M06 tends to give results in much better agreement with CCSD(T) than B3LYP, B3LYP with Grimme's D3 dispersion correction, M062X, MPWB1K, B97D or MP2. On the other hand, the effect of further enlarging the basis set has been analyzed by performing calculations with the augmented aug-cc-pVTZ basis sets.<sup>113</sup> All the results for three dimers in the table 4.2.

Isomer	Level of theory								
	B3LYP	B3LYP+Grimme	M06	M062x	MPWB1K	B97D	MP2	CCSD(T)	CCSD(T)/cc-pVTZ
dim1	6.72	6.70	9.54	11.66	8.84	11.88	-0.93	9.24	9.63
dim2	-1.60	-2.72	2.54	5.07	0.94	4.63	-7.50	3.26	2.42
dim3	0.00	0.00	0.00	0.00	0.00	0.00	0.00	0.00	0.00

**Table 4.2:** Relative Energies ( $\Delta E$ ) in kcal mol<sup>-1</sup> at different levels of theory.

Taking into account this previous study, based just on three dimers (dim1, dim2, dim3) we decided to exclude the follow functionals: B3LYP+Grimme, M062x, MPWB1K, B97D in the next study. Enlarging the basis set in the CCSD(T) calculations do not change the ordering and relative energy is almost the same as in case of CCSD(T)/6-311++G(d,p). Perfect agreement in terms of energy we can observe for M06 functional with respect to the CCSD(T) results. The latter functional has been chosen as the most appropriate for the optimization of cluster of  $\beta$ -alanine.

## Part III

# Results and Discussion



# Chapter 5

## Glycine

In this chapter we present an extensive conformational study of the neutral, cation and dication isomers of glycine in the gas phase. Isomerization of cations and dications, as well as their unimolecular decomposition were also studied. Both processes are presented in this chapter.

### 5.1 Conformational study

Geometry optimization is a key step to investigate the molecular structure, reactivity and fragmentation in all theoretical studies. To find equilibrium geometries we used ab initio molecular orbital density functional theory with analytical energy derivatives; methods that have been employed over the last decades. Our conformational study is based on these methods to find features such as minima, transition states and reaction paths.<sup>114</sup> Reaction path means the process that can be described by “connections” of all chemical species that appear in the fragmentation. Connections mean trajectories in which the whole molecular entity travels through the potential energy surface (PES) at a given velocity (changing the nuclear kinetic energy, NKE) until the desirable products are obtained or the reaction is complete. This was studied by ab initio molecular dynamics. However, it can be simplified by optimization methods and can be reduced to an exploration of the critical points in the PES<sup>115</sup>. This idea considers that reactants and products are connected by the line in the configuration space. Furthermore, all stationary points on the PES are described by minima and saddle points (the transition structure) and show the conformational rearrangement as well. This is the key step to reduce computational time and predict the most favorable structures and fragmentation channels.

We used the nomenclature showed in the table 5.1, for example **g9<sup>+</sup>** means **g**lycine **c**ation **n**umber **9**. We also kept the same numeration for the same neutral, cation and dication conformers for glycine and  $\beta$ -alanine i.e. if it exists one structure with the suitable geometry for neutral, cation and dication it will be called with the same number in the name: e.g. **g3**, **g3<sup>+</sup>** and **g3<sup>2+</sup>**, respectively.

Shortcut	Meaning
g	glycine
a	$\beta$ -alanine
f	important fragment
m	minor minimum
ts	transition state
f1	NH <sub>2</sub> CH <sub>2</sub>
f2	COOH
f3	NHCH
f4	NH <sub>2</sub> CHCO
f5	NH <sub>2</sub> CHCH <sub>2</sub> CO

**Table 5.1:** Nomenclature

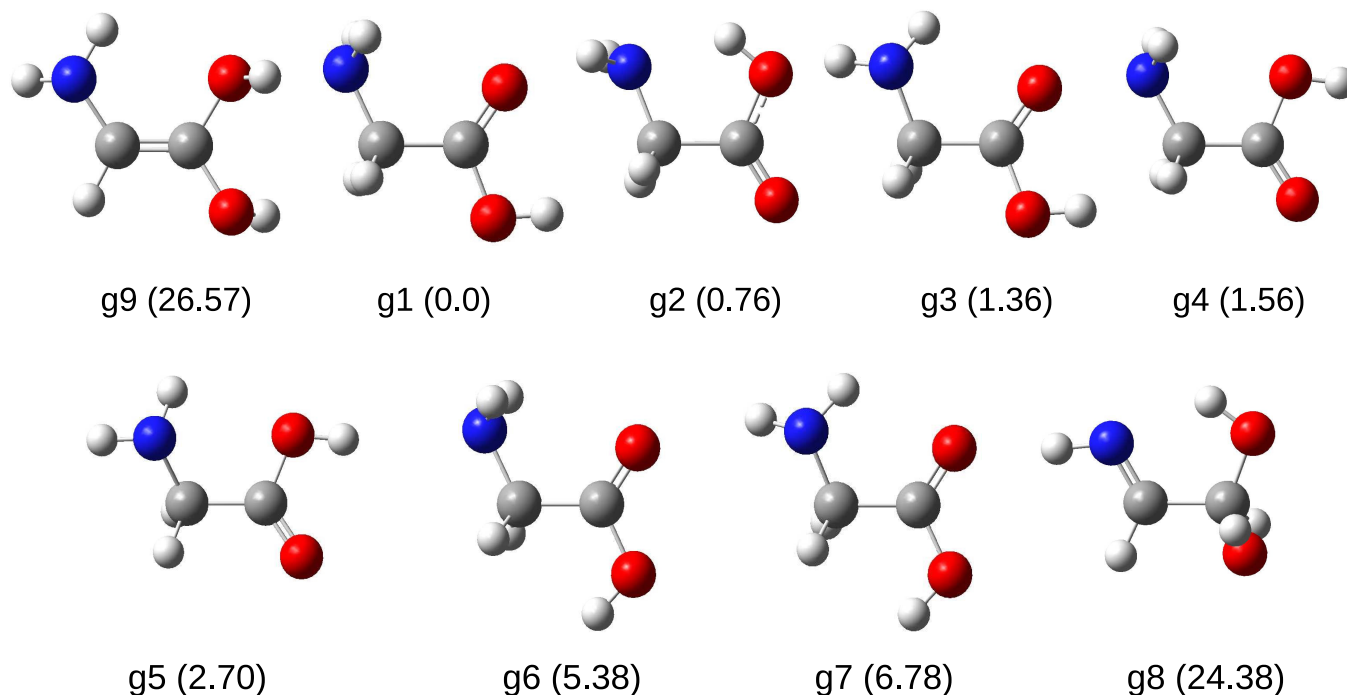


**Figure 5.1:** Optimized geometries for the neutral isomers of glycine at the B3LYP/6-311++G(d,p) level of theory. Relative energies ( $\Delta E$ ) in kcal mol<sup>-1</sup> with respect to most stable neutral (g1).

Using previous works by Mariona Sodupe et al.<sup>31</sup> and Attila G. Császár et al.<sup>116</sup>, we have chosen eight conformers of neutral glycine and one geminal diol form (g9). As it was shown in the previous paper<sup>31</sup>, the B3LYP functional in combination with the 6-31++G(d,p) basis gives relative energies in good agreement with single point calculations using coupled cluster method over geometries optimized at the MPWB1K/6-31++G(d,p) level (CCSD(T)/aug-pVTZ//MPWB1K/6-31++G(d,p)). Because of that we decide to use B3LYP/6-311++G(d,p) to re-optimize the structures. The results are shown in figure 5.1.

All conformers between g1 and g7 present the canonical structure of glycine and lie under 7 kcal/mol energy range. g8 isomer looks very strange and it appears in figure 5.1 just to show, that g9 (the geminal diol) is even less stable (26.57 kcal/mol) than the mentioned one (24.38 kcal/mol). That stability will change drastically after ionization, especially for doubly ionized glycine isomers, as we can observe in figures 5.2 and 5.4.

Starting from the geometry of the neutral conformers, we extract one electron and obtained six cations: g2<sup>+</sup>, g3<sup>+</sup>, g4a<sup>+</sup>, g4b<sup>+</sup>, g6<sup>+</sup>, g9<sup>+</sup>. In our exploration of the potential energy surface (PES) we get other minima (figure 5.2).  $\Delta E$  less than 45 kcal mol<sup>-1</sup> for neutral conformers ( $\approx 2$  eV) gives us certainty to populate the enols forms of glycine cations (g9<sup>+</sup> and g10<sup>+</sup>)<sup>13</sup>. Looking on the PES for isomerization of cations (figure 5.3), we can observe that theoretically all the conformers can be populated because minima<sup>+</sup> and ts<sup>+</sup> are close to the value described by Depke et al.<sup>117</sup> ( $\approx 2$  eV).

We used all minima (g<sup>+</sup>) and transition states (ts<sup>+</sup>) to build the PES for isomerization of cations (figure 5.3). We also calculated the 1<sup>st</sup> vertical ionization potential of the most stable neutral conformer (g1), which can be used as the reference energy entrance channel in single ionization. We can observe that removing an electron from neutral glycine leads to meaningful structural changes that depend strictly on the starting geometry of the amino acid. Starting from conformers g1, g3 and g5 we obtained the same conformer g3<sup>+</sup>. Glycine number nine (g9), despite its low stability in the neutral form, after extracting one electron (g9<sup>+</sup>) became the most stable cation (figure 5.2). This does not mean that g9<sup>+</sup> comes only from its neutral equivalent. This is due to the fact that ionization of glycine can lead to ultrafast hydrogen transfer leading to the diol cation. The extra stability of g9<sup>+</sup> can be explained through the core-core and lone pair-lone pair repulsion together with hydrogen atom-lone pair stabilizing interaction that this structure shows, and that correspond to the global minimum.<sup>13</sup> In consequence, it has minimal destabilizing effects of the well-organized lone pairs and hydrogen cores. We can also observe a very

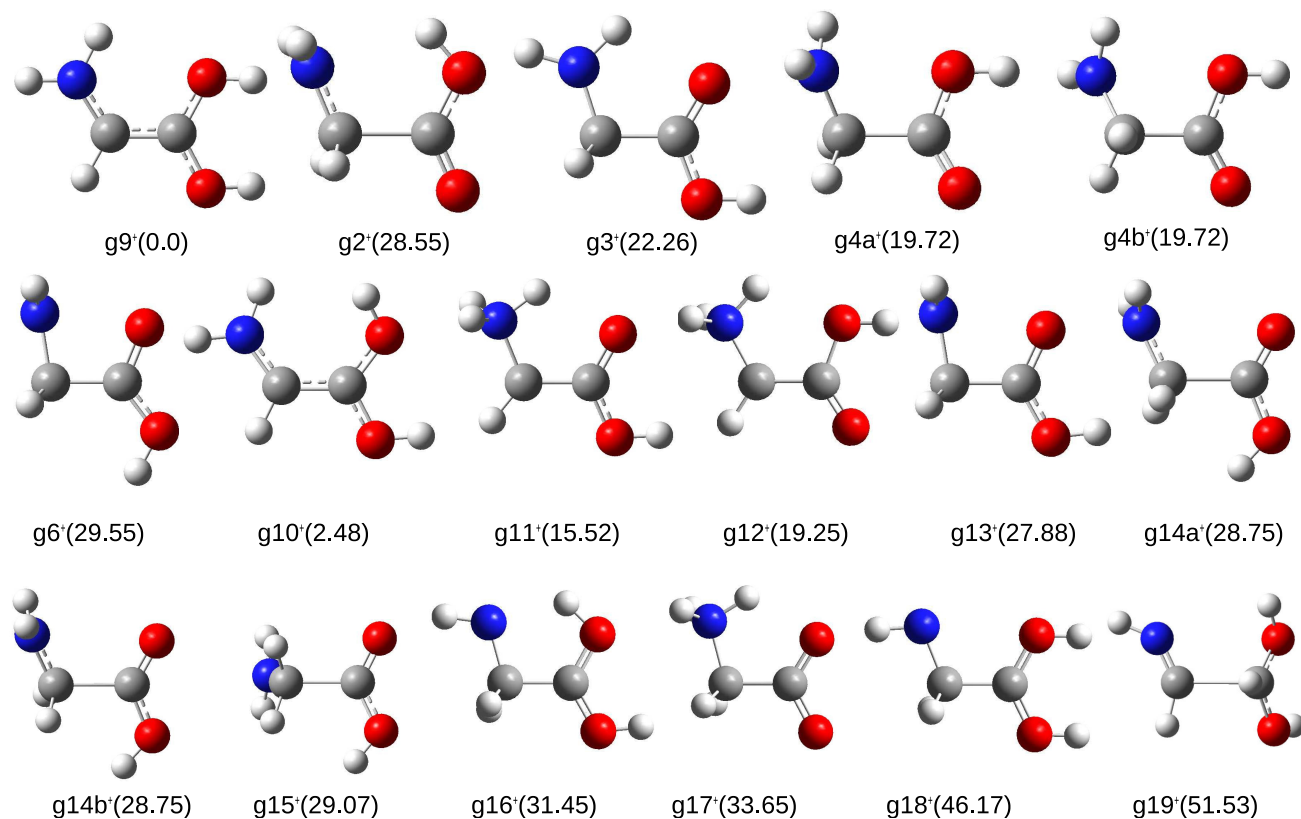


**Figure 5.2:** Optimized geometries for the cation isomers of glycine at the B3LYP/6-311++G(d,p) level of theory. Relative energies ( $\Delta E$ ) in kcal mol<sup>-1</sup> with respect to most stable cation ( $g9^+$ ).

stable  $g10^+$  isomer, which has almost the same geometry as  $g9^+$ : both are geminal di-enols forms with planar nitrogen and with different position of one hydrogen atom in one of the hydroxyl groups. The planar arrangement can be explained through an extra  $\pi$  conjugation (figure 5.2). Isomer  $g9^+$  has also  $C_1$  symmetry and presents a  $^2A$  ground electronic state. Despite of the problems of using the Mulliken population analysis,<sup>118</sup> including large changes of the computed atomic charges with small changes in the basic basis sets and the overestimation of the covalent character of a bond, we employed it for the most stable isomer— $g9^+$ . The Mulliken population analysis indicates that the radical character mainly lies on nitrogen (0.30) and one oxygen (0.2), whereas the positive charge is mainly located at both hydrogens from hydroxyl groups (0.32 and 0.31). The one positively charged group  $OH^+$  of  $g9^+$  acts as proton donor in an intramolecular hydrogen bond with the  $NH_2$  group. Through  $ts1^+$  and intramolecular hydrogen transfer with  $ts2^+$  leads to isomer  $g11^+$ , where we can obtain any of stationary points on the PES. It is observed (figure 5.3) that the two isomerizations  $g10^+ \rightarrow g16^+$  and  $g9^+ \rightarrow g18^+$  present a quite high energy barrier, 10.78 eV and 11.15 eV, respectively. This is due to the fact that both of them correspond to 1,2-H transfers, which require high geometry distortions. In contrast, the isomerizations  $g9^+ \rightarrow g10^+$  and  $g10^+ \rightarrow g11^+$  have significantly much smaller barriers, 8.28 and 9.04 eV. In the first case we observe just one hydroxyl group rotation, changing the position of one hydrogen and, in the second case, 1,4-H transfer. 1,4-H transfer is also observed for isomerization  $g3^+(NH_2CH_2COOH^+) \rightarrow g16^+(NHCH_2C(OH)_2^+)$  with a very flat transition state ( $ts15^+ = 9.49$  eV). These migrations are very easy to obtain and do not require large geometry distortions. On the other hand, 1,3-H transfer rearrangement, not observed in figure 5.3, should be even more energetically demanding than the three mentioned above.<sup>15</sup> It is remarkable that some regions of the PES are very soft: ( $g2^+ \rightsquigarrow ts11^+ \rightsquigarrow g15^+ \rightsquigarrow ts10^+ \rightsquigarrow g14a^+ \rightsquigarrow ts9^+ \rightsquigarrow g14b^+$ ); and particularly ( $g13^+ \rightsquigarrow ts13^+ \rightsquigarrow g3^+$ ).

Optimized rotamers of neutrals and cations were used as starting geometries to generate the dications by varying the necessary dihedral angles, hydrogen positions and bonds length. Extracting two electrons, we obtained just one conformer  $g9^{2+}$ , a geminal dienol structure. The rest of dications of glycine suffer Coulomb explosion during the optimization process, when we start with the neutral isomers. Three of the isomers that we found come from

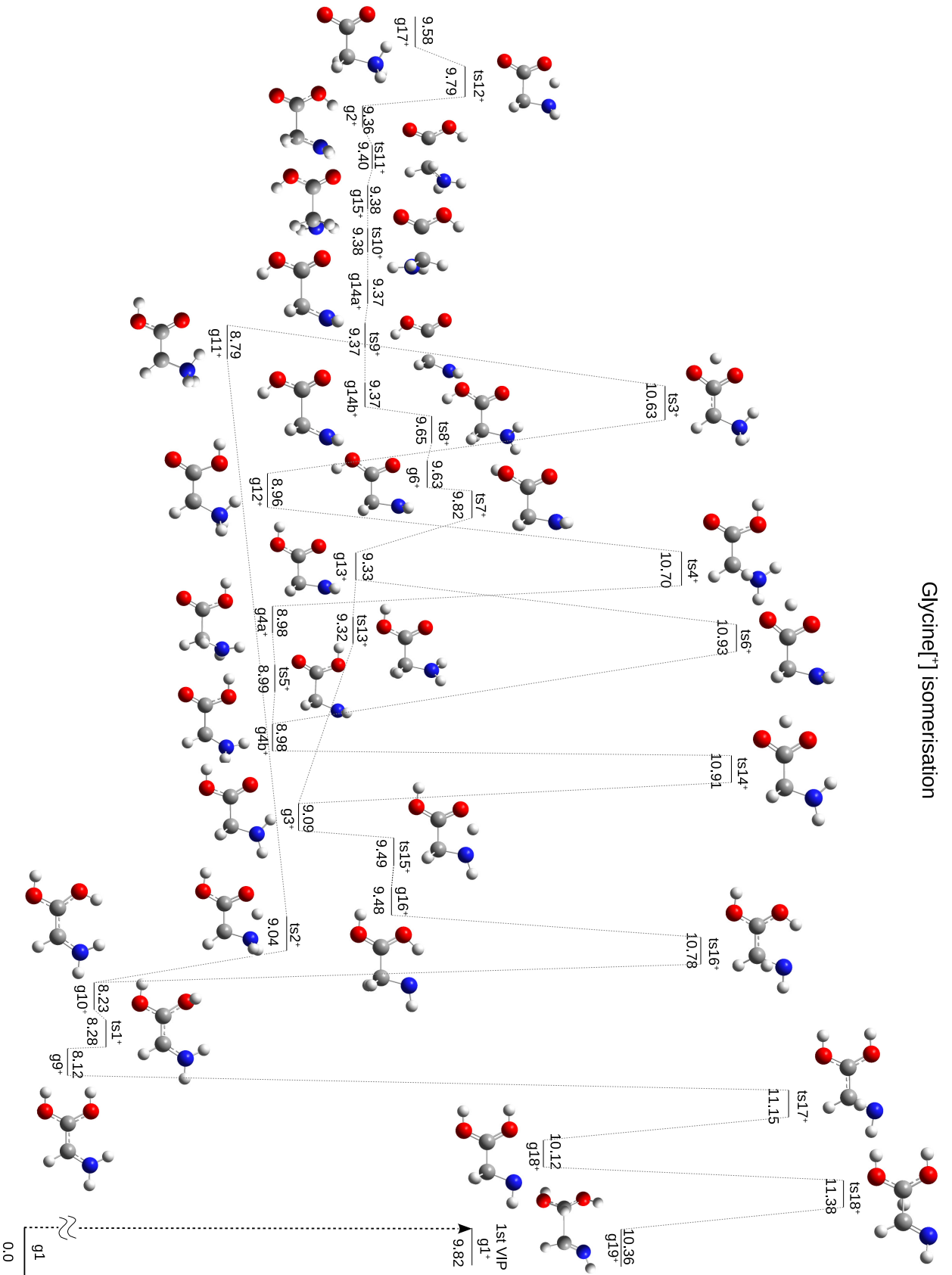


**Figure 5.3:** Stationary points on the isomerization part of the PES corresponding to the minima and transition states of glycine radical cation. Relative energies ( $\Delta E$ ) in eV with respect to most stable neutral glycine ( $g1$ ).

the cations ( $g_{10}^{2+}$ ,  $g_{12}^{2+}$ ,  $g_{18}^{2+}$ ) and the rest of the isomers are new structures (figure 5.4), found during the exploration of the PES. All of them are shown in figure 5.4.

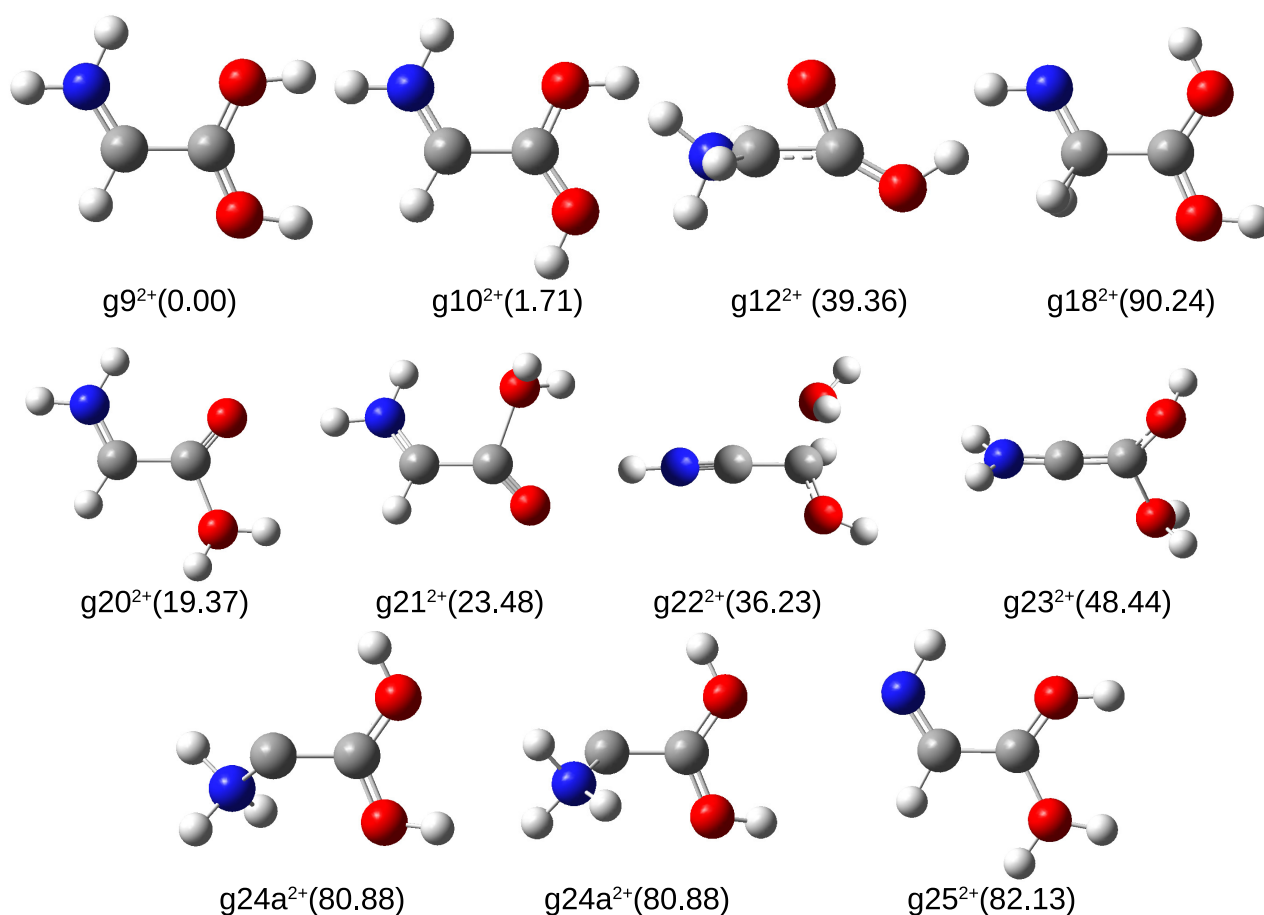


**Figure 5.4:** Optimized geometries for the dication isomers of glycine at the B3LYP/6-311++G(d,p) level of theory. Relative energies ( $\Delta E$ ) in  $\text{kcal mol}^{-1}$  with respect to most stable dication ( $g_{9}^{2+}$ ).

We used all minima ( $g^{2+}$ ) and transition states ( $ts^{2+}$ ) to built the PES for isomerization of dications (figure 5.5). We also calculated the first and second vertical ionization potentials (1<sup>st</sup> and 2<sup>nd</sup> VIPs) of the most stable neutral conformer ( $g_1$ ), which can be the reference for energy entrance channel for double ionization leading to dication  $g^{2+}$ . As we can observe on figure 5.5, the neutral system after ionization have to evolve via intra-molecular H migration keeping the two charges on the molecule. H can be transferred from:

- $C_\alpha$  once to produce the forms:  $\text{NH}_2\text{CHC}(\text{OH})_2^{2+}$  ( $g_{9}^{2+}$ ),  $\text{NH}_3\text{CHCOOH}^{2+}$  ( $g_{12}^{2+}$ ),  $\text{NH}_2\text{CHCOOH}_2^{2+}$  ( $g_{20}^{2+}$ );
- $C_\alpha$  twice:  $\text{NH}_2\text{CC}(\text{OH})(\text{OH}_2)^{2+}$  ( $g_{23}^{2+}$ ),  $\text{NH}_3\text{CC}(\text{OH})_2^{2+}$  ( $g_{24}^{2+}$ );
- N:  $\text{NHCH}_2\text{C}(\text{OH})_2^{2+}$  ( $g_{18}^{2+}$ );
- $C_\alpha$  once + N:  $\text{NHCHC}(\text{OH})(\text{OH}_2)^{2+}$  ( $g_{25}^{2+}$ );
- or  $C_\alpha$  twice + N:  $\text{NHCC}(\text{H})(\text{OH})(\text{OH}_2)^{2+}$  ( $g_{22}^{2+}$ ).

It is easy to notice that the minima obtained after single H transfer are more stable than those obtained after double proton transfer. Additionally, H transfer in  $g_9^+$  from  $C_\alpha$  to the direction of carboxyl group ( $ts_{22}^{2+}=24.98$  eV) dominates over H transfer in  $g_{10}^+$  from  $C_\alpha$  to the direction of amino group ( $ts_{28}^{2+}=25.73$  eV). It can be explained considering the radical character of ionized glycine. For that conformers the radical character is mainly located on  $C_\alpha$  and the acidity of the amino group is higher. Because of that the hydrogen bond in the  $\text{NH}_2$  group becomes strengthened. Moreover, the proton from  $C_\alpha$  prefers to move to the oxygen ( $ts_{22}^{2+}=24.98$  eV) rather

than to the nitrogen atom ( $ts28^{2+}=25.73$  eV). It can be explained due to the decreasing basicity of the amino group that caused the elongation of the intramolecular hydrogen bond. Isomer  $g9^{2+}$  is significantly more stable than any other ionized glycine isomer. The significant differences between the stability of dication conformers provide also an idea of the water loss process. The H transfer from one hydroxyl group of the enol to another hydroxyl group presents the lowest energy hydrogen migration barrier and leads to the  $g20^{2+}$  isomer. Metastable conformer  $g20^{2+}$  can easily loss neutral water leading to the doubly charged fragment  $NH_2CHCO^{2+}$  (figure 5.14). Preferable isomerization leading to one of the metastable conformers of glycine dications with the  $-OH_2$  group goes through hydrogen transfer from one hydroxyl group to another ( $ts23^{2+}$ ) and it is evidently more probable than 1,3-H transfer going through  $ts22^{2+}$  (it presents a lower barrier). It is worth to mention that the most stable glycine ion  $g9^{2+}$  does not isomerize to any other dicationic form with the exception of the less stable  $g10^{2+}$ , with a slightly different position of the hydrogen atom. Both isomers lie in a narrow energy range. It has to be mentioned that structures  $g9^{2+}$  and  $g10^{2+}$  looks like the one which presents a two-center three-electron bond between the OH and  $NH_2$  groups. The relative stability of these structures is found to be over stabilized by the DFT methods due to an overestimation of the self interaction of the exchange energy.<sup>119;120</sup>

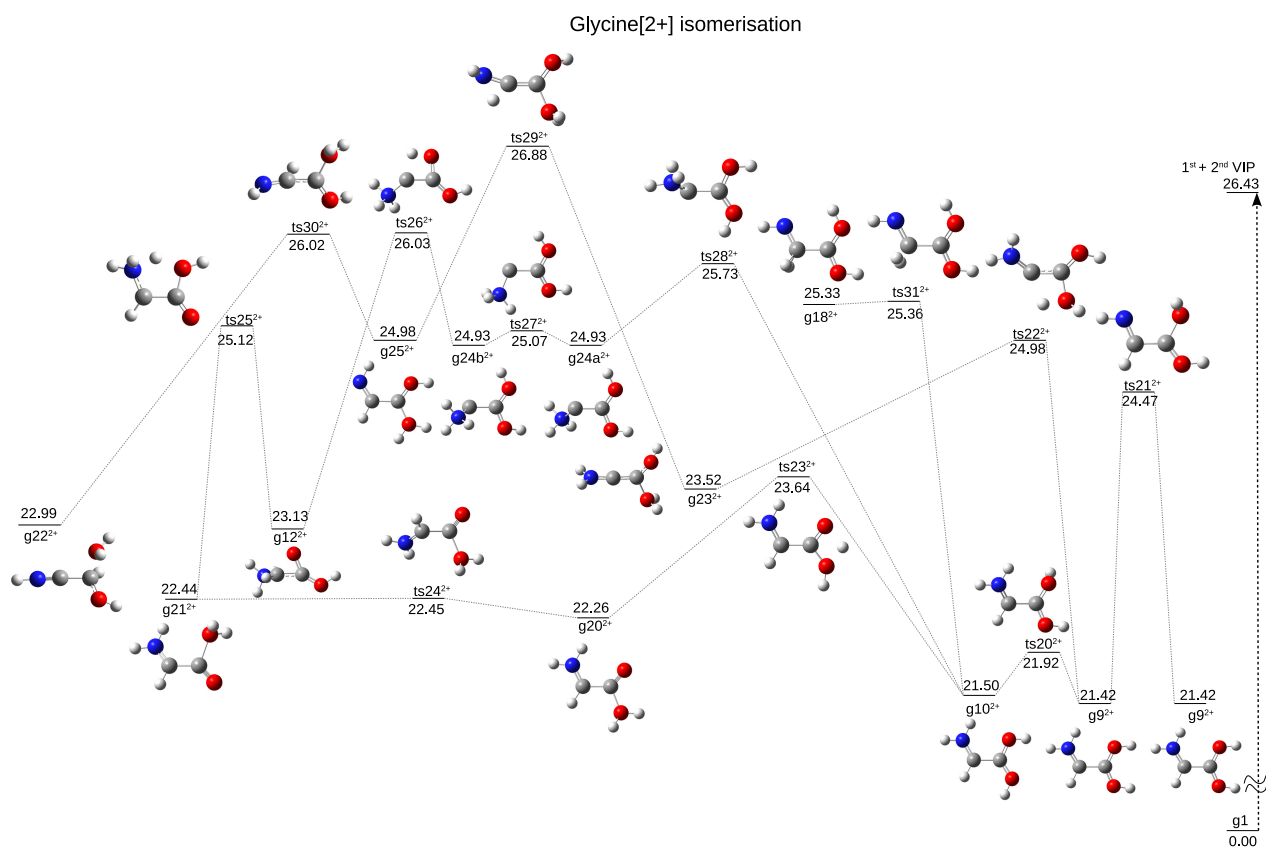


**Figure 5.5:** Stationary points on the isomerization part of the PES corresponding to the minima and transition states of glycine dication. Relative energies ( $\Delta E$ ) in eV with respect to most stable neutral glycine (g1).

## 5.2 Unimolecular decomposition

### 5.2.1 Experimental results

The experiments were performed at the Univeristé de Caen Basse-Normandie in Caen, France by Sylvain Maclot, Dr. Alicja Domaracka, Dr. Patrick Rousseau, Prof. Lamri Adoui and Prof. Bernhard A. Huber. The experimental

details can be found in<sup>121</sup>. The experiments consist in collisions of  $\text{Xe}^{25+}$  with glycine molecules in the gas phase. Charged molecular species are created in these collisions and analyzed with a time-of-flight mass spectrometer. Time-of-flight spectra are recorded in an event-by-event mode allowing to measure the correlation between the charged fragments proceeding from a single ion-molecule collision.<sup>121</sup>

Signals for glycine cation fragmentation are observed in figure 5.6. They were associated with the fragmentation patterns calculated on the PES for the cation (table 5.2) and will be explained in detail in the next section.

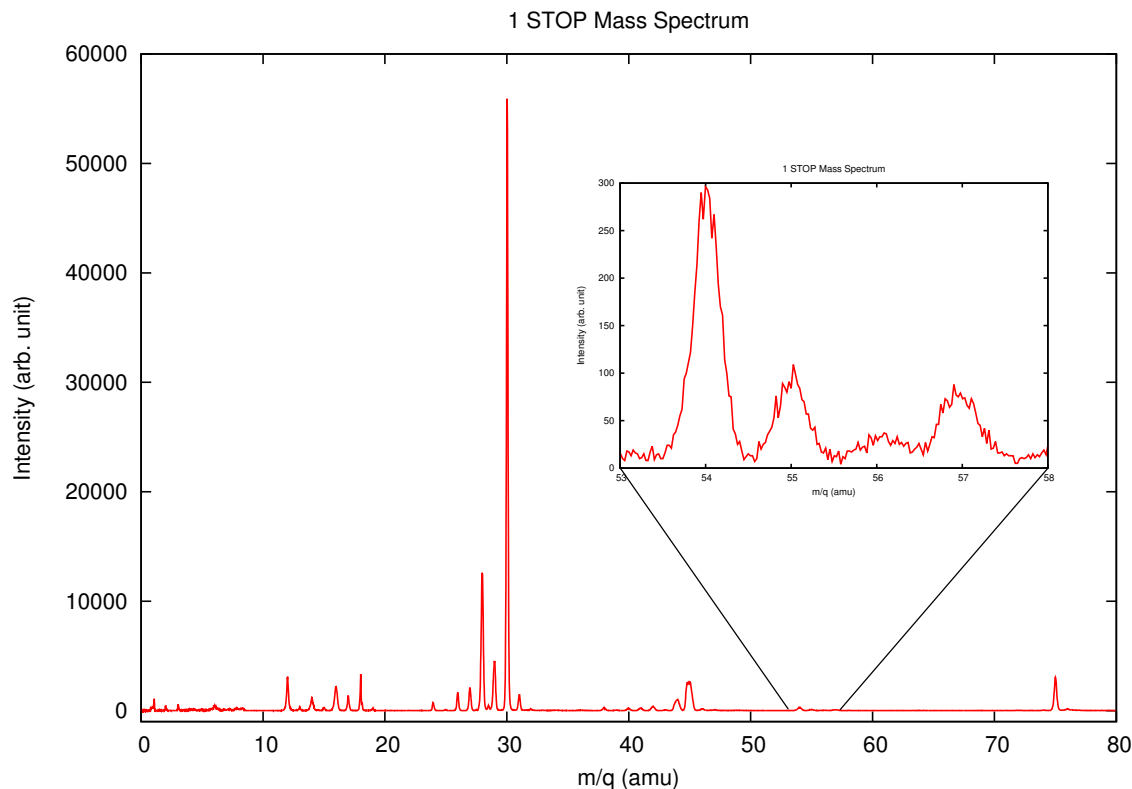


**Figure 5.6:** Mass spectrum of the cationic products obtained by fragmentation of the glycine cation in two charged fragments after the interaction of neutral glycine with  $\text{Xe}^{25+}$  ions at the energy of 387.5 keV.

The most important channel in glycine cation fragmentation corresponds to  $\text{C}_\alpha\text{-C}_{\text{carboxylic}}$  bond cleavage. The charge “prefer” to stay on the fragment containing the amino group ( $\text{NH}_2\text{CH}_2^+$ ) as shown by the high intensity of the peak at  $m/q=30^+$  amu.  $\text{COOH}^+$  fragment at  $m/q=45^+$  amu is only a minor channel in single ionization process. Further fragmentation of  $\text{NH}_2\text{CH}_2^+$  is clearly observed in the experiment (peaks at  $m/q=29^+$  and  $28^+$  amu are observed). We made a zoom in one of the regions of interest of figure 5.6, where we can see small peaks at  $m/q=57^+$ ,  $55^+$  and  $54^+$  amu. In fact singly-charged glycine is also observed in the spectrum ( $m/q=75^+$  amu). The assignation of these signals in the table is explained in the subsection 5.2.2.

Peak	Assignment
30	$\text{NH}_2\text{CH}_2^+$ ( $f1^+$ )
28	$\text{NHCH}^+$ ( $f3^+$ )
45	$\text{COOH}^+$ ( $f2^+$ )
75	$g^+$
57	$\text{NH}_2\text{CHCO}^+$
55	$\text{HNCCO}^+$
54	$\text{NCCO}^+$

**Table 5.2:** Assignment of the peaks corresponding to the regions of interest in the mass spectrum for glycine cation (see figure 5.6).

For glycine dication the most important peaks observed in the experiment are presented in the so-called 2 stop mass spectrum (figure 5.7) and in the coincidence map (figure 5.8). We assigned the main peaks observed in these

spectra in table 5.3 with a map of the fragmentation channels computed on the PES for dications (section 5.2.3).

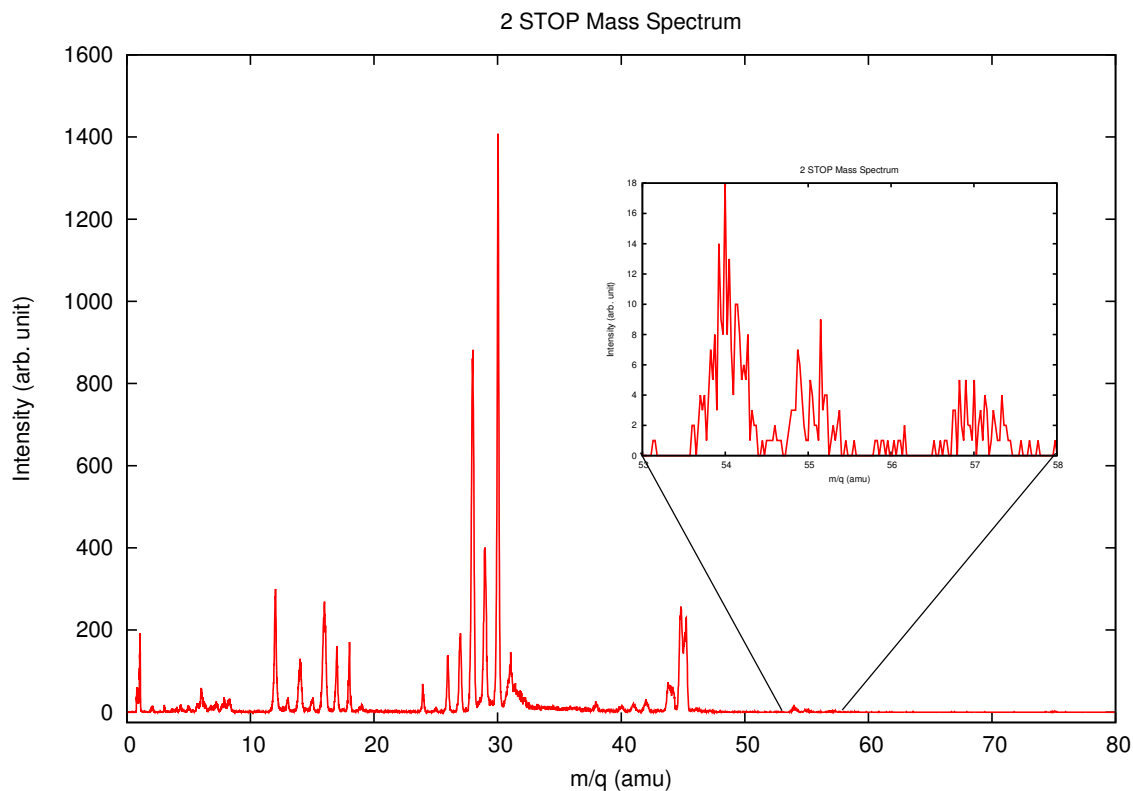


**Figure 5.7:** Mass spectrum of the cationic products obtained by fragmentation of the glycine dication in two charged fragments after the interaction of neutral glycine with  $\text{Xe}^{25+}$  ions at the energy of 387.5 keV.

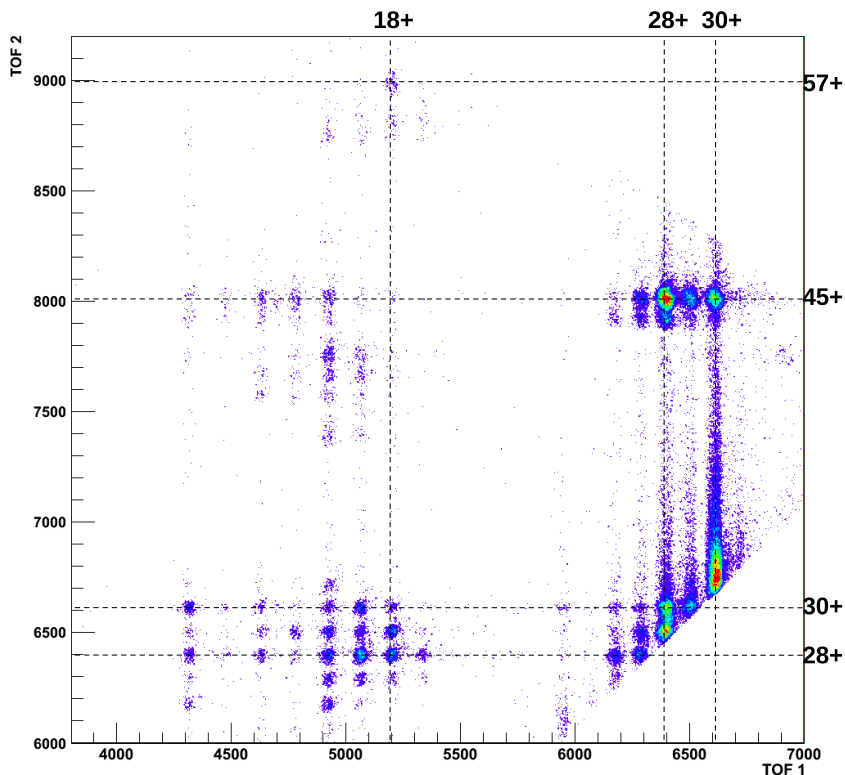


**Figure 5.8:** Coincidence map for the fragmentation of the glycine dication in two charged fragments after the interaction of neutral glycine with  $\text{Xe}^{25+}$  ions at the energy of 387.5 keV. The time-of-flight (in ns) of the heavier fragment (TOF2) is plotted as a function of the time-of-flight of the lighter one (TOF1).

M1	M2	Relative intensity	Assignment
28	45	100%	$\text{NHCH}^+ + \text{COOH}^+$
28	30	75.4%	$\text{CO}^+ + \text{NH}_2\text{CH}_2^+$
28	29	64%	$\text{NHCH}^+ + \text{COH}^+ / \text{CO}^+ + \text{NH}_2\text{CH}^+$
1	12	63.7%	
1	28	51.2%	
1	16	50%	
12	16	39.2%	
30	31	38.5%	
30	45	38.2%	$\text{NH}_2\text{CH}_2^+ + \text{COOH}^+$
29	45	32%	$\text{NH}_2\text{CH}^+ + \text{COOH}^+$
29	30	30.5%	$\text{COH}^+ + \text{NH}_2\text{CH}_2^+$
30	32	29.6%	
18	28	27%	$\text{H}_2\text{O}^+ + \text{NHCH}^+$

**Table 5.3:** Assignment of the correlation islands corresponding to the regions of interest in the coincidence map for glycine dication. Relative intensities are given in percentage of the total intensity of the map.

## 5.2.2 Cation

Glycine cation, despite its high stability (seventeen structures observed match to the peak at  $m/q=75^+$  amu) breaks up mainly into two fragments:  $\text{NH}_2\text{CH}_2^+/\text{COOH}$  (first fragment,  $f1^+$ /second fragment,  $f2$ ) or  $\text{NH}_2\text{CH}_2/\text{COOH}^+$  ( $f1/f2^+$ ) with different charge distribution, corresponding to the signals at  $m/q=30^+$  amu and  $45^+$  amu respectively (figure 5.9). This is explained due to the extra stability of  $\text{NH}_2\text{CH}_2^+$  and  $\text{COOH}^+$ , where the first pathway is about 2 eV lower in energy than the second one. A very intense peak at  $m/q=30^+$  prevails over  $45^+$  amu in the experiment. This is consistent with the energy required to create the immonium and carboxylic ions, indicating that our theoretical calculations are in agreement with the mass spectrometry experiments and with previous studies.<sup>30</sup>

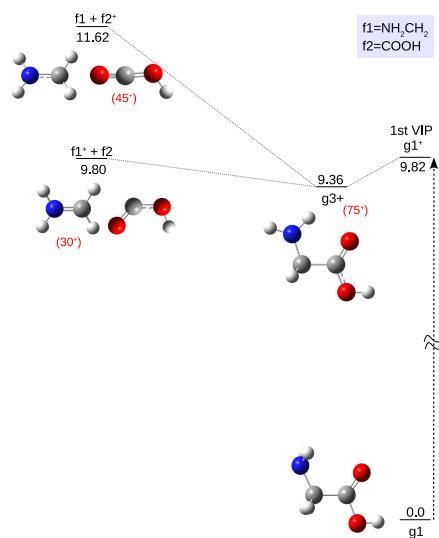


**Figure 5.9:** Fragmentation from glycine cation ( $g3^+$ ). 1<sup>st</sup> VIP from  $g1$  is given as entrance channel. Relative energies ( $\Delta E$ ) in eV with respect to most stable neutral glycine ( $g1$ ).

To interpret the experiments we also calculated the fragmentation of  $\text{NH}_2\text{CH}_2^+$ . We can observe that other intense peak  $m/q=28$  amu appears in the experiment. We assign this peak to losing hydrogen molecule from  $\text{NH}_2\text{CH}_2^+$  leading to  $\text{NHCH}^+$  ( $f3^+$ ) +  $\text{H}_2$  (figure 5.10). It is 3.86 eV higher in energy and indicates that in many cases the produced  $\text{NH}_2\text{CH}_2^+$  possesses enough internal energy to break continuously (figure 5.10). These channels appear as a result of the cleavage of the  $C_{\text{carboxylic}}-C_{\alpha}$  bond and are also observed in the experiment with high intensities:  $30^+$ ,  $28^+$  and  $45^+$ . In general, these ions are the characteristic features obtained in the fragmentation of ionized  $\alpha$ -amino acids.<sup>24;122;123</sup> Other channels are much higher in energy and, even without consideration of any barriers, lead to loss of neutral hydrogen from carbon or nitrogen side, 4.99 eV and 5.11 eV respectively. Figure 5.10

also presents dehydrogenation process which is very similar to the deprotonation–textbook example of, probably, one of the most important and one of the most extensively studied site–selective process among the reactions of organic radical cations. In the gas phase hydrogen atom loss may be the favorable process but in halocarbons or solid rare gases deprotonation will be favorable because of a large gain in polarization energy. As it is observed in this manuscript, the concept of selective bond weakening is also appropriate to the backbones in the radical cation and dication amino acids. Large elongation and weakening of the specific C–C  $\sigma$ –bond upon ionization has been reported for linear and branched pentanes<sup>124</sup> and alkanes.<sup>125</sup>

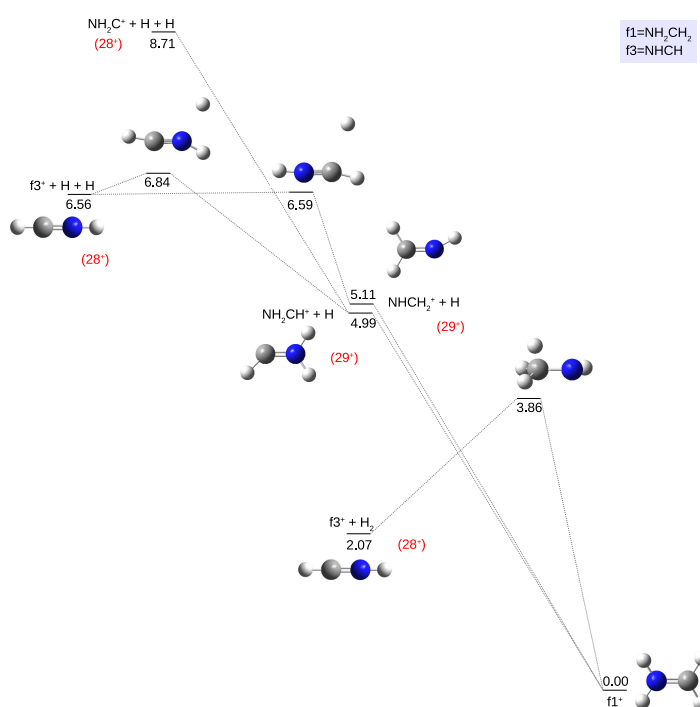


**Figure 5.10:** Fragmentation of  $\text{NH}_2\text{CH}_2^+$ . Relative energies ( $\Delta E$ ) in eV.

In figure 5.11 we can observe that easily we can get to the  $\text{NH}_2\text{CHCO}^+ + \text{H}_2\text{O}$  from  $\text{g13}^+$ , after obtaining a weakly–bounded molecule ( $\text{m1}^+$ ) and removing water molecule. This structure is rather stable (9.28 eV) and is found to readily equilibrate to  $\text{m2}^+$  prior to dissociation. The latter can loss hydrogen molecule with a quite high barrier (13.43 eV) leading to  $\text{HNCCO}^+$  ( $m/q=55^+$  amu) and finally complete the fragmentation path at  $m/q=54^+$  amu corresponding to linear  $\text{NCCO}^+ [+ \text{H}_2 + \text{H} + \text{H}_2\text{O}]$  ( $m/q=54^+$  amu), lying around 5 eV higher than the entrance channel. Since the peak at  $m/q=54^+$  amu is observed in the experiments, it shows that the excitation energy on the glycine molecule in the collision is at least of 5 eV.

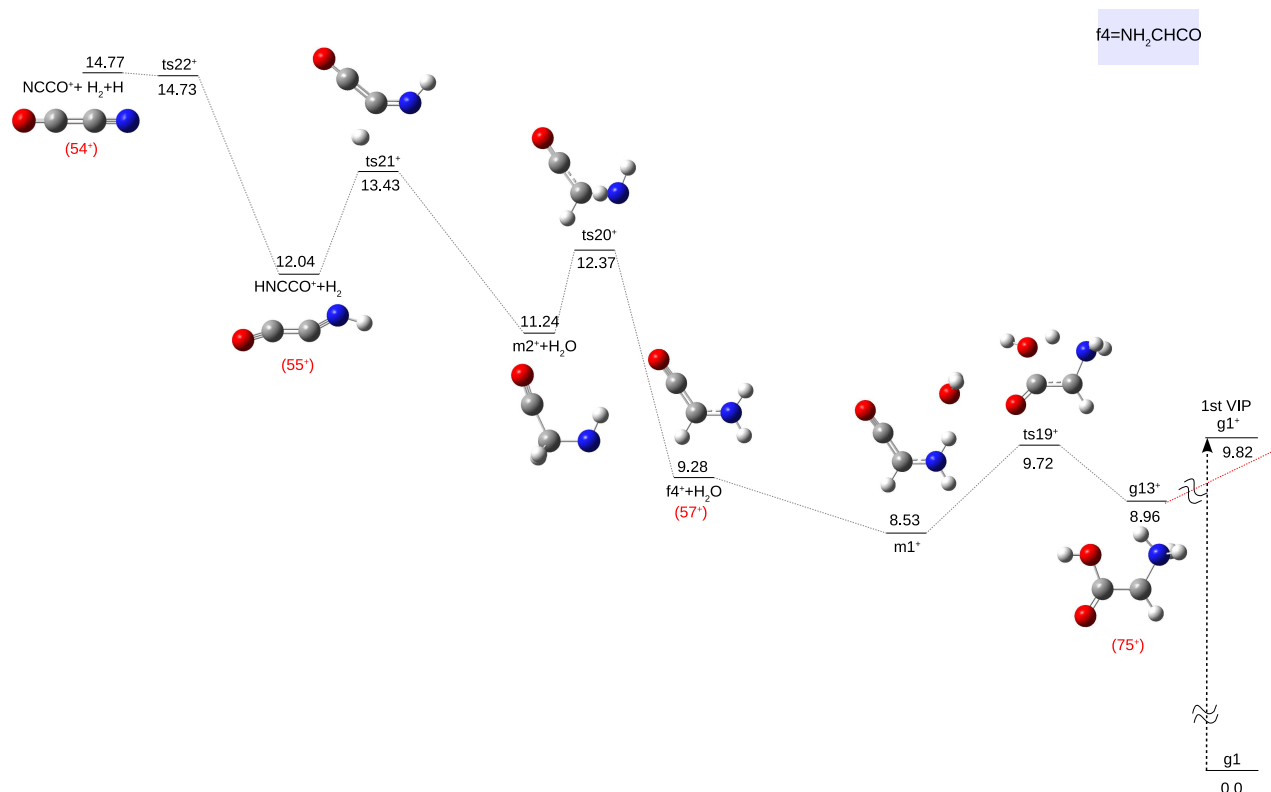
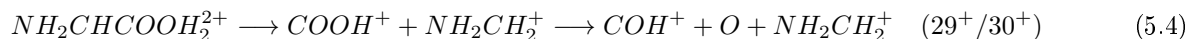
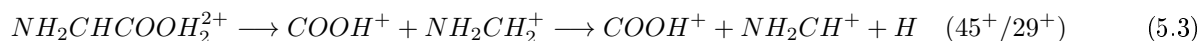
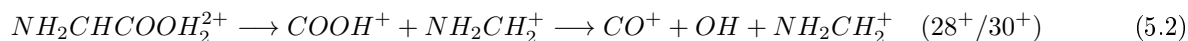
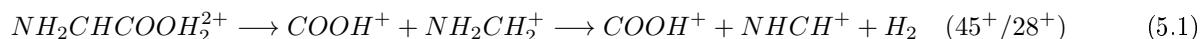


**Figure 5.11:** Additional fragmentation path of glycine cation. 1<sup>st</sup> VIP from g1 is given as entrance channel. Relative energies ( $\Delta E$ ) in eV with respect to most stable neutral glycine (g1).

### 5.2.3 Dication

In figure 5.12 we can observe the direct fragmentation into two charged fragments  $\text{NH}_2\text{CH}_2^+$  ( $f1^+$ ) and  $\text{COOH}^+$  ( $f2^+$ )  $m/q=(30^+/45^+)$  after  $\text{C}_\alpha\text{-C}_{\text{carboxylic}}$  break, which is the most characteristic fragmentation path of doubly-charged amino acids. Both ions are produced with enough internal energy to follow subsequent fragmentation, leading to loss of neutral moieties (H,  $\text{H}_2$ , O, OH):



Exploration of the PES reveals that the corresponding transition states and final products are below the energy of the entrance channel, explaining why channels 5.1 and 5.2 correspond to the most intense peaks observed in the experiment (figures 5.8 and 5.6). Note that  $g^{2+}$  is produced in a collision with a very energetic ion, so it is reasonable to assume that the produced fragments have enough internal energy to overcome the barriers needed to reach not only the four fragments mentioned above, but also  $29^+/28^+$ ,  $28^+/28^+$ ,  $27^+/28^+$  fragments (figure 5.12). In this respect, it is worth to mention that, for 5-fold ionization of Na clusters in collisions with  $\text{Xe}^{20+}$ , the measured transfer of energy can be as high as 4 eV.<sup>126</sup>

In addition, on the left-hand side in figure 5.12 we can observe the competitive pathways leading to the creation

of an enol form of dicationic glycine and to  $\text{NH}_3\text{CHCOOH}^{2+}$  ( $\text{g}12^{2+}$ ). In comparison with the most probable channel–Coulomb explosion, the production of stable dicationic forms of glycine ( $\text{g}9^{2+}$ ,  $\text{g}10^{2+}$ ,  $\text{g}12^{2+}$ ) is at least 3.36 eV higher in energy. We should also mention that we calculated all the possible ways of losing a neutral radical or cation i.e.  $\text{COOH}^+ + \text{NHCH}^+ + \text{H}_2$ ,  $\text{COOH}^+ + \text{NHCH} + \text{H}_2^+$  or  $\text{COOH} + \text{NHCH}^+ + \text{H}_2^+$  but only the most stable are reported. The preferences of losing neutral radical or cation can be explained analyzing the value of the ionization potential of the created species. In general, the more favorable process is the one leaving the charge on the fragment with lower ionization potential. This is a general conclusion reported by Simon et al.<sup>15</sup> and is confirmed in every further fragmentation pathway.

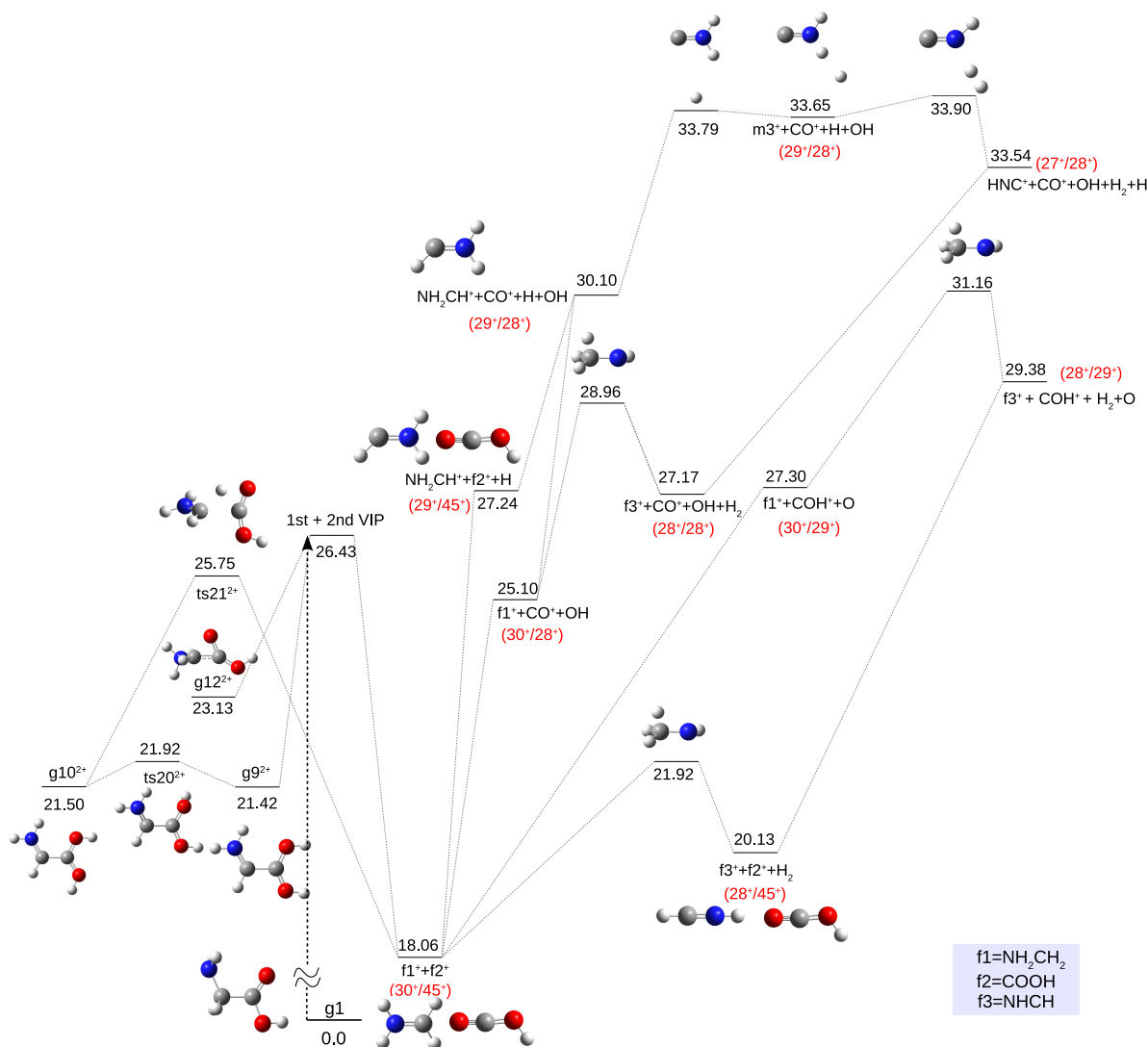


**Figure 5.12:** Fragmentations of dication of glycine in the wake of Coulomb explosion. Relative energies ( $\Delta E$ ) in eV with respect to most stable neutral glycine ( $\text{g}1$ ).

According to our results (figure 5.4), the dienol dication is significantly more stable than the other conformers and as shown in figure 5.12, it is slightly less stable than the typical Coulomb explosion ( $\text{NH}_2\text{CH}_2^+ + \text{COOH}^+$ ). The stability of doubly charged glycine diol requires an extra study in order to check if the structure can readily support different fragmentation channels, in addition to the Coulomb explosion  $\text{NH}_2\text{CH}_2^+ + \text{COOH}^+$ . Starting from diol  $\text{g}9^{2+}$  we calculated five possible channels, four are shown in figure 5.13 and one in figure 5.14. The latter corresponds to water loss, which remains the favored fragmentation pathway. We first focus on figure 5.13, where the channel with the lowest barrier ( $\text{ts}21^{2+} = 25.75$  eV) lead us to the same fragments as direct Coulomb explosion:  $\text{NH}_2\text{CH}_2^+$  and  $\text{COOH}^+$   $m/q = (30^+/45^+)$ . The same signal  $m/q = (30^+/45^+)$  can be obtained with a slightly higher transition state  $\text{ts}23^{2+}$  (26.65 eV) leading to the metastable fragment  $[\text{H}_2 \cdots \text{NHCH}]^+$ . The complementary and structurally

indicative fragments  $\text{NHCH}^+/\text{HC}(\text{OH})_2^+$   $m/q=(28^+/47^+)$  and  $\text{NH}_2\text{CH}^+/\text{C}(\text{OH})_2^+$   $m/q=(29^+/46^+)$  also appear in the experiment but are less abundant than those coming from the Coulomb explosion. Moreover,  $\text{HC}(\text{OH})_2^+$  can isomerise to  $\text{HOCO}_2^+$  ( $m/q=47^+$ ) and easily loss neutral water:  $\text{NHCH}^+ + \text{COH}^+ + \text{H}_2\text{O}$  ( $m/q=28^+/29^+$  with 21.79 eV) or ionized water:  $\text{NHCH}^+ + \text{COH} + \text{H}_2\text{O}^+$  ( $m/q=18^+/28^+$  with 26.11 eV). These channels are both accessible from the point of view of the entrance channel energy and the first one should be observed with quite higher probability. The most intense peak in the coincidence map  $m/q=28^+/45^+$  amu can be also obtained from dicationic diol form with small energy barriers (26.07 and 22.10 eV)  $\rightarrow \text{COOH}^+ + \text{NHCH}^+ + \text{H}_2$ . Furthermore, in figure 5.13 we can also observe three different channels leading to the signal at  $m/q=28^+/29^+$  amu. The lowest in energy is described above. The two others should not be accessible or very improbable because they need to go through many isomerization steps:  $\text{C}(\text{OH})_2^+ + \text{NH}_2\text{CH}^+ \rightarrow \text{H}_2\text{OCO}^+ + \text{NH}_2\text{CH}^+ \rightarrow \text{H}_2\text{O} + \text{CO}^+ + \text{NH}_2\text{CH}^+$  at 25.17 eV (unset in figure 5.13) or they are very high in energy  $\text{NHCH}^+ + \text{COH}^+ + \text{H}_2 + \text{O}$  (29.38 eV).

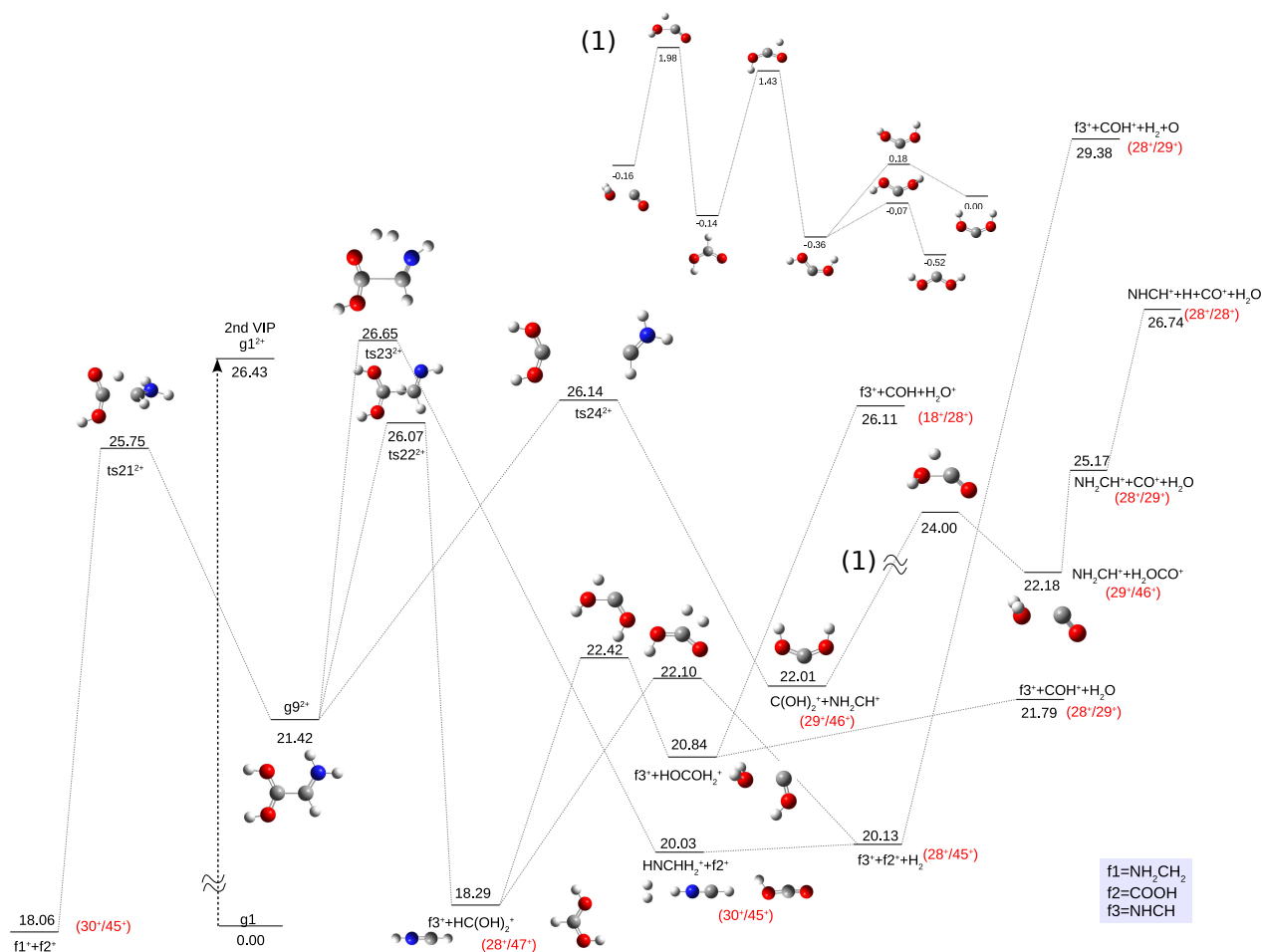
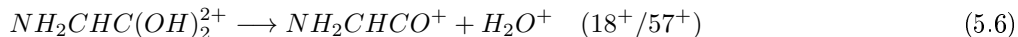
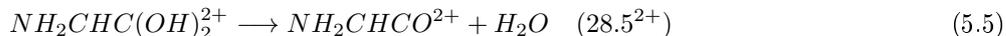


**Figure 5.13:** Fragmentations of dication of glycine: Coulomb explosion versus “enol” fragmentation paths. Relative energies ( $\Delta E$ ) in eV with respect to most stable neutral glycine ( $g1$ ). Inset (1): Isomerization of  $\text{C}(\text{OH})_2^+$ . Relative energies ( $\Delta E$ ) in eV.

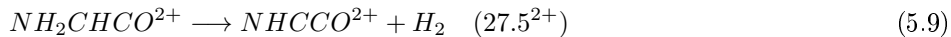
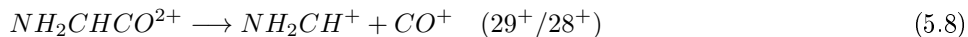
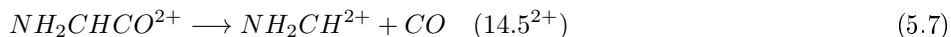
In the inset in figure 5.13 we can observe that  $\text{C}(\text{OH})_2^+$  can easily isomerize. However, the isomerization leading to the form which can loss carbon monoxide requires a three step reaction and 2 eV of internal energy. The most favorable process is isomerization to the structure found at 0.52 eV lower in energy than the molecule obtained after direct Coulomb bond breaking.

The high stability of glycine diol dications after ionization can be proved analyzing the further fragmentation mechanism theoretically predicted. The main attention of figure 5.14 should be paid on the very stable dication  $\text{NH}_2\text{CHCO}_2^+$  ( $m/q=28.5^+$  amu), which is obtained after water loss from  $g20^{2+}$ . The peak at  $m/q=28.5^+$  amu is observed in the experiment, confirming the mechanism proposed here. Additionally, fragmentation of this structure allowed to construct of the potential energy diagram which describes the participation of three other

dicationic forms:  $\text{NH}_2\text{CH}^{2+}$  (14.5<sup>+</sup>),  $\text{HCO}^{2+}$  (14.5<sup>+</sup>) and  $\text{HNCCO}^{2+}$  (27.5<sup>+</sup>) also measured in the coincidence map. Moreover, signals at  $m/q=18^+/57^+$  and  $18^+/55^+$ , are again observed in the experiment; As shown in figure 5.14 they correspond to  $\text{H}_2\text{O}^+ + \text{NH}_2\text{CHCO}^+$ . These fragmentation channels appear due to the competition between loss of the neutral water and the singly charged one:



The dehydration process can occur following two paths, one of which should be favored because it requires less energy (ts at 23.02 eV). Dehydration from the diol explains the peaks at  $m/q = 28.5^{2+}$  and  $18^+/57^+$ , which depends on the charge distribution after fragmentation. Charge can be localized on  $\text{NH}_2\text{CHCO}^{2+}$  or separated between  $\text{NH}_2\text{CHCO}^+$  and  $\text{H}_2\text{O}^+$ . These species can only be produced if one considers atomic rearrangement before Coulomb explosion. Thus, this detection is an experimental evidence of the intramolecular H transfer. Previous studies observing the peak at 28.5 amu<sup>127</sup> proposed a direct loss of OH and H from  $g^{2+}$ ; this route would require much more energy than the two-steps mechanism proposed here: isomerization + neutral water loss. Starting from the dehydrated cation,  $\text{NH}_2\text{CHCO}^+$ , a dissociation channel is found with one path sensibly favoured. On the other hand, starting from  $\text{NH}_2\text{CHCO}^{2+}$  we can distinguish 5 pathways: three paths lead to  $m/q=28^+/29^+$  amu, one path to  $m/q=14.5^{2+}$  amu and the last one to 27.5<sup>2+</sup> amu. Thus, the follow fragmentation of aminoketene dication ( $\text{NH}_2\text{CHCO}^{2+}$ ) leads to loss of CO,  $\text{CO}^+$  or  $\text{H}_2$  processes, which are also in competition:



CO and  $\text{H}_2$  loss from the aminoketene dication explain the peaks at  $m/q=14.5^{2+}$  amu and  $m/q=27.5^{2+}$  amu in the experiments, processes 5.7 and 5.9 respectively.

It is worth noting, however, that the  $\text{NH}_2\text{CHCO}^{2+}$  presents an energy that makes it accessible from the entrance channel but its possible dissociation pathways appear above this energy. Formation of  $\text{HNCCO}^{2+}$  and  $\text{NH}_2\text{CH}^{2+}$  become accessible channels if we assume that part of the population of initial doubly-charged glycine is formed with an internal energy of  $\approx 2.2$  eV. Thus, the computational study shows that for the formation of the observed doubly charged species, the excited aminoketene dication plays a central role. The characteristic (14.5<sup>2+</sup> and 27.5<sup>2+</sup>) peaks can be only explained in coincidence with the very stable  $\text{NH}_2\text{CHCO}^{2+}$  structure, and do not come from the typical  $\text{C}_{acid}-\text{C}_\alpha$  bond cleavage. It has been found that these two  $\text{NH}_2\text{CHCO}^+$  and  $\text{NH}_2\text{CHCO}^{2+}$  ions do not appear in other reaction channels, neither with the Coulomb explosion nor with any of the canonical nor  $\text{NH}_3\text{CHCOOH}$  glycine fragmentation structure. Such characteristics suggest that the typical signals observed in the experiment ( $28^+/29^+$ ) can be associated to fragments coming from fragmentation of  $\text{NH}_2\text{CHCO}^{2+}$  as well, and their presence should be consider in addition to the previous typical fragmentation paths.

The origin of the untypical fragmentation pathways, described above, is shown in figure 5.14 and is associated with an ultra-fast intramolecular hydrogen migration. This migration was previously studied on smaller molecules such as acetylene<sup>128;129</sup> and methanol<sup>130</sup> and reported that it occurs within a few tens of fs, being the responsible of the ultrafast decay of the excited dications.

We performed ab initio molecular dynamics calculations using the ADMP method to better understand the fragmentation mechanisms. The main fragmentation channel observed in the first steps of the dynamics leads



to fission of the dicationic glycine,  $g^{2+}$  into  $NH_2CH_2^+/COOH^+$  (figure 5.15a), the corresponding experimental coincidence measurement is noted  $m/q=(30^+/45^+)$  amu. However, the simulations also show fast intramolecular H transfer leading to two stable doubly charged isomers  $NH_2CHC(OH)_2^{2+}$  and  $NH_3CHCOOH^{2+}$  (figure 5.15b, c); both of them correspond to a minimum in the potential energy surface (PES) as shown in the previous section. This occurs only starting from certain conformers and for a given range of internal energy, thus a minimum excitation is required to initiate the intramolecular transfer; however above a certain value, the excitation is too high leading directly to the dissociation. These simulations confirm the mechanisms proposed above: Coulomb explosion in competition with intramolecular H transfer.

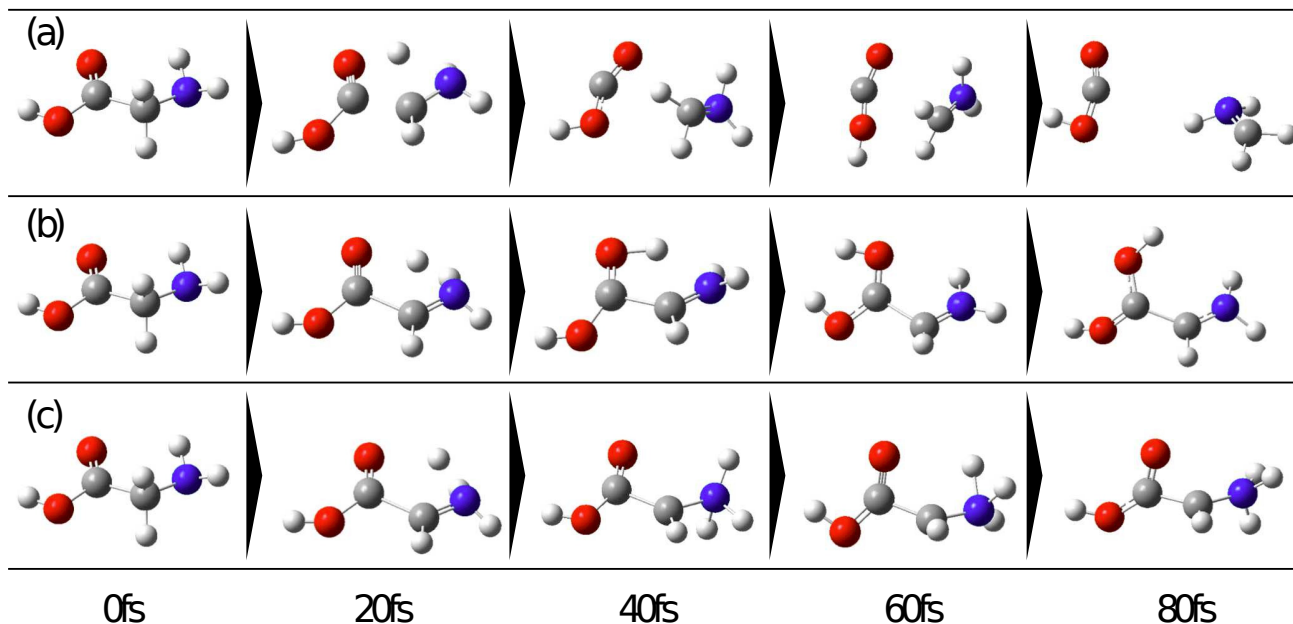


**Figure 5.15:** Snapshots of molecular dynamics simulations of a glycine dication with (a) 2.18 eV of internal energy giving a fission process leading to fragments  $NH_2CH_2^+/COOH^+$ , b) 2.45 eV and c) 2.72 eV leading the isomerization by H-transfer in diol  $NH_2CH(OH)^{2+}$  and  $NH_3CHCOOH^{2+}$ , respectively.

# Chapter 6

## $\beta$ -Alanine

Previous works have evaluated the conformers of neutral  $\beta$ -alanine in gas phase,<sup>28</sup> as well as in aqueous solution.<sup>131</sup> Furthermore the fragmentation of singly charged  $\beta$ -alanine have been also studied.<sup>30;123;132</sup> In this chapter we focus on the stability and fragmentation dynamics of doubly charged  $\beta$ -alanine. We present ab initio molecular dynamics simulations of the possible fragmentation pathways as a function of the excitation energy. We found seventeen different fragmentation mechanisms. Finally, the PES of several fragmentation pathways of  $(\beta\text{-alanine})^{2+}$  is also presented.

### 6.1 Conformational study– neutrals

We have first studied different conformers of neutral  $\beta$ -alanine in the gas phase. To do this, we used the same methodology as in the case of glycine.  $\beta$ -alanine has more group rotation degrees of freedom and because of that the existence of stable conformers with slight difference in relative energies scales rapidly. As it was mentioned in the case of glycine, amino acids are generally floppy molecules which can fall into many stable isomers during the exploration of the potential energy surface (PES). Each well on a PES corresponds to the most stable local minimum, where the geometry of one particular isomer changed and for which the forces on the nuclei vanish. We can not be sure, from a theoretical point of view that any of presented minima (figure 6.1) correspond to the global minimum on the PES. Some of the starting geometries were taken from the previous study of McGlone and Godfrey.<sup>133</sup> Other starting geometries have been taken from Sanz et al.<sup>28</sup>. In our exploration we found sixteen isomers as shown in figure 6.1. The relative energy between the isomers shows a high degree of degeneracy; nine of the isomers lie in a range of less than 2 kcal/mol (relative energy with respect to the most stable conformer a1).

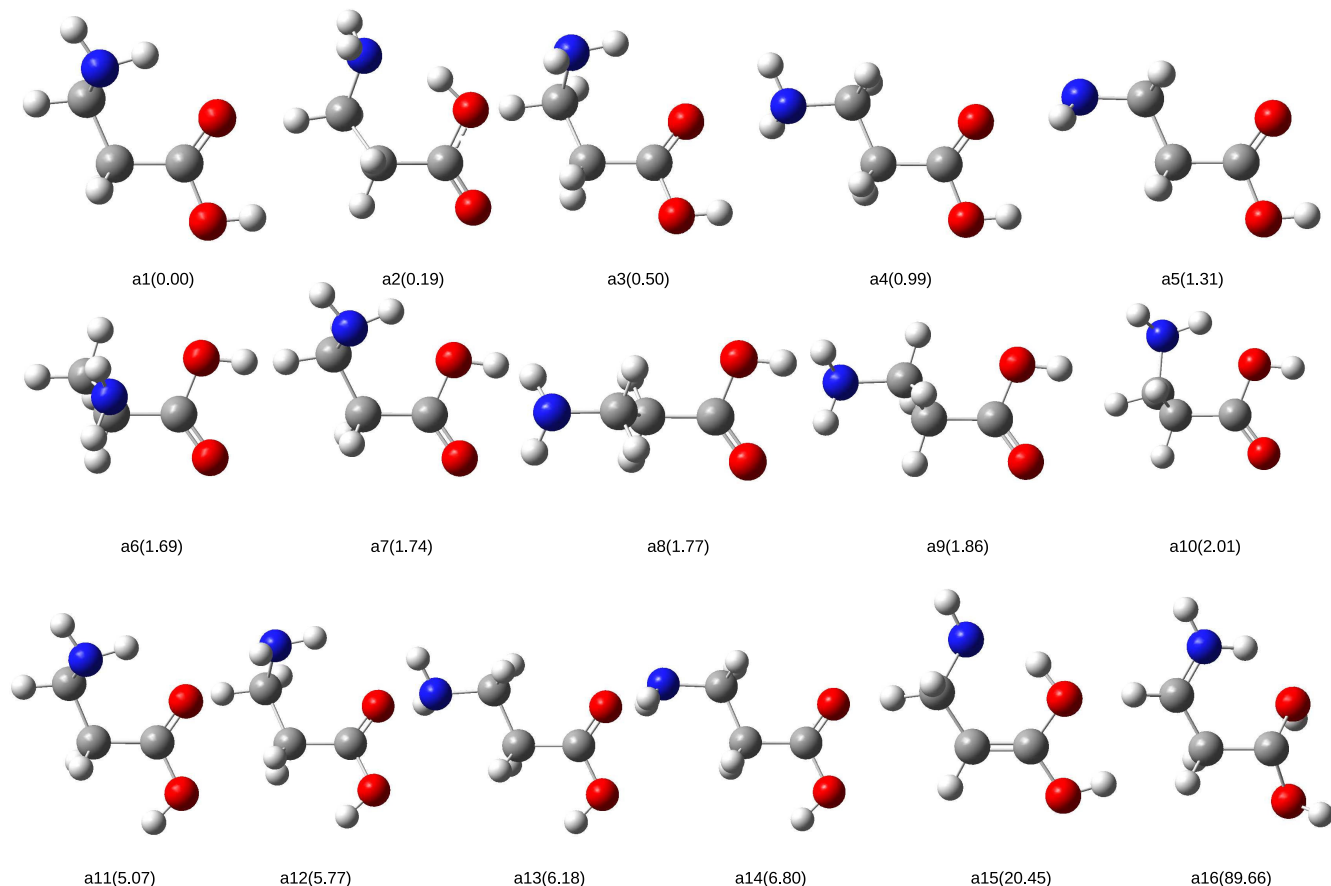


**Figure 6.1:** Optimizing geometries for the neutral isomers of  $\beta$ -Alanine at the B3LYP/6-311++G(d,p) level of theory. Relative energies ( $\Delta E$ ) in kcal mol<sup>-1</sup> with respect to most stable neutral (a1).

## 6.2 Experimental results

The experiments for  $\beta$ -alanine were performed by the same group as for glycine at the Univeristé de Caen Basse-Normandie in Caen (France) by Sylvain Maclot, Dr. Alicja Domaracka, Dr. Patrick Rousseau, Prof. Bernhard A. Huber and Prof. Lamri Adoui. The methods used for  $\beta$ -alanine, accordingly to section 5.2.1 are the same as for glycine. The most important peaks observed for dication of  $\beta$ -alanine are presented in the 2-stop mass spectrum and in the coincident map 6.3. We assigned them (table 5.3) to the computed fragmentation channels (section 6.5).

Collision with highly charged ions like Xe<sup>25+</sup> or He<sup>2+</sup> is a very fast process. Therefore, the electrons of the target molecule are rapidly extracted. The charged molecules are also excited and undergo fragmentation. Then, the produced charged fragments resulting from the fragmentation are detected. Results are plotted as the time-of-flight of one fragment as the function of the time-of-flight of second fragment on the so-called coincidence map.

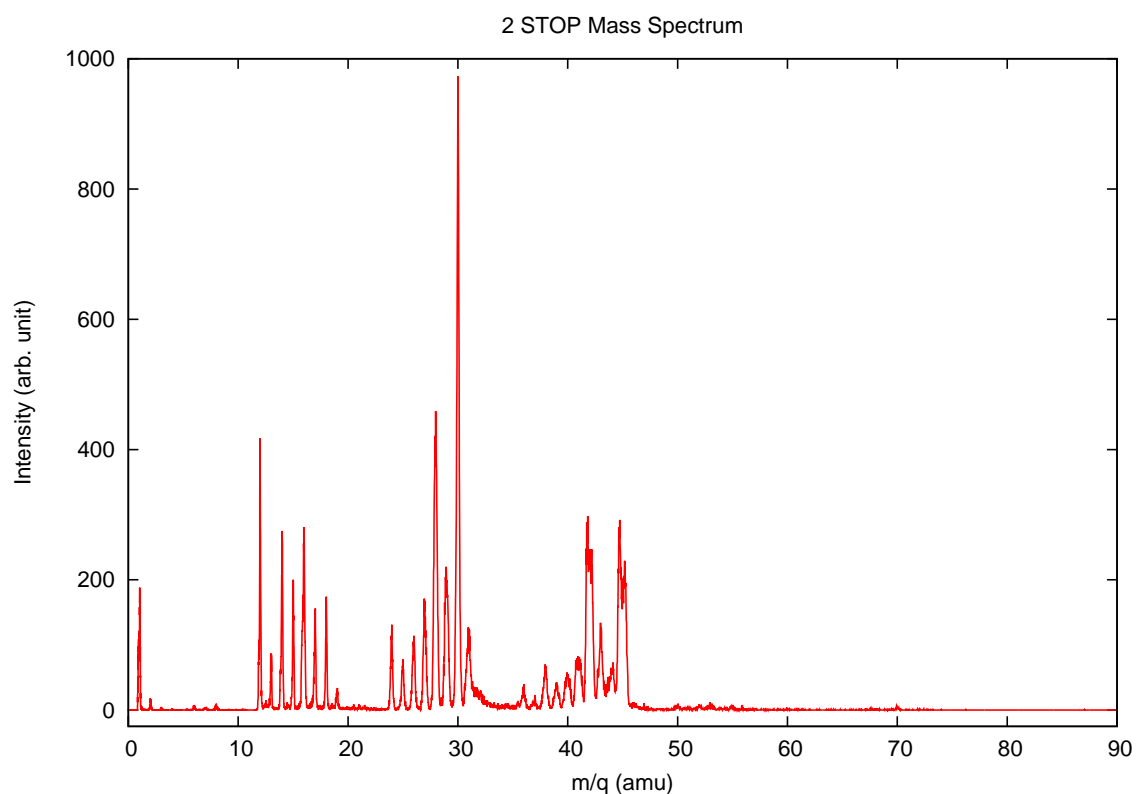


**Figure 6.2:** Mass spectrum of the cationic products obtained by fragmentation of  $\beta$ -alanine dication in two charged fragments after the interaction of neutral glycine with  $\text{Xe}^{25+}$  ions at the energy of 387.5 keV.

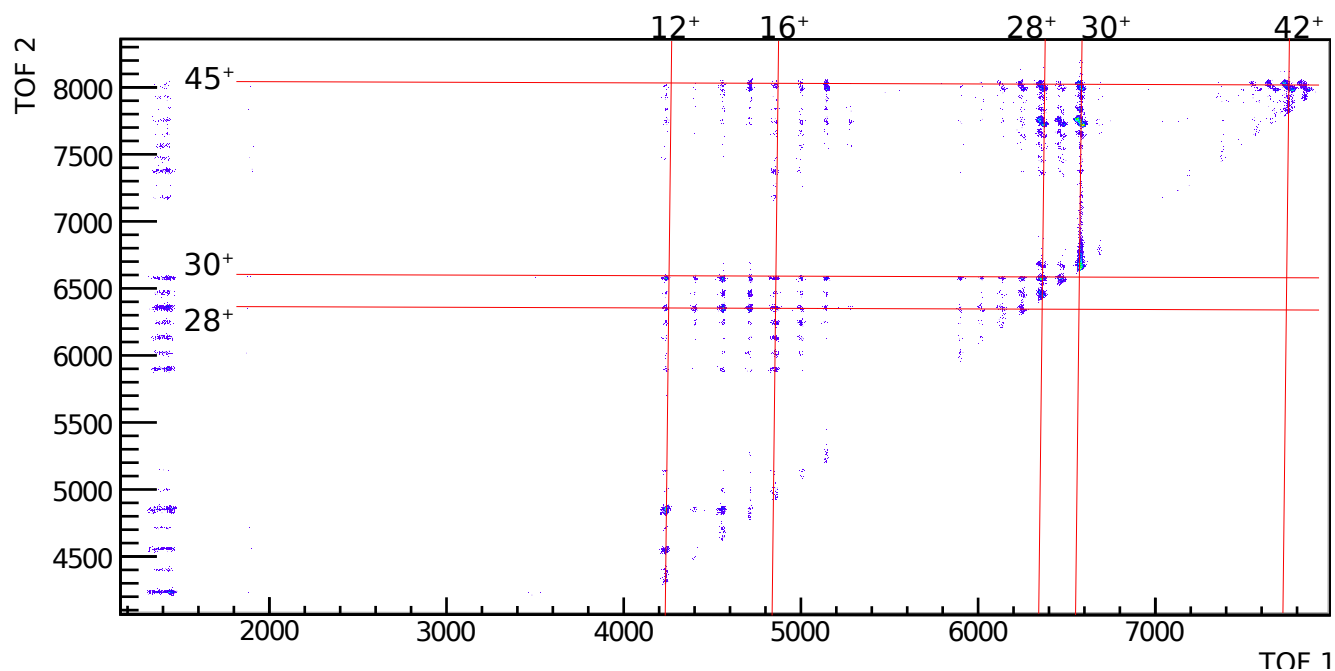


**Figure 6.3:** Coincidence map for the fragmentation of the  $\beta$ -alanine dication in two charged fragments after the interaction of neutral  $\beta$ -alanine with  $\text{Xe}^{25+}$  ions at the energy of 387.5 keV. The time-of-flight (in ns) of the heavier fragment (TOF2) is plotted as a function of the time-of-flight of the lighter one (TOF1).

M1	M2	Relative intensity	Assignment
30	42	100%	$\text{NH}_2\text{CH}_2^+ + \text{CH}_2\text{CO}^+$
30	31	80%	$\text{NH}_2\text{CH}_2^+ + \text{HOCH}_2^+$
42	45	58%	$\text{NH}_2\text{CCH}_2^+ + \text{COOH}^+$
28	42	47%	$\text{NHCH}^+ + \text{CH}_2\text{CO}^+$
30	45	45%	$\text{NH}_2\text{CH}_2^+ + \text{COOH}^+$
1	12	39%	
28	45	39%	$\text{COOH}^+ + \text{NHCH}^+$
12	16	35%	
28	29	35%	$\text{NHCH}^+ + \text{COH}^+$
30	32	34%	
28	30	31%	$\text{NH}_2\text{CH}_2^+ + \text{CO}^+$
43	45	30%	$\text{COOH}^+ + \text{NH}_2\text{CHCH}_2^+$
29	42	29%	$\text{NH}_2\text{CH}^+ + \text{CHCOH}^+ / \text{COH}^+ + \text{NHCCH}_3^+$
1	16	29%	
1	28	28%	
29	30	28%	
41	45	22%	$\text{NHCCH}_2^+ + \text{COOH}^+$
1	24	21%	
14	28	21%	$\text{CH}_2^+ + \text{NHCH}^+$

**Table 6.1:** Assignment of the correlation islands corresponding to the regions of interest in the coincidence map for  $\beta$ -alanine dication (see Fig. 2 in the main article). Relative intensities are given in percentage of the total intensity of the map.

Comparing the experimental data with our calculations (AIMD simulations and PES fragmentation) we can notice that the easiest way of breaking the molecule is through the  $\text{C}_\alpha\text{-C}_{\text{carboxylic}}$  bond cleavage ( $\text{NH}_2\text{CHCH}_3^+ + \text{COOH}^+$ ), not like the experiments show  $\text{C}_\alpha\text{-C}_\beta$  ( $\text{NH}_2\text{CH}_2^+ + \text{CH}_2\text{COOH}^+$ ). The most intense peak at  $m/q=30^+/42^+$  coming from  $\text{C}_\alpha\text{-C}_\beta$  bond breaking is seen as the strongest fragmentation channel. This is because the further fission of the molecule in this channel is less favorable than fission of the fragments coming from the  $\text{C}_\alpha\text{-C}_{\text{carboxylic}}$  bond breaking. Moreover, the elimination of the carbon monoxide followed by the migration of the OH group is observed with much lower barrier than the emission of the OH, leading to the peak at  $m/q=30^+/42^+$ . The loss of CO from  $\text{HOCH}_2\text{CO}^+$  followed by observation of a metastable  $m1^+$  is reported and assigned in the mass spectra to the second most important channel with intensity 80% (table 6.1). Additionally, two electron extraction does not affect to the  $\text{COOH}^+$  fragment and does not preferred further fragmentation of this ion. Observation the corresponding  $\text{COOH}^+$  fragment at  $m/q = 45^+$ , which is a major fragment in coincidence with many other small charge fragments, confirmed the high stability in double ionization of this molecular ion (table 6.1). As we show in the next section, our results indicate also that isomerization in the first femto seconds after ionization is also a very probable process and further fragmentation leading to stable dicationic moieties should be carefully investigated by experimentalists.

### 6.3 Fragmentation dynamics (with ADMP)

To better understanding the mechanisms and what is happening during the fragmentation of the excited ( $\beta$ -alanine) $^{2+}$ , we employ in this case a different type of analysis (in comparison with glycine) based on ab initio molecular dynamics. In particular, we have studied the fragmentation dynamics of doubly-charged  $\beta$ -alanine using the ADMP method. In our simulations we mimic the experimental conditions by extracting the two outermost electrons from the neutral conformers and introducing a certain amount of excitation energy ( $\approx 0.03\text{-}4.08$  eV) randomly distributed among the internal (vibrational) degrees of freedom of the molecule. In this way, we reproduce the sudden ionization and excitation produced in the collision of neutral gas phase  $\beta$ -alanine molecules with highly charged ions. Considering reasonable conditions for a statistical study we have chosen the twelve most stable neutral conformers of  $\beta$ -alanine (figure 6.1). For each conformer we increase the internal energy starting from 0.001 through 0.005, 0.010, 0.020, 0.030, 0.040, 0.050, 0.060, 0.070, 0.080, 0.090, 0.100, 0.110, 0.120, 0.130, 0.140, until

0.150 Hartrees. For each conformer and each value of internal energy we have performed 20 trajectories, i.e. a total of 4080 simulations. To simulate the internal energy we used a random velocity distribution over all atoms. Dynamics calculations were carried out using the B3LYP functional with a slightly reduced 6-31G++(d,p) basis set with respect to the optimization calculations.<sup>101</sup>

From all the 4080 simulations we can observe three different kinds of dynamics: Coulomb explosion (figure 6.4), isomerization (figure 6.5) and combined processes (figure 6.6).

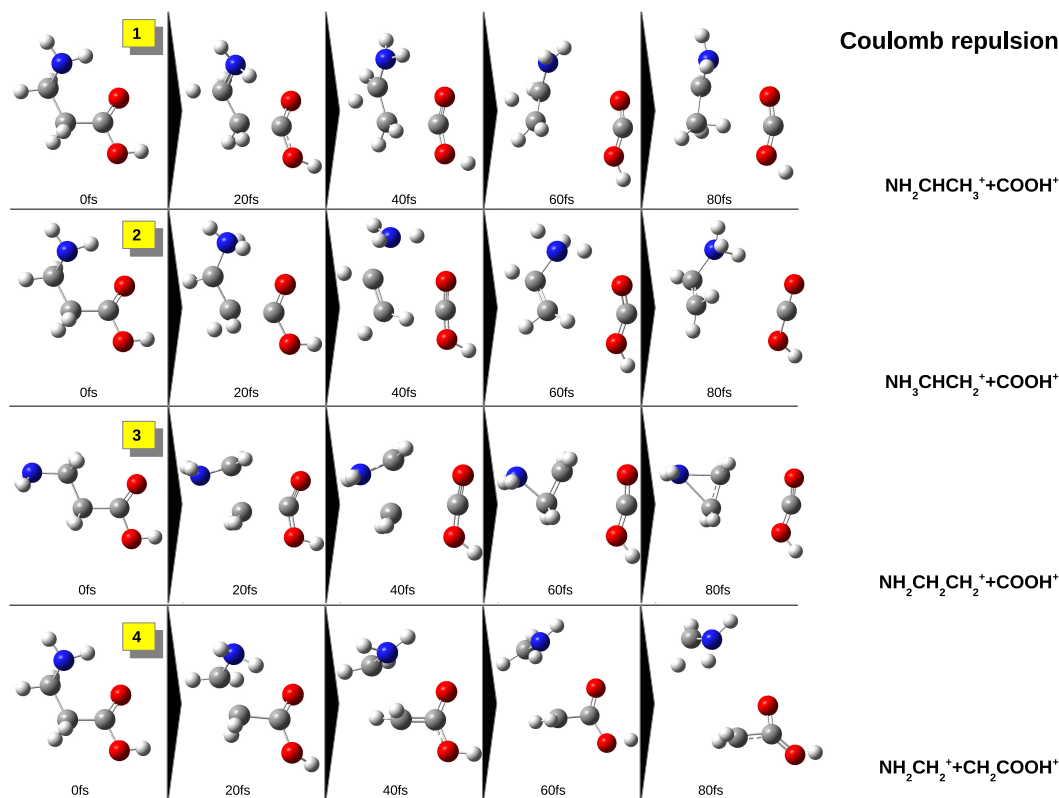


**Figure 6.4:** Snapshots of molecular dynamics simulations of a  $\beta$ -alanine dication giving a fission processes and leading to fragments with a)  $\text{C}_\alpha\text{-C}_{\text{carboxylic}}$  bond breaking: (1)  $\text{NH}_2\text{CHCH}_3^+/\text{COOH}^+$ , (2)  $\text{NH}_3\text{CHCH}_2^+/\text{COOH}^+$ , (3)  $\text{NH}_2\text{CH}_2\text{CH}_2^+/\text{COOH}^+$ ; b)  $\text{C}_\alpha\text{-C}_\beta$  bond breaking: (4)  $\text{NH}_2\text{CH}_2^+/\text{CH}_2\text{COOH}^+$ .

As we can observe in figure 6.4 there are four different Coulomb explosion processes I(1-3) and II(1):

**I.**  $\text{C}_\alpha\text{-C}_{\text{carboxylic}}$  bond cleavage leading to:

1.  $\text{NH}_2\text{CHCH}_3^+ + \text{COOH}^+$  (1)
2.  $\text{NH}_3\text{CHCH}_2^+ + \text{COOH}^+$  (2)
3.  $\text{NH}_2\text{CH}_2\text{CH}_2^+ + \text{COOH}^+$  (3)

**II.**  $\text{C}_\alpha\text{-C}_\beta$  bond cleavage leading to:

1.  $\text{NH}_2\text{CH}_2^+ + \text{CH}_2\text{COOH}^+$  (4)

In the dynamics (1) and (2) we can observe H migration to the terminal C atom or to the terminal N atom, respectively, stabilizing the produced cation. On the other hand dynamic (3) is an example of geometry reorganization to create the stable cyclic form of the  $\text{NH}_2\text{CH}_2\text{CH}_2^+$  cation. Simulation (4) does not follow any of these trends, it is just a direct bond breaking.

In figure 6.5 we present four different isomerization processes. They lead to four stable isomers of dication of  $\beta$ -alanine:

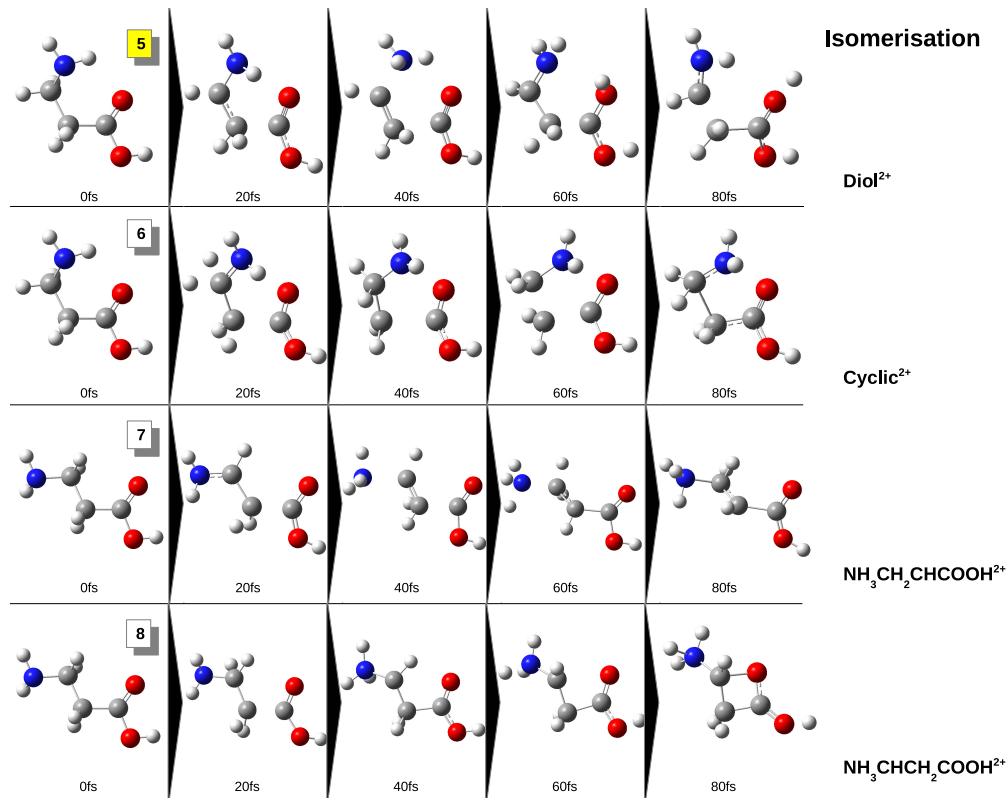


**Figure 6.5:** Snapshots of molecular dynamics simulations of a  $\beta$ -alanine dication leading to the isomerization by H-transfer in (5)  $\text{Diol}^{2+}$ , (6) 5-membered ring dication, (7) linear  $\text{NH}_3\text{CH}_2\text{CHCOOH}^{2+}$  and (8) 4-membered ring dication.

- The most common event of isomerization is dynamics number (5). Geminal diol dication formation after fast H migration is a favorable process similar like in the case of glycine. We also observe that in the first 40 fs H is migrating to the  $\text{NH}_2$  group (leading to  $\text{NH}_3$ ) and after, a further H transfer to the carboxyl group leads to the diol:



In our simulations we observe three further processes of isomerization:

- 5-member ring formation, dynamic (6); we can recognize here the stability effect produced through the intramolecular N–O bond formation;
- linear form of dication of  $\beta$ -alanine:  $\text{NH}_3\text{CH}_2\text{CHCOOH}^{2+}$ , dynamic (7); H transfer takes place as follows:

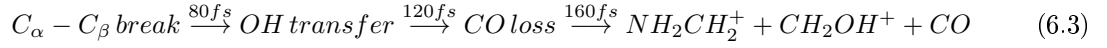


- 4-member ring formation is observed in dynamic (8) with a stabilizing effect of the charge with the bonds between C–C–O–C and the two terminal groups:  $\text{NH}_3$  and  $\text{OH}$ ;

For all these isomerization processes, we observe that if  $\beta$ -alanine $^{2+}$  becomes stable in the first 60 fs, it will not undergo fragmentation even after 400 fs of the simulation. The stable cyclic $^{2+}$  (5-membered ring) has not been reported for  $\beta$ -alanine yet, but a similar 5-membered ring intermediate (oxazolone) was reported by Harrison,<sup>134</sup> due to the fragmentation of a peptide and further elimination of water.

In figure 6.6 we can distinguish six different mechanisms of fragmentation:

- Coulomb explosion+isomerization+fragmentation:
  - $\text{NH}_2\text{CH}_2^+ + \text{CH}_2\text{OH}^+ + \text{CO}$  (9);  $C_\alpha$ – $C_\beta$  bond cleavage (c.a. 80 fs), then OH transfer ( $\sim 120$  fs) and finally loss of neutral CO ( $\sim 160$  fs); mechanism in eq. 6.3



- Coulomb explosion+fragmentation:

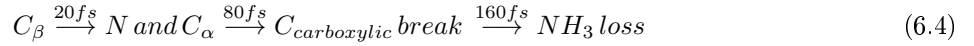
- $NH_2CCH_2^+ + COOH^+ + H_2$  (10);  $C_\alpha - C_{carboxylic}$  bond cleavage ( $\sim 50$  fs), then neutral  $H_2$  loss ( $\sim 80$  fs);
- $NH_2CH_2^+ + CH_2 + COOH^+$  (17);  $C_\alpha - C_{carboxylic}$  bond cleavage ( $\sim 60$  fs) and neutral  $CH_2$  loss ( $\sim 60$  fs);

- fragmentation+isomerization:

- $H_2 + HNCCH_2C(OH)_2^{2+}$  (11); loss of neutral hydrogen molecule ( $\sim 80$  fs) and  $H_N$  transfer to O ( $\sim 100$  fs);

- isomerization+Coulomb explosion+fragmentation:

- $NH_3 + CH_2CH^+ + COOH^+$  (12); H transfer ( $\sim 20$  fs), then  $C_\alpha - C_{carboxylic}$  bond cleavage ( $\sim 80$  fs) and neutral loss of  $NH_3$  ( $\sim 160$  fs);

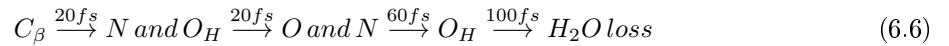


- isomerization+dehydration:

- $NH_2CHCH_2CO^{2+} + H_2O$  (13); H transfer and water loss;



- $NH_2CHCH_2CO^{2+} + H_2O$  (14); H transfer and water loss;



- $NH_2CHCH_2CO^{2+} + H_2O$  (15);



- isomerization+Coulomb explosion:

- $NH_3CHCH_3^{2+} + CO_2$  (16); H transfer ( $\sim 40$  fs), then  $C_\alpha - C_{carboxylic}$  bond cleavage ( $\sim 60$  fs)



## Combined processes

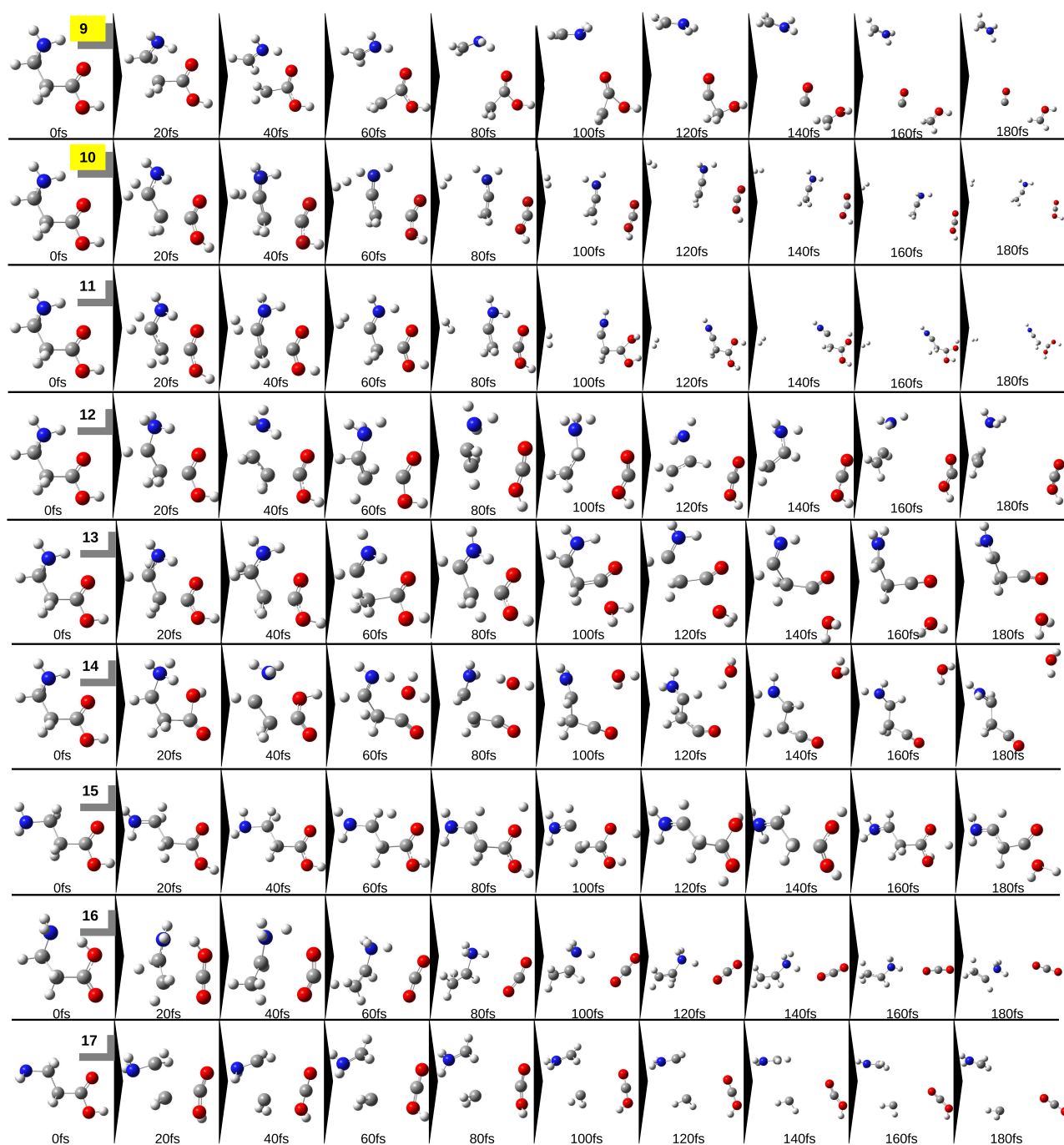


**Figure 6.6:** Snapshots of molecular dynamics simulations of a  $\beta$ -alanine dication giving a combined processes and leading to a) Coulomb explosion+isomerization+fragmentation: (9); b) Coulomb explosion+fragmentation: (10), (17); c) fragmentation+isomerization: (11); d) isomerization+Coulomb explosion+fragmentation: (12); e) isomerization+dehydration: (13), (14), (15); f) isomerization+Coulomb explosion: (16).

H transfer leading to water remove is observed in dynamics (13), (14) and (15) with different mechanisms as shown in figure 6.6. Two of them are indirect mechanisms (equations 6.9 and 6.10) one of them is a direct one (equation 6.11):



•



The mechanism 6.11 is much faster than 6.9 and 6.10; it occurs in the first 40 fs after ionization. Accordingly we observe on the PES a lower barrier of the H transfer following 6.11 (mechanism shown in the next section), it is therefore more probable than the other mechanisms.

The results of the statistical study performed over the 4080 trajectories are shown in figures 6.7, 6.8 and 6.9. Figure 6.7 shows that the fragmentation pattern depends a lot on the geometry of the conformers. This can be explained due to the fact that the electronic structure of a dication formed at the initial stage of the fragmentation determines the reaction path and thus the fragmentation products. Moreover, the structure of the neutral conformer leads us to a large variety of obtained products when increasing the internal energy. The general dependency of each isomer can be classified as a preferable way for fission and gather into four groups:

- $\text{NH}_2\text{CHCH}_3^+ + \text{COOH}^+(1)$ : isomers a1, a2, a6, and a11;
- $\text{NH}_2\text{CHCH}_3 + \text{COOH}^+(1)$  in competition with  $\text{NH}_2\text{CH}_2^+ + \text{CH}_2\text{OH}^+ + \text{CO}$  (9): isomers a3 and a12;
- $\text{NH}_2\text{CH}_2^+ + \text{CH}_2\text{COOH}^+(4)$ : isomers a7, a8, a9, a10;
- $\text{NH}_2\text{CH}_2^+ + \text{CH}_2\text{OH}^+ + \text{CO}$  (9) in competition with  $\text{NH}_2\text{CH}_2\text{CH}_2^+ + \text{COOH}^+(3)$ : isomer a5;

The isomer a4 is unclassified because of the wide variety of possible fragmentation pathways. Its geometry is slightly similar to a5, but very different from the other isomers. Indeed, conformer a5 also present a different fragmentation behavior than the others. The detailed description of each of the investigated isomers is as follows:

1. a1: the most populated fragmentation channel is  $\text{NH}_2\text{CHCH}_3^+ + \text{COOH}^+$  (1). For an excitation energy lower than 0.05 Hartree ( $E_{exc} < 0.05$  Hartree) we only observe this channel. When we increase the excitation energy we can observe nine different pathways. I. e. there is also a trend showing a highest contribution of different fragmentation pathways after increasing the internal energy of the molecule.
2. a2: the most populated fragmentation channel is  $\text{NH}_2\text{CHCH}_3^+ + \text{COOH}^+$  (1). The fragmentation of this conformer does not depend on  $E_{exc}$  in all investigated range  $\langle 0.001; 0.150 \rangle$ . Only a 5% of probability, just one trajectory for one value of  $E_{exc} = 0.07$  Hartree, correspond to the  $\text{NH}_2\text{CH}_2^+ + \text{CH}_2\text{OH}^+ + \text{CO}$  pathway. The other  $\text{C}_{\alpha}-\text{C}_{\beta}$  bond cleavage:  $\text{NH}_2\text{CH}_2^+ + \text{CH}_2\text{COOH}^+$  is observed with 5% and 10% of probability for 0.1 and 0.14 Hartree, respectively.
3. a3: competition between  $\text{NH}_2\text{CH}_2^+ + \text{CH}_2\text{OH}^+ + \text{CO}$  (9) and  $\text{NH}_2\text{CHCH}_3^+ + \text{COOH}^+$  (1) channels is observed. For  $E_{exc} < 0.06$  Hartree the dominant pathway is (9). For the higher excitation energies we observe about 40%/60% ratio (9)/(1) with a very small participation of the  $\text{NH}_2\text{CH}_2^+ + \text{CH}_2\text{COOH}^+(4)$  fragments.
4. a4: we observe competition between  $\text{diol}^{2+}$  (5),  $\text{NH}_2\text{CH}_2\text{CH}_2^+ + \text{COOH}^+$  (3) and  $\text{NH}_2\text{CHCH}_3^+ + \text{COOH}^+(1)$ . When we increase the excitation energy, we can observe a decreasing of the two the most probable fragmentation channels: (5) and (3). From  $E_{exc} = 0.03$  Hartree channel (1) increases systematically its participation with the energy. The geometry of this conformer after ionization allows us to obtain a very high variety of other possible fragmentation pathways; the most significant are:

- $\text{NH}_3\text{CHCH}_2^+ + \text{COOH}^+$  appearing since  $E_{exc} \geq 0.05$  Hartree
- $\text{NH}_2\text{CCH}_2^+ + \text{H}_2 + \text{COOH}^+$  appearing for  $E_{exc} = \{0.05\} \wedge \geq 0.1$  Hartree

Three observed channels that also contribute to the fragmentation of a4 are:  $\text{NH}_2\text{CH}_2^+ + \text{CH}_2\text{OH}^+ + \text{CO}$  (9),  $\text{NH}_2\text{CH}_2^+ + \text{CH}_2\text{COOH}^+$  (4) and  $\text{NH}_3\text{CH}_2\text{CHCOOH}^{2+}$  (7) and do not depend on the excitation energy. Isomer

a4 also posses the geometry characteristic to occur the H transfer leading to diol<sup>2+</sup> or NH<sub>3</sub>CH<sub>2</sub>CHCOOH<sup>2+</sup> and therefore these paths are also seen.

5. a5: competition between three channels is observed: NH<sub>2</sub>CH<sub>2</sub>CH<sub>2</sub><sup>+</sup>+COOH<sup>+</sup>(3), NH<sub>2</sub>CH<sub>2</sub><sup>+</sup>+CH<sub>2</sub>OH<sup>+</sup>+CO(9) and NH<sub>2</sub>CH<sub>2</sub><sup>+</sup>+CH<sub>2</sub>COOH<sup>+</sup>(4). When increasing the excitation energy, we observe the decreasing of channel (3) and increasing of (9) and (4), where the latter is significantly less important. Fragmentation of this conformer gives us also NH<sub>3</sub>+CHCH<sub>2</sub><sup>+</sup>+COOH<sup>+</sup> at  $E_{exc} = 0.14$  Hartree, which is observed only once over the 4080 simulations.(3-aminopropanoic acid)
6. a6: very similar to isomer a2, there is only one principal fragmentation channel: NH<sub>2</sub>CHCH<sub>3</sub><sup>+</sup>+COOH<sup>+</sup>(1). The minor fragments: NH<sub>2</sub>CH<sub>2</sub><sup>+</sup>+CH<sub>2</sub>COOH<sup>+</sup> and NH<sub>3</sub>CHCH<sub>2</sub><sup>+</sup>+COOH<sup>+</sup> appear at  $E_{exc} \geq 0.09$  Hartree .
7. a7: the most populated fragmentation channel is NH<sub>2</sub>CH<sub>2</sub><sup>+</sup>+CH<sub>2</sub>COOH<sup>+</sup>(4). The geometry of a7 after ionization allows us to remove neutral water molecule. This isomer gives the highest contribution to the channel: NH<sub>2</sub>CHCH<sub>2</sub>CO<sup>2+</sup>+H<sub>2</sub>O.
8. a8: competition between NH<sub>2</sub>CH<sub>2</sub><sup>+</sup>+CH<sub>2</sub>COOH<sup>+</sup>(4) and NH<sub>2</sub>CH<sub>2</sub>CH<sub>2</sub><sup>+</sup>+COOH<sup>+</sup>(3) is observed. The channel (4) dominates over all the excitation energy range covered, being less important for higher  $E_{exc}$ . Starting from  $E_{exc} \geq 0.02$  Hartree we can observe an increment of channel (3). Moreover we can see almost the 10% of NH<sub>2</sub>CH<sub>2</sub><sup>+</sup>+CH<sub>2</sub>OH<sup>+</sup>+CO(9) and it does not depend on the energy, appearing for  $E_{exc} = \{0.01, 0.04\} \wedge \geq 0.06$  Hartree.
9. a9: the most populated fragmentation channel is NH<sub>2</sub>CH<sub>2</sub><sup>+</sup>+CH<sub>2</sub>COOH<sup>+</sup>(4). From  $E_{exc} \geq 0.06$  Hartree we can observe an increasing contribution of NH<sub>2</sub>CH<sub>2</sub>CH<sub>2</sub><sup>+</sup>+COOH<sup>+</sup>(3). Similar to isomer a8 we can also see almost an equal presence of NH<sub>2</sub>CH<sub>2</sub><sup>+</sup>+CH<sub>2</sub>OH<sup>+</sup>+CO(9), that neither depends on the excitation energy and appear for  $E_{exc} = \{0.05, 0.06\} \wedge \geq 0.11$  Hartree. An insignificant presence of NH<sub>2</sub>CCH<sub>2</sub><sup>+</sup>+H<sub>2</sub>+COOH<sup>+</sup>, NH<sub>3</sub>CHCH<sub>2</sub><sup>+</sup>+COOH<sup>+</sup> and diol<sup>2+</sup> for  $E_{exc} \geq 0.12$  Hartree is also appreciated.
10. a10: the most populated fragmentation channel is NH<sub>2</sub>CH<sub>2</sub><sup>+</sup>+CH<sub>2</sub>COOH<sup>+</sup> with two “oscillating” pathways with the energy: NH<sub>2</sub>CH<sub>2</sub><sup>+</sup>+CH<sub>2</sub>OH<sup>+</sup>+CO(9) and NH<sub>2</sub>CHCH<sub>3</sub><sup>+</sup>+COOH<sup>+</sup>(1) appearing since  $E_{exc} = 0.03 \wedge E_{exc} = 0.5$  Hartree, respectively.
11. a11: the most populated fragmentation channel is NH<sub>2</sub>CHCH<sub>3</sub><sup>+</sup>+COOH<sup>+</sup>(1). Indeed, for  $E_{exc} \leq 0.06$  Hartree only (1) is observed. Increasing the excitation energy allows a higher geometry distortion leading to six other pathways, where two of them are standing out over the rest: NH<sub>3</sub>CHCH<sub>2</sub><sup>+</sup>+COOH<sup>+</sup>(2) and NH<sub>2</sub>CCH<sub>2</sub><sup>+</sup>+H<sub>2</sub>+COOH<sup>+</sup>(10).
12. a12: competition between NH<sub>2</sub>CHCH<sub>3</sub><sup>+</sup>+COOH<sup>+</sup>(1) and NH<sub>2</sub>CH<sub>2</sub><sup>+</sup>+CH<sub>2</sub>OH<sup>+</sup>+CO(9) is observed. Increasing the excitation energy the probability to obtain (9) increases and automatically decreases the possibility to get (1). The third minor channel observed: NH<sub>2</sub>CH<sub>2</sub><sup>+</sup>+CH<sub>2</sub>COOH<sup>+</sup>(4) also decreases when the excitation energy arises.

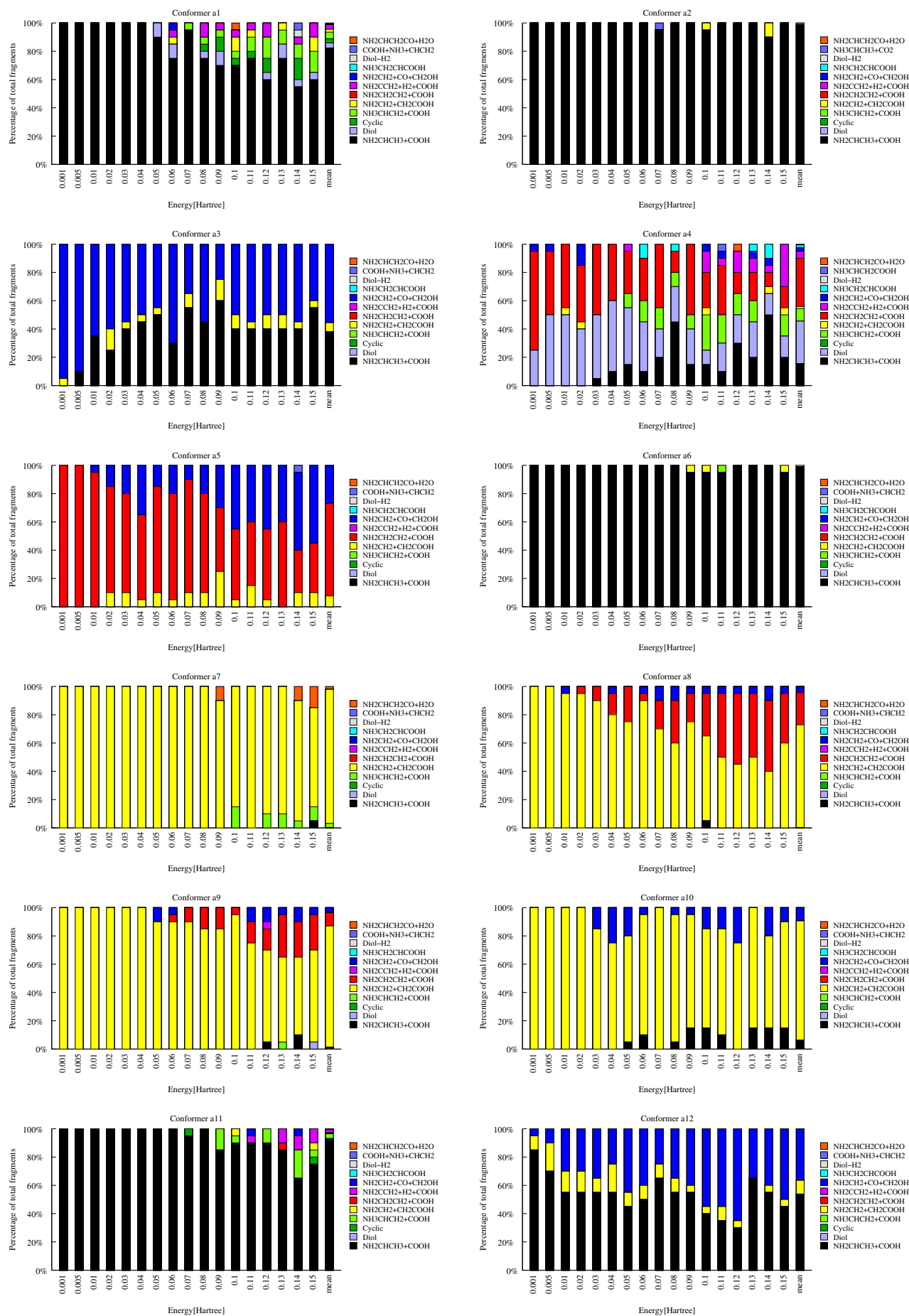


**Figure 6.7:** Ab initio molecular dynamics statistics for each neutral conformer of  $\beta$ -alanine with relative energy  $\approx 2$  kcal/mol<sup>-1</sup>.

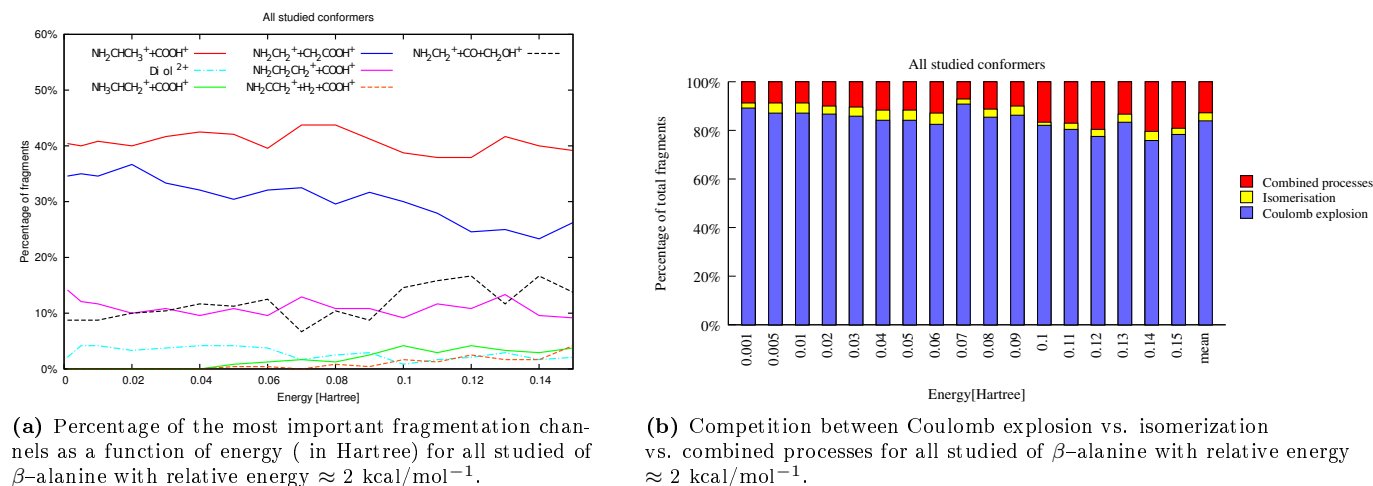


**Figure 6.8:** Ab initio molecular dynamics statistic for all neutral conformers of  $\beta$ -alanine; percentage of the most important fragmentation channels as a function of energy (in Hartree).

Taking into account all data from the 4080 molecular dynamic simulations we prepared the general statistics shown in figure 6.8. In the left part of the figure (6.8a) we can observe all the fragmentation channels for whose there are linear dependencies on the energy. In the right part of the figure (6.8b) we can see competition between different processes occurring during molecular dynamics simulations: Coulomb explosion vs. isomerization vs. combined processes. We first analyzed the left part, where we can observe that two channels dominates over the rest:  $\text{NH}_2\text{CHCH}_3^+ + \text{COOH}^+$  and  $\text{NH}_2\text{CH}_2^+ + \text{CH}_2\text{COOH}^+$  with around 40% and 30% of probability to occur. Moreover, there are three different trends:

- the percentage of probability to occur  $\text{NH}_2\text{CHCH}_3^+ + \text{COOH}^+$  and  $\text{NH}_2\text{CH}_2\text{CH}_2^+ + \text{COOH}^+$  is almost constant and does not depend on energy;
- the percentage of probability to occur  $\text{NH}_2\text{CH}_2^+ + \text{CH}_2\text{COOH}^+$  and  $\text{diol}^{2+}$  decreases with the excitation energy;
- the percentage of probability to occur  $\text{NH}_2\text{CH}_2^+ + \text{CH}_2\text{OH}^+ + \text{CO}$  (9),  $\text{NH}_3\text{CHCH}_2^+ + \text{COOH}^+$  and  $\text{NH}_2\text{CCH}_2^+ + \text{H}_2 + \text{COOH}^+$  increases when the excitation energy increases. This can be explained due the fact that process (9) is a further stage of  $\text{NH}_2\text{CH}_2^+ + \text{CH}_2\text{COOH}^+$  with the OH migration. The two latter processes appear only when the excitation energy is big enough ( $E_{exc} \geq 0.04$  Hartree).

In figure 6.8b we can observe that Coulomb explosion dominates over isomerization and combined processes but when increasing the excitation energy this process becomes weaker and we can observe more complicated combined processes. This is what we can expect because of the fact of easier  $\text{C}_\alpha\text{-C}_{\text{carboxylic}}$  or  $\text{C}_\alpha\text{-C}_\beta$  bond cleavages than other more complicated processes, require higher geometry distortions and therefore, higher excitation energy.

Another type of analysis that we did corresponds to detailed statistics of each of the three processes: Coulomb explosion (figure 6.9a), isomerization (figure 6.9b) and combined processes (figure 6.9c). First of all, we focus in figure 6.9a, where we can observe that Coulomb explosion leading to  $\text{C}_\alpha\text{-C}_{\text{carboxylic}}$  bond cleavage dominates over  $\text{C}_\alpha\text{-C}_\beta$ . This is over all the excitation energies, where that rule is even stronger for the highest  $E_{exc}$  because of the competition with combined processes (mainly (9)), which finally makes the  $\text{C}_\alpha\text{-C}_\beta$  fragmentation less competitive than the  $\text{C}_\alpha\text{-C}_{\text{carboxylic}}$ .

Figure 6.9b shows the results of the isomerization leading to diol, 4-membered ring, 5-membered ring and linear  $\text{NH}_3\text{CH}_2\text{CHCOOH}$  forms of dication of  $\beta$ -alanine as a function of excitation energy. All these processes are populated less than 5% of the total intensity. Proton transfer is more favorable on the oxygen atom of the carboxyl group leading to  $\text{diol}^{2+}$ . This behavior is mainly observed for lower values of excitation energy. For higher excitation energies,  $E_{exc} \geq 0.06$  Hartree, we can see competitive processes, where the one does not need H transfer leading to stable cyclic form of  $\beta$ -alanine (structures  $\text{a1}^{2+}$  or  $\text{a2}^{2+}$  in figure 6.10). The other competitive action

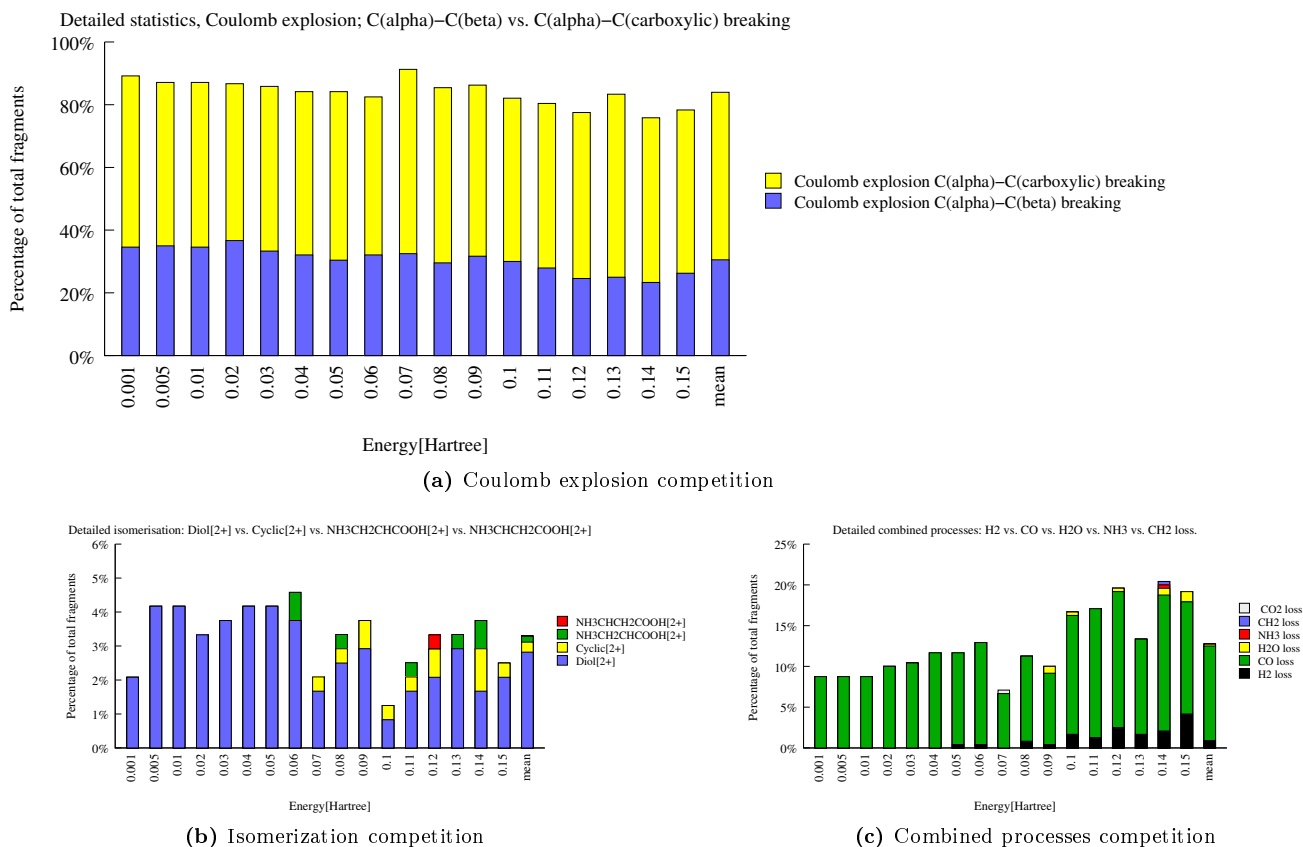


**Figure 6.9:** Ab initio molecular dynamics statistic for all neutral conformers of  $\beta$ -alanine; percentage of the most important fragmentation channels as a function of energy ( in Hartree) for all studied of  $\beta$ -alanine with relative energy  $\approx 2$  kcal/mol<sup>-1</sup>.

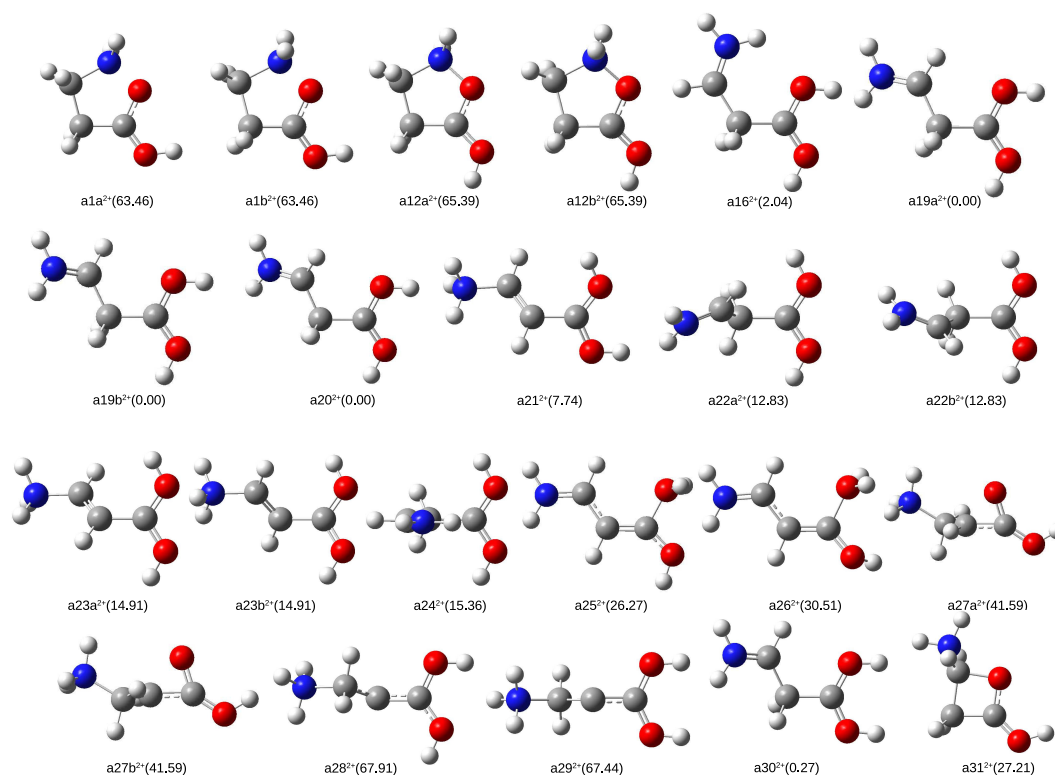
is the formation of linear  $\text{NH}_3\text{CH}_2\text{CHCOOH}^{2+}$ , which demands H transfer as well as the creation of diol<sup>2+</sup> and appears randomly when  $E_{exc}$  achieves 0.06 Hartree. The dication of 4-membered ring structure was obtained once, for  $E_{exc} = 0.12$  Hartree.

Figure 6.9c shows the competition between combined fissions. The most important and dominant channel is  $\text{NH}_2\text{CH}_2^+ + \text{CH}_2\text{OH}^+ + \text{CO}$  leading to emission of neutral carbon monoxide. The other slightly observed channels are  $\text{NH}_2\text{CCH}_2^+ + \text{H}_2 + \text{COOH}^+$  and  $\text{NH}_2\text{CHCH}_2\text{CO}^{2+} + \text{H}_2\text{O}$  appearing for  $E_{exc} \geq 0.05 \wedge E_{exc} \geq 0.09$  Hartree and leading to emissions of neutral hydrogen molecule and water, respectively. Fragmentation of neutral  $\text{CO}_2$ ,  $\text{NH}_3$  and  $\text{CH}_2$  are very rare processes appearing with  $1/4080$  probability each.

## 6.4 Conformational study– dications

The isomerization mechanisms obtained in the molecular dynamic simulations lead to four different stable conformers of  $\beta$ -alanine: diol (a20<sup>2+</sup>), 4-membered ring (a31<sup>2+</sup>), 5-membered ring (a1a<sup>2+</sup> or a1b<sup>2+</sup> which are enantiomers) and linear  $\text{NH}_3\text{CH}_2\text{CHCOOH}$  (a27a<sup>2+</sup> or a27b<sup>2+</sup> which are also enantiomers). The optimized structures for this isomers together with the others species found during the exploration of the potential energy surface (PES) are shown in figure 6.10.

Linear conformers  $\text{NH}_2\text{CH}_2\text{CH}_2\text{COOH}^{2+}$  and  $\text{NH}_3\text{CHCH}_2\text{COOH}^{2+}$  are unstable and starting optimization from these geometries leads to other geometries. One of the hydrogens connected to  $\text{C}_\alpha$  (or even two H in the cases of a29<sup>2+</sup> and a30<sup>2+</sup>) prefer to transfer to  $\text{C}_\beta$  (a27<sup>2+</sup>) or to O (a23<sup>2+</sup>) leading to the enol form together with a  $\text{NH}_3$  group. Two hydrogens in the position  $\text{C}_\alpha$  are observed only for the cyclic or enol forms. The stability depends mainly of the number of hydrogens located in the amino and carboxylic groups and the schematic pattern can be shown with increasing relative energy as follows:  $\text{NH}_2 \dots \text{C}(\text{OH})_2^{2+} \rightarrow \text{NH}_3 \dots \text{C}(\text{OH})_2^{2+} \rightarrow \text{NH}_3 \dots \text{COH}^{2+}$  (cyclic form)  $\rightarrow \text{NH}_2 \dots \text{C}(\text{OH})_2(\text{OH})^{2+} \rightarrow \text{NH}_3 \dots \text{COOH}^{2+} \rightarrow \text{NH}_2 \dots \text{COOH}^{2+}$  (cyclic form). We can observe that the 5-membered ring structures show the lowest stability, similar to the metastable a28<sup>2+</sup> or linear a29<sup>2+</sup> and a30<sup>2+</sup> and



**Figure 6.10:** Optimizing geometries for the dication isomers of  $\beta$ -Alanine at the B3LYP/6-311++G(d,p) level of theory. Relative energies ( $\Delta E$ ) in kcal mol<sup>-1</sup> with respect to most stable isomer (a20<sup>2+</sup>).

these compounds are the only canonical forms of dication of  $\beta$ -alanine. We found four dicationic forms with O – N bonds of  $\beta$ -alanine which has not been found for cationic conformers of bigger amino acids like  $\gamma$ -aminobutyric acid (GABA).<sup>121</sup> The 4-membered dicationic structure (a31<sup>2+</sup>) is more stable  $\approx 14$  kcal/mol<sup>-1</sup> than the corresponding linear form a27<sup>2+</sup>. The two isomers a29<sup>2+</sup> and a30<sup>2+</sup> are linear and possess two protonated stabilizing groups NH<sub>3</sub>...C(OH)<sub>2</sub><sup>2+</sup>, but the lack of hydrogens in C <sub>$\alpha$</sub>  unstabilizes these structures.

We explored the PES (figure 6.11) and connected all the dicationic isomers that we have found. For completeness we included other minima on the PES that did not appear in the molecular dynamic simulations but they play a role of links. We show these structures in comparison and with the observed in the dynamics with their relative energies in the figure. We can see in figure 6.11 four different energy levels:

- diols<sup>2+</sup>  $\approx 19.5$  eV
- 4-member ring<sup>2+</sup>  $\approx 21$  eV
- NH<sub>3</sub>CH<sub>3</sub>CHCOOH<sup>2+</sup>  $\approx 21.5$  eV
- 5-member ring<sup>2+</sup>  $\approx 22.5$  eV

As we can observe the relative energy of diols (with respect to the most stable neutral isomer of  $\beta$ -alanine) is  $\sim 2$  eV lower than for the other isomers. This can explain why the diols are the favorable isomerization products of the molecular dynamic simulations. After the results obtained in the MD simulations, we were surprised to observe the 5-membered ring structures, since obtaining this form of  $\beta$ -alanine from the diol form requires a large amount of energy (ts5<sup>2+</sup> = 25.40 eV). The only explanation that this process is the second favorable isomerization event is due to the fact that it does not require any H transfer, but just a small geometry reorganization is enough; even if this cyclic form does not belong to the most stable region of PES.

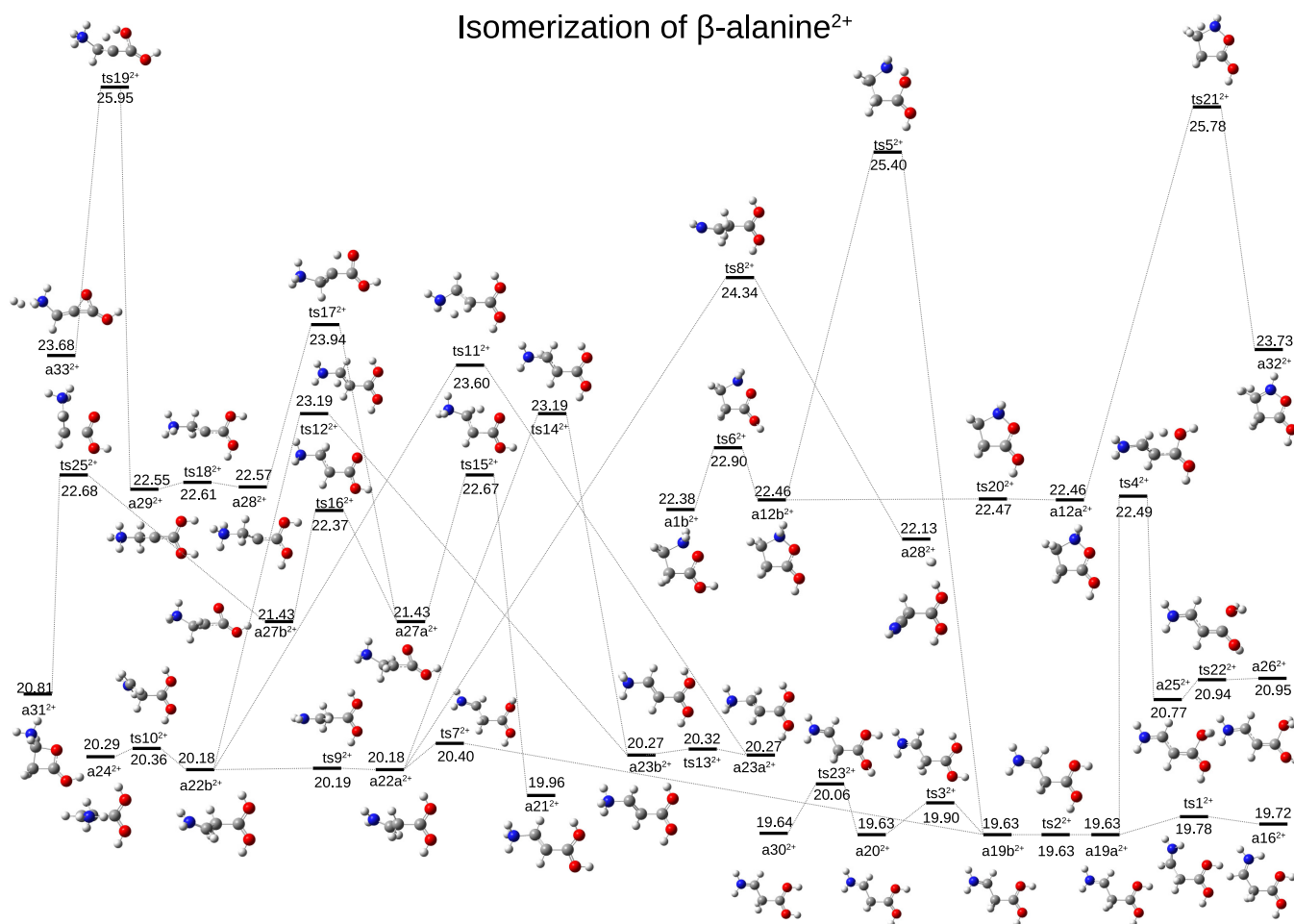


**Figure 6.11:** Stationary points on the PES corresponding to the minima and transitions states of  $\beta$ -Alanine dications. Relative energies ( $\Delta E$ ) in eV with respect to most stable neutral  $\beta$ -alanine (a1).

## 6.5 Unimolecular decomposition

The fragmentation pathways of singly-charged  $\beta$ -alanine have been already investigated.<sup>132;135;136</sup> We present here an exploration of the potential energy surface (PES) for the doubly-charged  $\beta$ -alanine. The exploration of the PES has been performed starting from the most probable processes as observed in the statistics of the molecular dynamics: processes (1), (2), (3), (4), (5), (9), and (10). The results are shown in figures 6.12, 6.13, 6.14 and 6.15. Firstly, we calculate all of the pathways corresponding to products obtained in the molecular dynamic simulations. Peaks corresponding to the charged fragments are also observed in the coincidence map obtained in the experiments (figure 6.3) and a summary is presented in the table 6.1.

Since the experimentalists observe a peak at  $m/q=30^+/31^+$  amu we assigned it to the process (9):  $\text{NH}_2\text{CH}_2^+ + \text{CH}_2\text{OH}^+ + \text{CO}$  reaction observed in the dynamics. We propose in figure 6.12 (showing the fragmentation after processes (4) and (9)) the fragmentation path leading through hydroxyl group migration and Coulomb explosion to  $\text{NH}_2\text{CH}_2^+ + \text{HOCH}_2\text{CO}^+$ . We revealed that in the loss of the neutral carboxyl group, presumably the metastable  $\text{HOCH}_2\text{CO}^+$  structure is involved in the formation of  $\text{NH}_2\text{CH}_2^+$  and  $\text{HOCH}_2^+$  ions. The fragmentation process, which is preceded by the migration of the OH group, has to occur at the femtosecond timescale and is the only possibility to explain the coincidence peak at  $m/q=30^+/31^+$  amu. The driving force for this fragmentation process seems to be the stability of the  $\text{NH}_2\text{CH}_2^+ + \text{HOCH}_2^+$  ions (18.25 eV), where the relative energy is 8 eV lower than the entrance channel and much lower than the channel appearing in competition  $\text{NH}_2\text{CH}_2^+ + \text{HOCH}_2 + \text{CO}^+$  (24.72 eV). The latter is exactly the same as the previous one but with different charge distribution. Additionally, we calculated the pathways at  $28^+/31^+$  for  $\text{CO}^+ + \text{HOCH}_2^+$  coming from doubly charged  $\text{HOCH}_2\text{CO}^{2+}$ , which

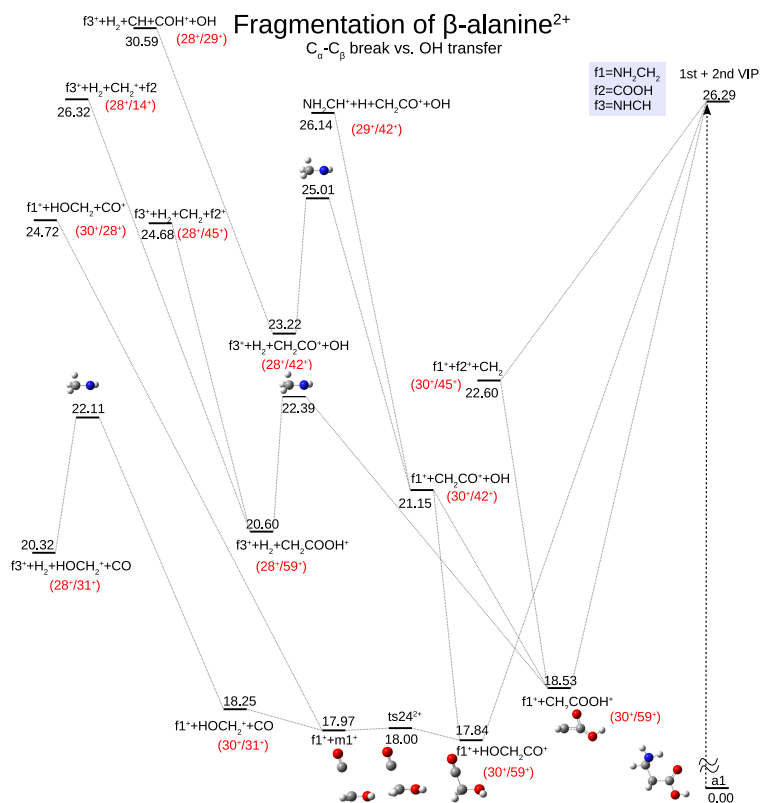


**Figure 6.12:** Fragmentations of dication of  $\beta$ -alanine: Coulomb C<sub>α</sub>-C<sub>β</sub> bond cleavage in competition with combined process NH<sub>2</sub>CH<sub>2</sub><sup>+</sup>+CH<sub>2</sub>OH<sup>+</sup>+CO (9). Relative energies ( $\Delta E$ ) in eV with respect to most stable neutral  $\beta$ -alanine (a1).

is very high in energy (29.04 eV, not presented in figure 6.12). The same mass/charge ratio (28<sup>+</sup>/31<sup>+</sup>) can be also obtained for different molecules: (NHCH<sup>+</sup>)/(HOCH<sub>2</sub><sup>+</sup>) just after removing the hydrogen molecule from NH<sub>2</sub>CH<sub>2</sub><sup>+</sup>, which is not observed in the experiment, despite its low energy barrier (22.11 eV). This seems to be an opposite trend to fragmentation of glycine (see figure 5.12) and the others channels like NH<sub>2</sub>CH<sub>2</sub><sup>+</sup>+CH<sub>2</sub>COOH<sup>+</sup> (30<sup>+</sup>/59<sup>+</sup>) → NHCH<sup>+</sup>+CH<sub>2</sub>COOH<sup>+</sup>+H<sub>2</sub> (28<sup>+</sup>/59<sup>+</sup>) or NH<sub>2</sub>CH<sub>2</sub><sup>+</sup>+CH<sub>2</sub>CO<sup>+</sup> (30<sup>+</sup>/42<sup>+</sup>) → NHCH<sup>+</sup>+CH<sub>2</sub>CO<sup>+</sup>+H<sub>2</sub> (28<sup>+</sup>/42<sup>+</sup>) which are analogous and correspond to the removing the hydrogen molecule (figure 5.10). Further fragmentation NHCH<sup>+</sup>/CH<sub>2</sub>CO<sup>+</sup> (28<sup>+</sup>/42<sup>+</sup>) leads to NHCH<sup>+</sup>/COH<sup>+</sup> with emission of neutral CH (30.59 eV).

The absence of the signal at 59<sup>+</sup> in coincidence with any other signals in the experiment and the relatively low energies calculated for that charged fragment (HOCH<sub>2</sub>CO<sup>+</sup> or CH<sub>2</sub>COOH<sup>+</sup>) allow us to draw the conclusion that the fragment at 59<sup>+</sup> have to undergo further fragmentation processes [signals at (30<sup>+</sup>/42<sup>+</sup>), (30<sup>+</sup>/45<sup>+</sup>), (28<sup>+</sup>/45<sup>+</sup>) and (28<sup>+</sup>/14<sup>+</sup>)]. The observation of these signals indicates that the molecule has enough energy to break C<sub>α</sub>-C<sub>carboxylic</sub> bond leading to CH<sub>2</sub> and COOH<sup>+</sup> or CH<sub>2</sub><sup>+</sup> and COOH, where the latter is not presented in figure because is very high in energy. Finally, the peaks with intensities around 21 % at 14<sup>+</sup>/28<sup>+</sup> are assigned to CH<sub>2</sub><sup>+</sup> and NHCH<sup>+</sup> ions (table 6.1).

In figure 6.13 we present the channels coming after C<sub>α</sub>-C<sub>carboxylic</sub> bond cleavage. We first focus on the minimum at 17.32 eV (the right part of the figure). This is the strongest observed channel in the dynamic calculations. We can see now that it is not a surprising information because energetically it is the lowest pathway ( $\approx$  1.2 eV lower than C<sub>α</sub>-C<sub>β</sub> break and about 0.5 eV lower than combined process NH<sub>2</sub>CH<sub>2</sub><sup>+</sup>+HOCH<sub>2</sub>CO<sup>+</sup>). Starting from COOH<sup>+</sup>+NH<sub>2</sub>CHCH<sub>3</sub><sup>+</sup> on the PES we can follow four different fragmentation channels:

1. removing H<sub>2</sub> leading to:

(a) COOH<sup>+</sup>+NH<sub>2</sub>CCH<sub>2</sub><sup>+</sup>+H<sub>2</sub> (19.43 eV) with ts25<sup>2+</sup> (20.62 eV).

From this point the lowest possible fragmentation pathways correspond to the loss of a neutral hydrogen atom:

i. COOH<sup>+</sup>+NHCCH<sub>2</sub><sup>+</sup>+H<sub>2</sub>+H (23.06 eV);

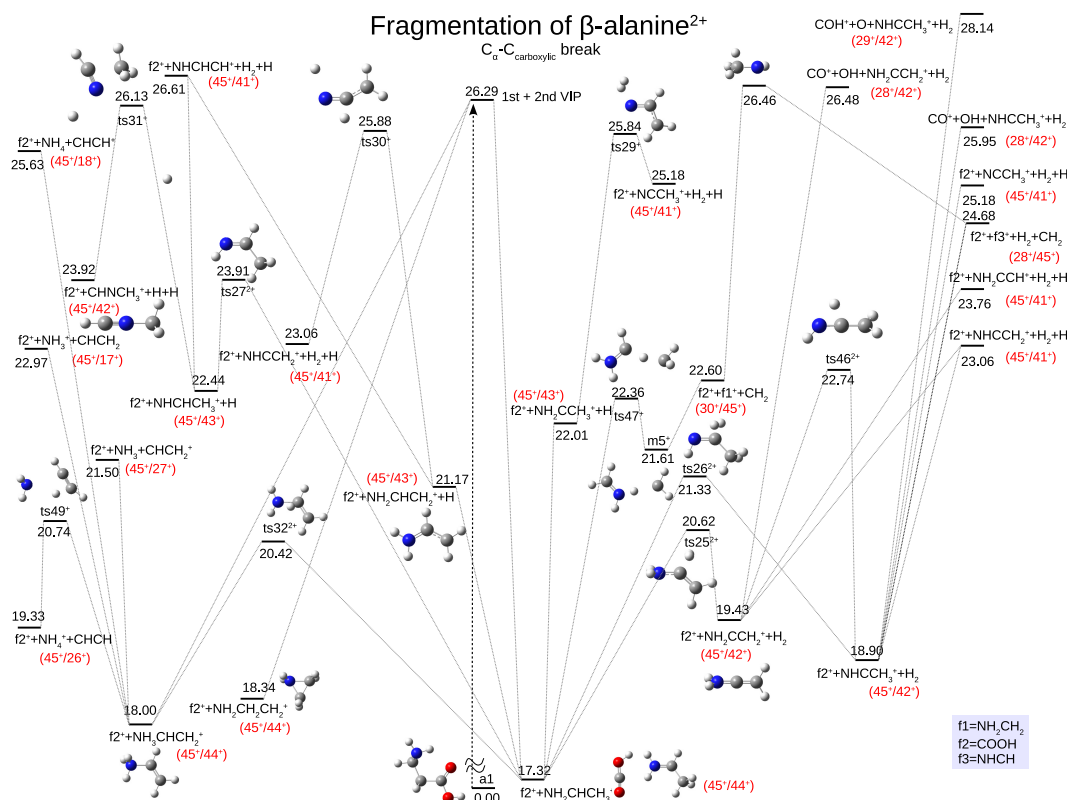


**Figure 6.13:** Fragmentations of dication of  $\beta$ -alanine: Coulomb explosion additional channels. Relative energies ( $\Delta E$ ) in eV with respect to most stable neutral  $\beta$ -alanine (a1).

- ii.  $\text{COOH}^+ + \text{NH}_2\text{CCH}^+ + \text{H}_2 + \text{H}$  (23.76 eV);  
or to breaking the  $\text{COOH}^+$  leading to emission of neutral OH:
- iii.  $\text{CO}^+ + \text{OH}^+ + \text{NH}_2\text{CCH}_2^+ + \text{H}_2$  (26.48 eV).

(b)  $\text{COOH}^+ + \text{NHCCH}_3^+ + \text{H}_2$  (18.90 eV) with  $\text{ts}26^{2+}$  (21.33 eV).

Further fragmentation leads to five different channels on the PES:

- i.  $\text{COOH}^+ + \text{NHCCH}_2^+ + \text{H}_2 + \text{H}$  (23.06 eV);
- ii.  $\text{COOH}^+ + \text{NHCH}^+ + \text{H}_2 + \text{CH}_2$  (24.68 eV);
- iii.  $\text{COOH}^+ + \text{NCCH}_3^+ + \text{H}_2 + \text{H}$  (25.18 eV);
- iv.  $\text{CO}^+ + \text{OH} + \text{NHCCH}_3^+ + \text{H}_2$  (25.95 eV);
- v.  $\text{COH}^+ + \text{O} + \text{NHCCH}_3^+ + \text{H}_2$  (28.14 eV);

Channel 1(a) and 1(b) can isomerize with slightly low barrier ( $\text{ts}46^{2+}$  22.74 eV). Removing hydrogens (1(a)i) or 1(a)ii) leading to one of the isomers with  $m/q=41^+$  is about 3 eV more favorable process than breaking of  $\text{COOH}^+$ . The similar trend is observed starting from channel (b), where we can observe additionally two different pathways. One corresponds to the removal of neutral  $\text{CH}_2$  from  $\text{NHCCH}_3^+$  and the second to the removal of neutral oxygen leading to  $\text{COH}^+$  from  $\text{COOH}^+$  fragment. The latter needs much more energy to occur ( $\approx 3.5$  eV). The first one can be also obtained through weakly bounded species (see point 3).

2. removing H leading to:

(a)  $\text{COOH}^+ + \text{NH}_2\text{CHCH}_2^+ + \text{H}$  (21.17 eV);

This reaction pathway leads to the same isomer as previously observed with  $m/q=41^+$  amu:

- i.  $\text{COOH}^+ + \text{NHCCH}_2^+ + \text{H} + \text{H}_2$  (23.06 eV);  
or alternatively to a very unstable isomer with  $m/q=41^+$  amu, which is about 0.3 eV above the  $1^{st} + 2^{nd}$  vertical ionization potential:

- ii.  $\text{COOH}^+ + \text{NHCHCH}^+ + \text{H} + \text{H}_2$  (26.61 eV);
- (b)  $\text{COOH}^+ + \text{NH}_2\text{CCH}_3^+ + \text{H}$  (22.01 eV), from which the reaction barrier through  $\text{ts29}^{2+}$  (25.84 eV) leads to:
  - i.  $\text{COOH}^+ + \text{NHCCH}_3^+ + \text{H}_2 + \text{H}$  (25.28 eV);
- (c)  $\text{COOH}^+ + \text{NHCHCH}_3^+ + \text{H}$  (22.44 eV); This reaction pathway leads to the same isomer as the previous (2(a)ii):
  - i.  $\text{COOH}^+ + \text{NHCHCH}^+ + \text{H} + \text{H}_2$  (26.61 eV);  
and to new isomer with  $m/q=42^+$  amu;
  - ii.  $\text{COOH}^+ + \text{CHNCH}_3^+ + \text{H} + \text{H}$  (23.92 eV) through  $\text{ts31}^+$  (26.13 eV);

3. removing  $\text{CH}_2$  leading to :

- (a) a weakly bounded species  $m5^+$ , crossing barrier at  $\text{ts47}^+$  (22.36 eV) and then emission of neutral  $\text{CH}_2$  (22.60 eV). Further fragmentation leads through common  $\text{H}_2$  loss from  $\text{NH}_2\text{CH}_2^+$  to a minimum previously mentioned (see point 1(b)ii):
  - i.  $\text{COOH}^+ + \text{NHCH}^+ + \text{H}_2 + \text{CH}_2$  (24.68 eV);

4. isomerization to  $\text{NH}_3\text{CHCH}_2^+$  (18.00 eV) with  $\text{ts32}^+$  (20.42 eV);

Starting from  $\text{NH}_3\text{CHCH}_2^+$  we can easily obtain different fragmentation pathways than from  $\text{NH}_2\text{CHCH}_3^+$ . The calculated channels are itemized in order of increasing relative energies:

- (a)  $\text{COOH}^+ + \text{NH}_4^+ + \text{CHCH}$  (19.33 eV) with  $\text{ts49}^+$  (20.64 eV);
- (b)  $\text{COOH}^+ + \text{NH}_3 + \text{CHCH}_2^+$  (21.50 eV);
- (c)  $\text{COOH}^+ + \text{NH}_3^+ + \text{CHCH}_2$  (22.97 eV);
- (d)  $\text{COOH}^+ + \text{NH}_4 + \text{CHCH}^+$  (25.63 eV).

We can also see another pathways from our MD simulations in the breaking of  $\text{C}_\alpha\text{-C}_{\text{carboxylic}}$  bond:  $\text{COOH}^+ + \text{NH}_2\text{CH}_2\text{CH}_2^+$  (3). This channel was not consider to the further investigation because it will be similar to the two channels previously shown and do not bring any new energetic information.

From the analysis of the figure 6.13, carefully described above, together with the molecular dynamics calculations, we can draw the conclusion that the most probable channels are those corresponding to further fragmentation of the specie  $\text{NH}_2\text{CHCH}_3^+$ :  $m/q=45^+/42^+$ , then  $45^+/43^+$  and  $45^+/41^+$  amu and with small contribution of  $m/q=30^+/45^+$  amu ( $\text{CH}_2$  loss); Further fission of the  $\text{COOH}^+$  is much higher in energy. Other fragmentation pathways coming from  $\text{NH}_3\text{CHCH}_2^+$  should be less populated ( $m/q=45^+/26^+$  and  $45^+/27^+$  amu) despite its high stability. This can be easily explained with the dynamics simulations, where the probability of  $\text{COOH}^+ + \text{NH}_3\text{CHCH}_2^+$  is much smaller than  $\text{COOH}^+ + \text{NH}_2\text{CHCH}_3^+$ .

On the other hand, the isomerization process is energetically more favorable ( $\text{ts32}^+ = 20.42\text{eV}$ ) than the lowest fragmentation channel:  $\text{NH}_2\text{CHCH}_3^+ - \text{H}_2 \xrightarrow{\text{ts25}^{2+}(20.62\text{eV})} \text{NH}_2\text{CCH}_2^+ + \text{H}_2$ . The coincident peak with  $m/q=43^+$  and  $45^+$  amu could be obtained from both  $\text{NH}_2\text{CHCH}_3^+$  and  $\text{NH}_3\text{CHCH}_2^+$  without any barrier. Despite that, and despite its high stability (comparable with  $m/q=30^+/42^+$   $\text{NH}_2\text{CH}_2^+ + \text{CH}_2\text{CO}^+$ ) removing atomic hydrogen is not preferable in comparison with removing hydrogen molecule. The question is: why the experimentalists do not observe the signals at  $m/q=45^+/44^+$  amu instead of the observation of  $m/q=30^+/42^+$  amu ( $\text{NH}_2\text{CH}_2^+ + \text{CH}_2\text{CO}^+$ )? The answer to this question, even after dynamics which lead us to this channel is difficult. The only possible explanation is that the internal energy of the two fragments, mainly  $\text{NH}_2\text{CHCH}_3^+$  or  $\text{NH}_3\text{CHCH}_2^+$  with coincident with  $\text{COOH}^+$  ( $m/q=44^+/45^+$  amu) is high enough to overcome the energy barriers and leads with a certain probability to further fragmentation steps.

In the next figure 6.14 we focus on the isomerization processes occurring during dynamics simulations—we present further fragmentation processes in the PES after the formation of the dication of diol. In that figure we

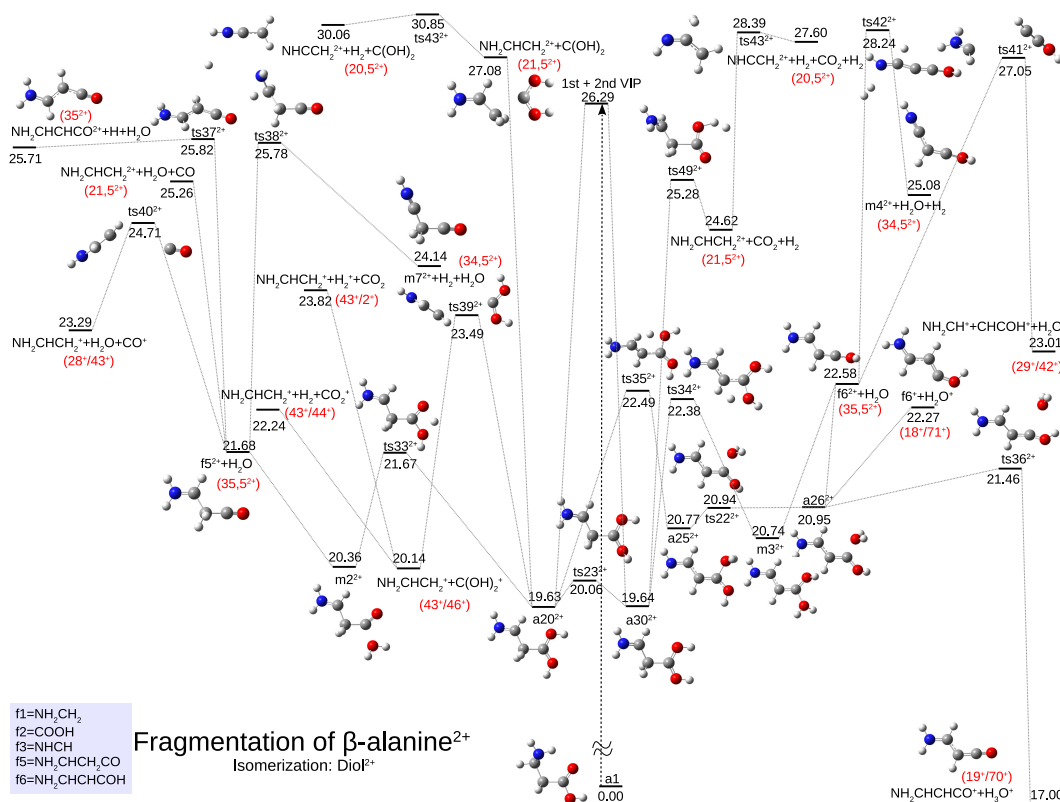


**Figure 6.14:** Fragmentations of dication of  $\beta$ -alanine: “enol” versus “cyclic” versus “linear” fragmentation paths. Relative energies ( $\Delta E$ ) in eV with respect to most stable neutral glycine (g1).

can see competitions, similar to the one observe for glycine, between fragmentation channels with different charge distribution. The most important fragmentation implies the four channels presented in figure 6.14:

1.  $\text{NH}_2\text{CHCHCOH}^{2+} + \text{H}_2\text{O}$  (22.58 eV)
2.  $\text{NH}_2\text{CHCHCOH}^+ + \text{H}_2\text{O}^+$  (22.27 eV)
3.  $\text{NH}_2\text{CHCHCO}^+ + \text{H}_3\text{O}^+$  (17.00 eV) with  $\text{ts36}^{2+}$  (21.46 eV);
4.  $\text{NH}_2\text{CHCH}_2\text{CO}^{2+} + \text{H}_2\text{O}$  (21.68 eV)

Fragmentation from  $\text{a26}^{2+}$  (20.95 eV) favors the 3<sup>rd</sup> channel, even if we do not consider any barrier for the 1<sup>st</sup> and 2<sup>nd</sup>. The channel with signal 19<sup>+</sup>/70<sup>+</sup> is not observed in the experiment despite its very high stability. This can be explained in two ways:

1. The paths of arriving to  $\text{a26}^{2+}$  imply several steps and it is thus dynamically very improbable. As we can observe in the right part of the figure 6.14 there are two ways of remove water:
  - one step:  $\text{a30}^{2+}$  (19.64 eV)  $\longrightarrow$   $\text{m3}^{2+}$  (20.74 eV) with  $\text{ts34}^{2+}$  (22.38 eV);
  - two steps:  $\text{a20}^{2+}$  (19.63 eV)  $\longrightarrow$   $\text{a25}^{2+}$  (20.77 eV) with  $\text{ts35}^{2+}$  (22.49 eV)  $\longrightarrow$   $\text{a26}^{2+}$  (20.95 eV) with  $\text{ts22}^{2+}$  (20.94 eV)
2. One step isomerization leading to  $\text{m2}^{2+}$  (20.36 eV) with  $\text{ts33}^{2+}$  (21.67 eV) from where emission of neutral water is the most probable channel leading to  $\text{NH}_2\text{CHCH}_2\text{CO}^{2+}$ . This channel is observed in the dynamics as the only one among the ones mention above. This shows that is is much probable to loss  $\text{H}_2\text{O}$  through  $\text{m2}^{2+}$  rather than produce  $\text{a26}^{2+}$ . For the further fragmentation of  $\text{NH}_2\text{CHCHCOH}^{2+} + \text{H}_2\text{O}$  (22.58 eV) we found two possible pathways leading to:
  - two singly charged fragments:  $\text{NH}_2\text{CH}^+ + \text{CHCOH}^+ + \text{H}_2\text{O}$  (23.01 eV) with barrier  $\text{ts41}^{2+}$  (27.05 eV);

- one doubly charged fragment:  $\text{NHCCHCOH}^{2+} + \text{H}_2\text{O} + \text{H}_2$  (25.08 eV) with barrier  $\text{ts}42^{2+}$  (28.24 eV).

The first path is energetically more favorable, although the second one leads to the peak at  $34.5^{2+}$  with just hydrogen molecule loss might be observed in the experiment (similar to the glycine case).

Another way of obtaining stable dicationic forms is to consider possible fragmentation of  $\text{a}30^{2+}$ . Just with one fragmentation step through  $\text{ts}49^{2+}$  (25.28 eV) we can remove two neutral fragments ( $\text{CO}_2$  and  $\text{H}_2$ ) leading to the doubly charged  $\text{NH}_2\text{CHCH}_2^{2+}$  ( $m/q=21.5$  amu). Further fragmentation is 2 eV above the entrance channel ( $\text{ts}43^{2+} = 28.39$  eV) leading to  $\text{NHCCH}_2^+$  ( $m/q=20.5$  amu) with additional removed of one hydrogen molecule:  $\text{NHCCH}_2^+ + \text{H}_2 + \text{CO}_2 + \text{H}_2$  (27.60 eV). Taking into account the left part of the figure 6.14 we can observe the most probable dehydration channel, which is also seen in the dynamics simulation:  $\text{NH}_2\text{CHCH}_2\text{CO}^{2+} + \text{H}_2\text{O}$  (21.68 eV). This very stable dicationic specie ( $m/q=35.5^{2+}$  amu) can easily follow further fragmentation through four paths, all of them below the entrance channel:

1.  $\text{NH}_2\text{CHCH}_2^+ + \text{H}_2\text{O} + \text{CO}^+$  (23.29 eV) with  $\text{ts}40^{2+}$  (23.29 eV) leading to a signal  $m/q=28^+/43^+$  amu or removing neutral carbon monoxide without any barrier:
2.  $\text{NH}_2\text{CHCH}_2^{2+} + \text{H}_2\text{O} + \text{CO}$  (25.26 eV) leading to a signal at  $m/q=21.5^{2+}$  and two processes in competition with very similar energy barriers leading to emission of neutral hydrogen atom:
3.  $\text{NH}_2\text{CHCHCO}^{2+} + \text{H}_2\text{O} + \text{H}$  (25.71 eV) through  $\text{ts}37^{2+}$  (25.82 eV) at  $m/q=35^{2+}$  amu and:
4.  $\text{NHCCH}_2\text{CO}^{2+} + \text{H}_2 + \text{H}_2\text{O}$  (24.14 eV) through  $\text{ts}38^{2+}$  (25.78 eV) at  $m/q=34.5^{2+}$  amu.

Despite the very similar energy barriers between channels 3 and 4, the latter leads to a minima at  $\sim 1.5$  eV lower in energy than the channel 3. As we can see the flat molecule  $\text{NH}_2\text{CHCHCO}^{2+}$  is less stable than the one with angle C-C-C around  $180^\circ$  and two hydrogen in middle carbon position  $\text{NH}_2\text{CCH}_2\text{CO}^{2+}$  ( $34.5^{2+}$ ). Two other possible fragmentation channels arising from  $\text{a}20^{2+}$  imply  $\text{C}_\alpha\text{-C}_{\text{carboxylic}}$  fragmentation. In one of them the charge is located on the  $\text{NH}_2\text{CHCH}_2^+$  moiety and in the second case (more favorable), the charge is separated between  $\text{NH}_2\text{CHCH}_2^+$  and  $\text{C}(\text{OH})_2^+$ . The latter pathway is more than 2 eV lower in energy and can undergo further fission according to:

- $\text{NH}_2\text{CHCH}_2^+ + \text{H}_2 + \text{CO}_2^+$  (22.24 eV) with  $m/q=43^+/44^+$  amu:
- $\text{NH}_2\text{CHCH}_2^+ + \text{H}_2^+ + \text{CO}_2$  (23.82 eV) with  $m/q=43^+/2^+$  amu.

Both channels are not observed in the experiment. Absence of the signals at  $m/q=43^+/44^+$  and  $43^+/2^+$  amu is due to the competition with the dehydrogenation process, which is more favorable since it requires less energy to cross the barrier ( $\text{ts}33^{2+} = 21.67\text{eV}$ ). Moreover, the one step fission process ( $\text{ts}49^{2+} = 25.28\text{eV}$ ) with emission of two neutral fragments should be a more favorable process than  $\text{NH}_2\text{CHCH}_2^+ + \text{C}(\text{OH})_2^+$ .

In figure 6.15 we propose different fragmentation paths starting from other products obtained in the molecular dynamics simulations:  $\text{NH}_3\text{CH}_2\text{CHCOOH}^{2+}$  and dications of 4-membered and 5-membered rings. On the left part of the figure we can see four pathways, where the most favorable one corresponds to the fragments, which we can get directly after Coulomb explosion:  $\text{NH}_3\text{CHCH}_2^+ + \text{COOH}^+$  with  $\text{ts}55^{2+}$  (23.32 eV). The three additional channels are unique. The presence of peaks at  $m/q: 17^+/62^+, 22^{2+}$  and  $36^{2+}$  amu in the experiment might be a proof of the isomerization to  $\text{NH}_3\text{CH}_2\text{CHCOOH}^{2+}$  prior to fragmentation. We can not observe the signals mentioned above if there will not be a hydrogen transfer leading to  $\text{a}27^{2+}$ . The most probable fission is the one with  $\text{ts}54^{2+}$  (24.45 eV) leading to equal charge separation:  $\text{NH}_3^+ + \text{CH}_2\text{CHCOOH}^+$ . We calculated the competition channel with the dicationic fragment  $\text{NH}_3 + \text{CH}_2\text{CHCOOH}^{2+}$  (26.32 eV) for which further fragmentation is around 6.5 eV over the entrance channel. This pathway should not be accessible and the dicationic form  $\text{CHCH}_2^{2+}$  ( $m/q=13.5^{2+}$  amu) is not observed in the experiment. The right part of the figure presents the fission processes of the 4-membered and 5-membered rings. The  $\text{a}1^{2+}$  can undergo the follow fragmentations:

1.  $C_\alpha$ - $C_\beta$  fission with  $ts44^{2+}$  (24.09 eV) together with isomerization leading to  $NH_2CH_2^+ + HOCH_2CO^+$  (17.84 eV) at  $m/q=30^+/59^+$  amu. Further fragmentation will be exactly the same as channel (9) in figure 6.6; i.e.  $NH_2CH_2^+ + CO + CH_2OH^+$ ;
2. Neutral hydrogen molecule emission with a simultaneous hydrogen transfer to the carboxyl group:  $HNCCH_2C(OH)_2^{2+} + H_2$  with  $ts45^{2+}$  (24.39 eV) at  $m/q=43.5^{2+}$  amu. Further fragmentation leads to a weakly-bounded  $HNCCH_2COOH_2^{2+}$  ( $m6^{2+}$ ) and then to signal at  $34.5^{2+}$  amu ( $NHCCH_2CO^{2+}$ ) after emission of neutral water (24.14 eV).

We can observe that  $a31^{2+}$  is 1.5 eV more stable than  $a1^{2+}$ . Dehydration of dication of 4-membered ring can lead to the 3-membered dicationic specie with emission of neutral water (25.90 eV) or to a cationic fragment with different 4-membered ring with emission water cation (24.83 eV) at  $m/q=71^+/18^+$ . The latter is more preferable ( $\sim 1$  eV) but requires the production of a weakly bounded moiety between  $ts56^{2+}$  and  $NH_3CHCHOC^+ + H_2O^+$ . The lowest barrier ( $ts57^{2+} = 23.03$  eV) corresponds to the fission into  $NH_3CHO^+ + CH_2COH^+$  (18.75 eV) at  $m/q=46^+/43^+$ , which is not observed in the experiment but could prove the existence of a 4-membered specie.

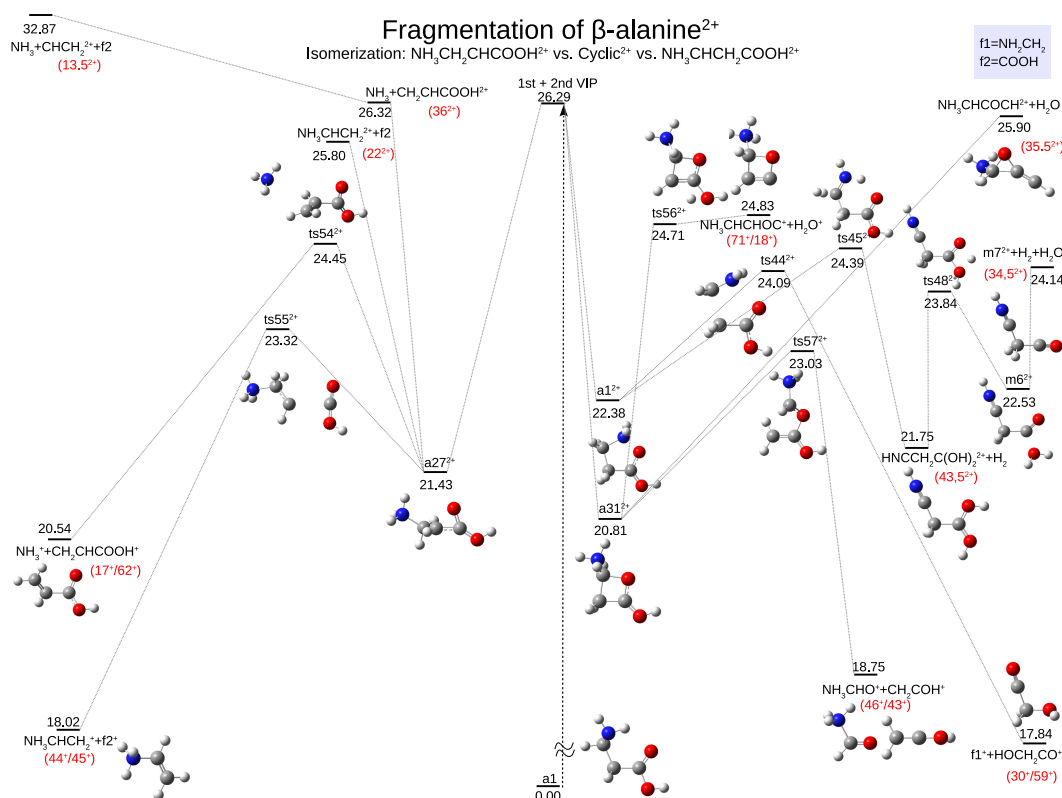


**Figure 6.15:** Fragmentations of dication of  $\beta$ -alanine: “enol” versus “cyclic” fragmentation paths. Relative energies ( $\Delta E$ ) in eV with respect to most stable neutral glycine (g1).

Figure 6.16 presents a summary of all combined processes observed in the molecular dynamics simulations together with other complementary channels. The ordering in terms of increasing relative energies are as follow:

1.  $NH_2CH_2^+ + HOCH_2^+ + CO$  (18.25 eV) through  $ts24^+$  (18.00 eV) and weakly-bounded  $OC \cdots CH_2OH^+$  ( $m1^+$ );
2.  $COOH^+ + NH_2CHCH_2^+ + H_2$  (19.43 eV) with  $ts46^{2+}$  (20.62 eV);
3.  $COOH^+ + NH_3 + CHCH_2^+$  (21.50 eV);
4.  $NH_2CHCH_2CO^+ + H_2O^+$  (21.62 eV) with  $ts33^{2+}$  (21.67 eV); *not observed in the dynamics*
5.  $NH_2CHCH_2CO^{2+} + H_2O$  (21.68 eV) with  $ts33^{2+}$  (21.67 eV);
6.  $NH_3CHCH_3^+ + CO_2^+$  (21.89 eV); *not observed in the dynamics*

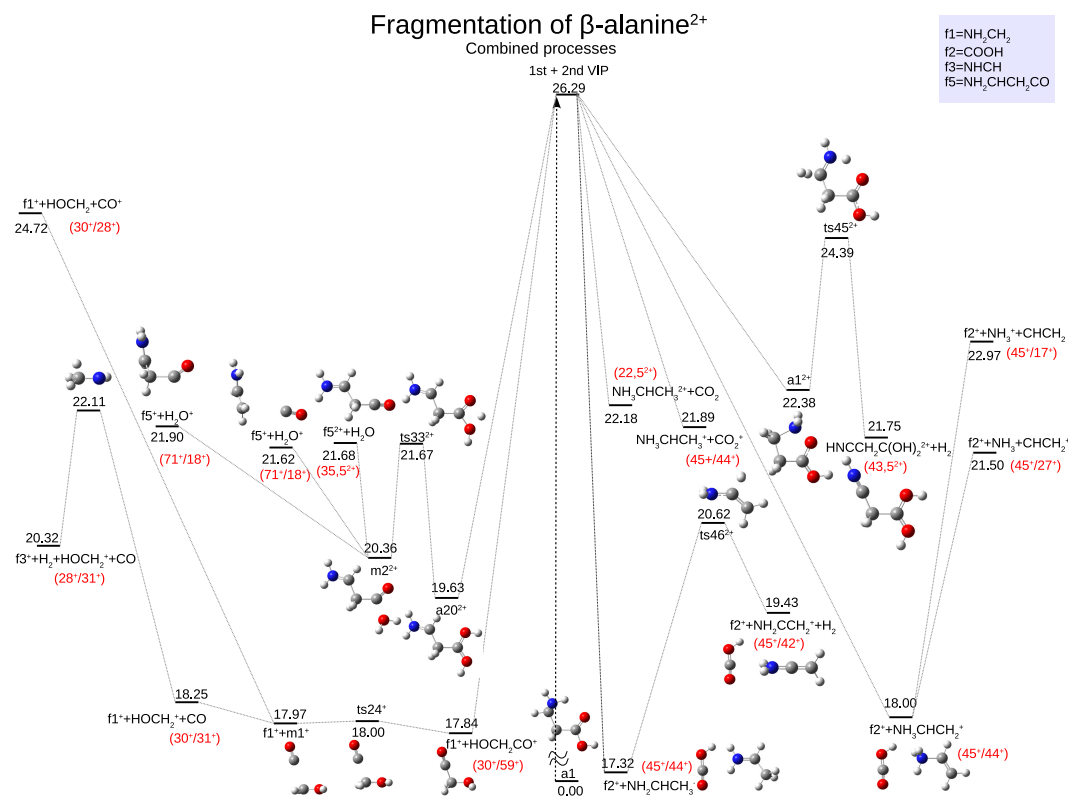


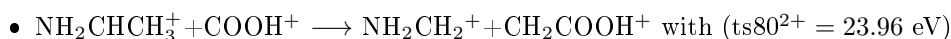
**Figure 6.16:** Fragmentations of dication of  $\beta$ -alanine: summary of combined fragmentation paths. Relative energies ( $\Delta E$ ) in eV with respect to most stable neutral glycine (g1).

7. Hydrogen molecule emission from  $\text{NH}_2\text{CH}_2^+$  (20.32 eV) with typical  $t_s=22.11$  eV; *not observed in the dynamics*
8.  $\text{NH}_3\text{CHCH}_3^{2+}+\text{CO}_2$  (22.18 eV)
9.  $\text{COOH}^++\text{NH}_3^++\text{CHCH}_2$  (22.97 eV);
10.  $\text{HNCCH}_2\text{C}(\text{OH})_2^{2+}+\text{H}_2$  (21.75 eV) with  $t_{s45^{2+}}$  (24.39 eV);
11.  $\text{NH}_2\text{CH}_2^++\text{HOCH}_2+\text{CO}^+$  (24.72 eV) through  $t_{s24^+}$  (18.00 eV) and weakly-bounded  $\text{OC}\cdots\text{CH}_2\text{OH}^+$  ( $m1^+$ ); *not observed in the dynamics.*

The fissions 4,6 and 10 are not observed in dynamics. From our calculations of the PES, the charge prefers to delocalize over two fragments (4 and 6) but MD calculations shows that, despite that, small molecules like water, carbon dioxide or hydrogen molecule prefer to be neutrals (5 and 7). Moreover charge distribution between CO and HOCH<sub>2</sub> in coincidence with NH<sub>2</sub>CH<sub>2</sub><sup>+</sup> prefers definitely the latter moiety. On the other hand, channel NHCH<sup>+</sup>+H<sub>2</sub>+HOCH<sub>2</sub><sup>+</sup>+CO is not observed neither in the dynamics neither in the experiment despite its low energy barrier, as explained in the beginning of this section.

## 6.6 Reactions between two singly charged fragments

We also calculated the energy barriers for chemical reactions between two singly charged molecules on the PES of  $\beta$ -alanine dication. The connections between the most important fragmentation products of  $\beta$ -alanine are showed in figure 6.17. We can observe that if the position of the hydrogen from the carboxyl group is closer to the amino group the chemical reaction involves a lower energy barrier:



than the reaction with the hydrogen in opposite position ( $t_{s82^{2+}} = 24.99$  eV). This trend is observed also for the reaction:

- $\text{NH}_2\text{CH}_2^+ + \text{CH}_2\text{COOH}^+ \rightarrow \text{COOH}^+ + \text{NH}_2\text{CH}_2\text{CH}_2^+$  with ( $\text{ts}84^{2+} = 23.90$  eV).

The reaction between  $\text{NH}_2\text{CH}_2^+ + \text{CH}_2\text{COOH}^+$  leading to  $\text{COOH}^+ + \text{NH}_2\text{CH}_2\text{CH}_2^+$  can take place through two different transition states:  $\text{ts}84^{2+} = 23.90$  eV and  $\text{ts}51^{2+} = 24.15$  eV.  $\text{NH}_2\text{CHCH}_2\text{CO}^+$  is involved in two reactions:

- $\text{NH}_2\text{CH}_2^+ + \text{CH}_2\text{COOH}^+ \rightarrow \text{NH}_2\text{CHCH}_2\text{CO}^+ + \text{H}_2\text{O}^+$  with ( $\text{ts}50^{2+} = 24.29$  eV);
- $\text{COOH}^+ + \text{NH}_2\text{CHCH}_2^+ \rightarrow \text{NH}_2\text{CHCH}_2\text{CO}^+ + \text{H}_2\text{O}^+$  with ( $\text{ts}52^{2+} = 23.20$  eV).

Both channels are accompanied by emission of cationic water. The second pathway is energetically more probably (it presents a lower activation energy).

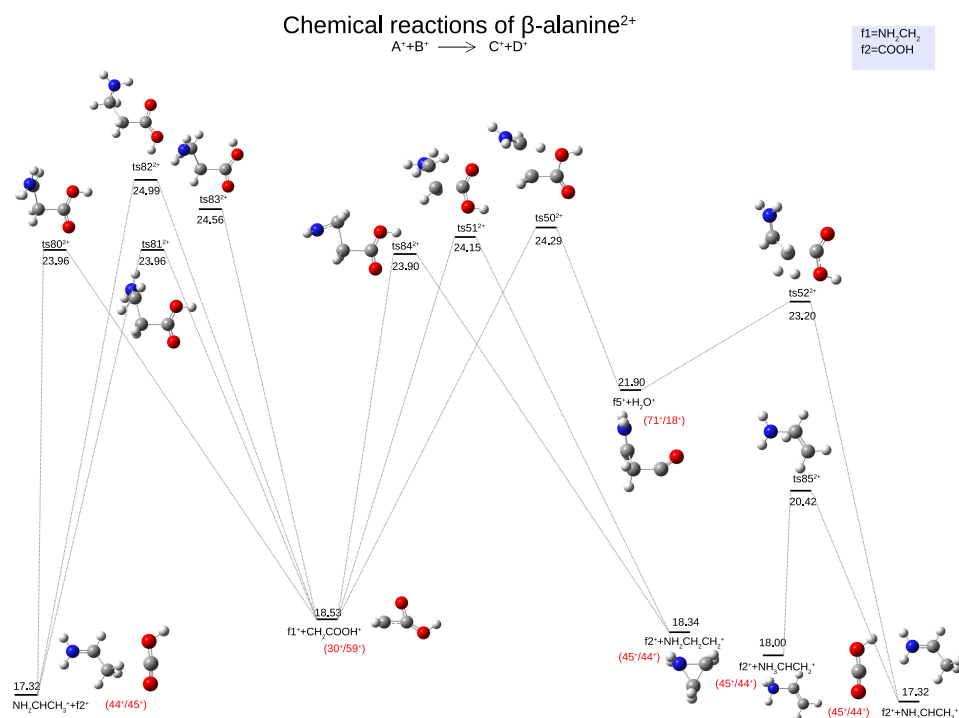


**Figure 6.17:** Chemical reactions between two cation in the PES of dication of  $\beta$ -alanine. Relative energies ( $\Delta E$ ) in eV with respect to most stable neutral  $\beta$ -alanine (a1).



## Chapter 7

# Clusters of $\beta$ -alanine

In this chapter we present the evolution of single  $\beta$ -alanine molecules into clusters. With respect to glycine and  $\beta$ -alanine, the clusters of  $\beta$ -alanine are more CPU demanding and are mainly characterized by the non-covalent interactions between the molecules. Recently, they become the interests of experimental and theoretical chemists. On the one hand, because they possess different internal interactions than single molecules such as intermolecular forces as van der Waals interactions or hydrogen bonds. On the other hand, because they present similar properties than foldamers (discrete chain of molecules or oligomers) and therefore they can adopt a secondary structure, which is stabilized by the non-covalent interactions. The latter attracts the attention because the secondary structures,<sup>137;138</sup> that they are able to adopt are essential in the rational design of nucleic acid structures for DNA nanotechnology and DNA computing.<sup>139</sup> In a future study, we will consider that via ionization and excitation of the neutral clusters we can form covalently bonded residues. Due to that, we should first perform a careful investigation of the geometry of the neutral clusters of  $\beta$ -alanine as the first step towards understanding the main properties of these structures before ionization. The recent experiments performed by P. Rousseau et al. (private communication) shows strong correlations between the temperature of exposition of the neutral clusters and their further reactions after ionization. After ionization, the obtained positively charged  $\beta$ -peptides will have new properties, such as the secondary structures (beta helix or beta sheets). Those structures do not suffer proteolytic degradation (breakdown of the peptide bond) in contrast to the conventional peptides (build of  $\alpha$ -amino acids) and they can present abundant conformational stability at relatively short lengths in water.<sup>140 141</sup> Furthermore, clusters of  $\beta$ -amino acids, can be employed as a medium to the rational synthesis of  $\beta$ -peptides; this could be a first stage of the creation of this biologically active molecules.<sup>142</sup> Additionally, considering the formations of peptide bonds in the clusters of  $\beta$ -amino acids leading to  $\beta$ -peptides, we have to take into account their potential to form a new platform technology for the design and synthesis of peptidomimetic materials (very stable compounds designed to mimic a biologically active peptide).<sup>143</sup>

Clusters of  $\beta$ -alanine do not present the covalent bonds between the residues and only the non-covalent effects can stabilize the neutral clusters. Moreover, it has been proposed experimentally<sup>144</sup> that oligomers constructed from  $\beta$ -amino acids will avoid the hydrogen bonds between the nearest neighbors the amide groups along the backbone. Thus, they become an attractive “material” to build the foldamers, due to the fact that abstention of attractive interactions with the nearest neighbor appears to be important for acceptance of compact secondary structures.<sup>144</sup>

On the other hand, clusters of  $\beta$ -alanine are challenging systems to investigate theoretically for several reasons. One of them is that the single residues are not covalently bonded, thus many stable conformers of the clusters may be found. Moreover, the van der Waals interactions between the residues in the cluster should be easily broken when the temperature increases.

In this chapter we present the average geometry of the clusters of  $\beta$ -alanine obtained from classical molecular dynamics (CMD) simulations for different values of the temperature and clusters size. Moreover, geometry optimization at the DFT level of theory (B3LYP and M06 functionals) was performed for different isomers with 2,3,4

and 5 residues of  $\beta$ -alanine. We used the nomenclature based on parameters taken from the CMD simulations:  $(\beta\text{-Ala})_n300\text{K}_{200\text{ps}}$ , where  $n$  is the cluster size, 300K is the temperature used in the dynamics and the third element is the time of the CMD simulation (table 7.1). The shape of the geometry after the optimization with the B3LYP and the M06 functionals is very similar and we present in the figures only geometries optimized at the M06 level of theory. We also show the relative energy, root mean square deviation (RMSD) and binding energies (BE) for the different conformers at the two levels of theory (M06 and B3LYP) for the clusters of  $\beta$ -alanine with 2,3,4 and 5 residues. Relative energies are calculated with respect to the most stable conformer. RMSD is the answer to the question how much did the optimized structure changed with respect to the average one taken from a molecular dynamics simulation. The geometries are compared after an alignment-fitting of the molecules based on the selected atoms (in our case all atoms). RMSD is defined as:

$$RMSD = \sqrt{\frac{\sum_{i=1}^{N_{atoms}} (r_i(\text{average}) - r_i(\text{optimized}))^2}{N_{atoms}}} \quad (7.1)$$

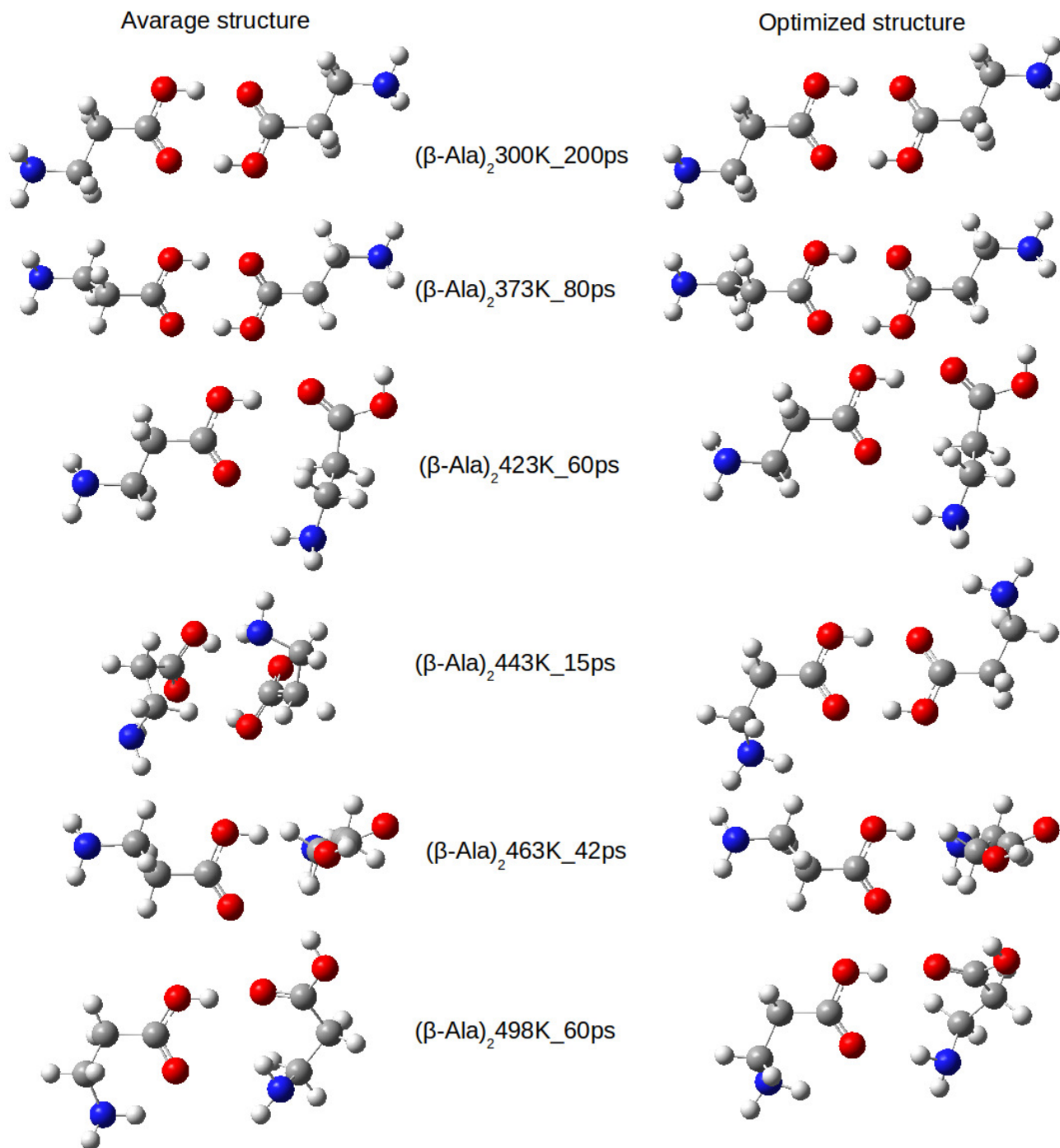
where,  $N_{atoms}$  is the number of atoms and  $r_i$  is the position of atom  $i$ .

The stability of the cluster can be presented in terms of binding energies ( $BE$ ) as well.  $BE$  was calculated as:

$$BE = E_n - NE \quad (7.2)$$

where,  $E_n$  is the energy of the cluster,  $N$  is the residues number and  $E$  is the energy of the most stable neutral  $\beta$ -alanine conformer. The binding energies give us an idea of the participation of the hydrogen bonds and van der Waals interactions for the stabilization of the cluster. When  $BE$  is negative, it means that the cluster is stable and as more negative value as larger the intramolecular interactions.

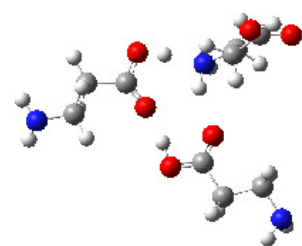
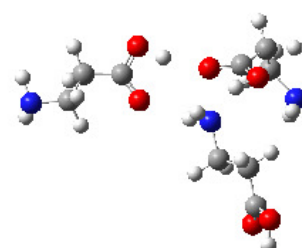
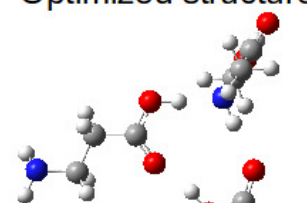
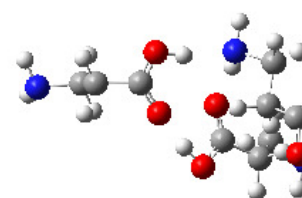
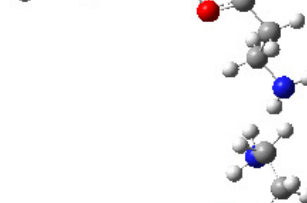
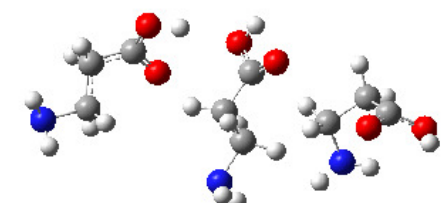
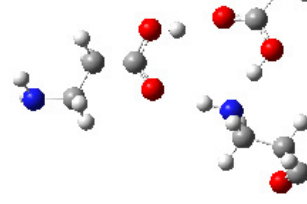
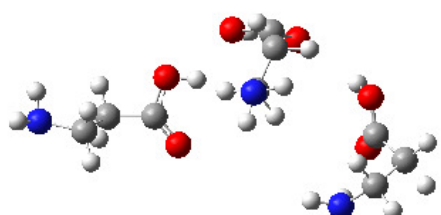
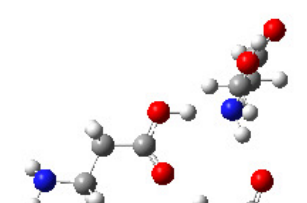
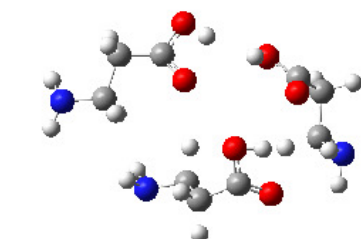
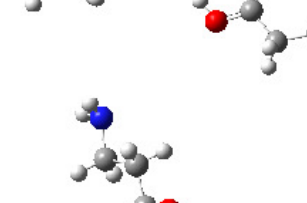
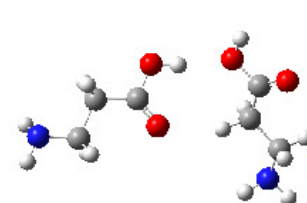
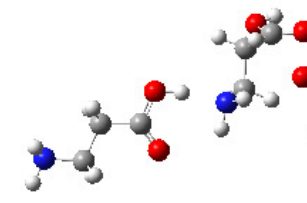
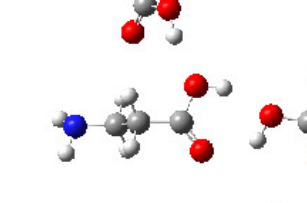
We performed CMD calculations to create the cluster distribution with different sizes. In the dynamics we can observe that smaller the molecule and higher the temperature, shorter the dynamics because the clusters fragment at higher temperature. This trend is mainly observed for the odd residues ( $n = 2, 4$ ). The residues prefer to destabilize the van der Waals interactions and break the hydrogen bonds, thus separating into smaller clusters or even into single residues. Because of that, we needed to control the parameters of the simulations (simulation time, time step, equilibration, etc.) to obtain the reliable average structure. The average structure is an artificial structure of a conformation which mostly represents the behavior of the cluster at a certain temperature. Because of that the temperature has an indirect influence on the potential well, in which the molecule fall down (minimum) after optimization. Results of the average structure of neural clusters of  $\beta$ -alanine for  $2 \leq n \leq 10$  and 20 are presented in figures 7.1 to 7.10. Moreover, in that figures for  $2 \leq n \leq 5$  we can see the structure obtained after optimization at the DFT level using the average MCD geometry as initial guess.



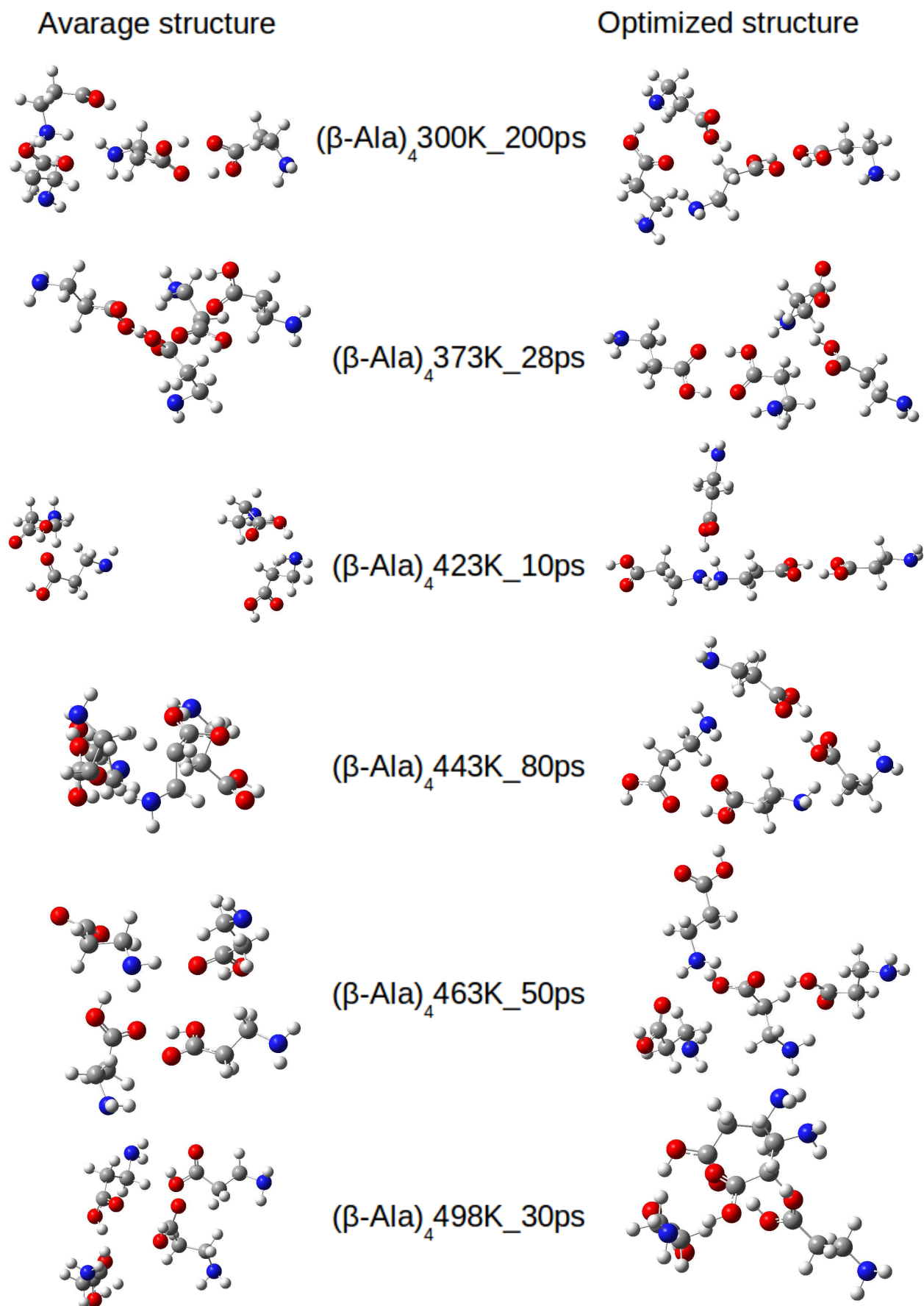
**Figure 7.1:** Average geometries of the six neutral conformers ( $\beta$ -Ala)<sub>2</sub> taken from classical molecular dynamics calculations for different temperature: 300K, 423K, 443K, 463K, 498K and optimized geometries for each structure at the M06/6-311++G(d,p) level of theory.

Average structure

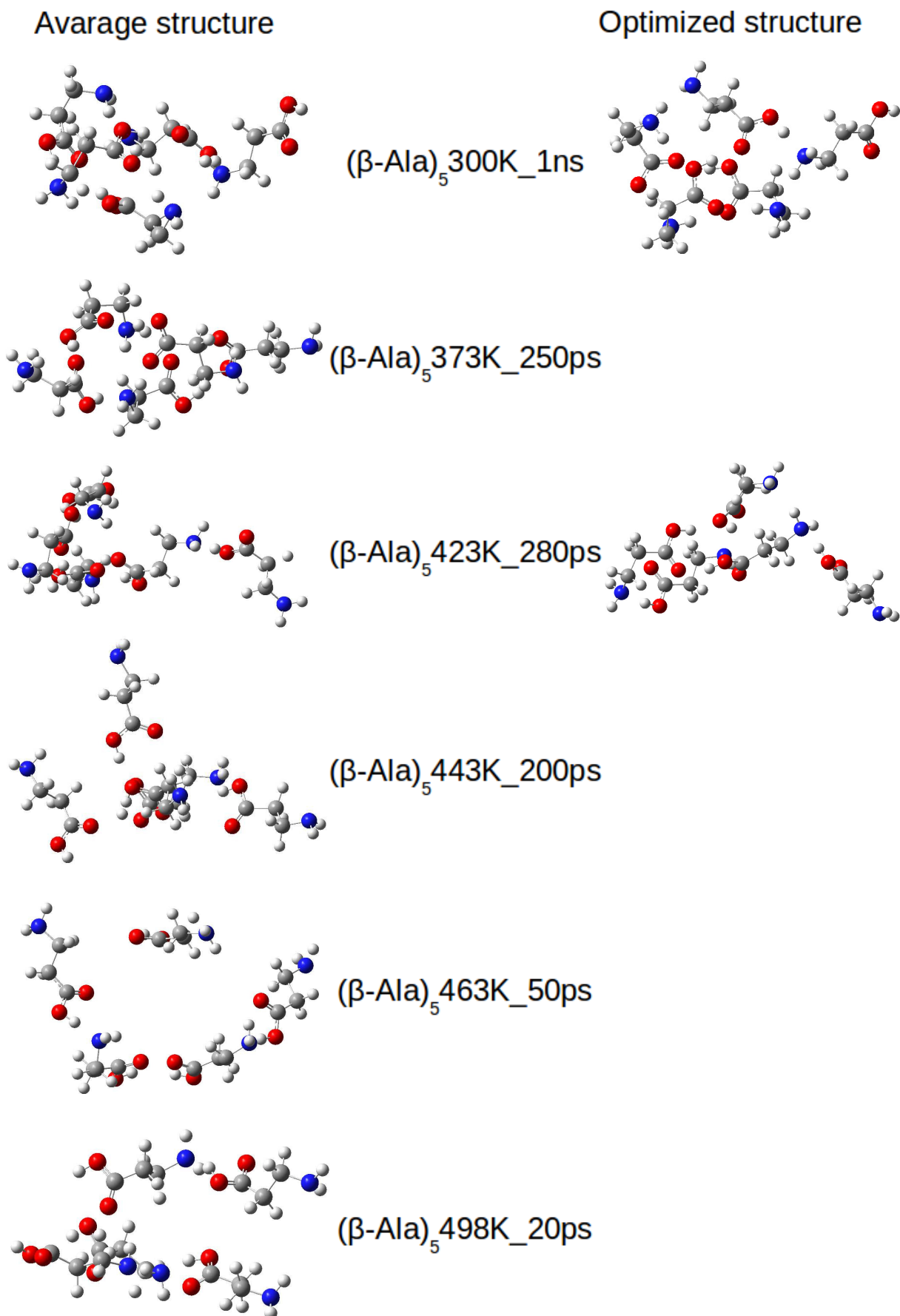
Optimized structure

 $(\beta\text{-Ala})_3$ 300K\_1ns $(\beta\text{-Ala})_3$ 373K\_600ps $(\beta\text{-Ala})_3$ 423K\_60ps $(\beta\text{-Ala})_3$ 443K\_35ps $(\beta\text{-Ala})_3$ 463K\_50ps $(\beta\text{-Ala})_3$ 498K\_50ps

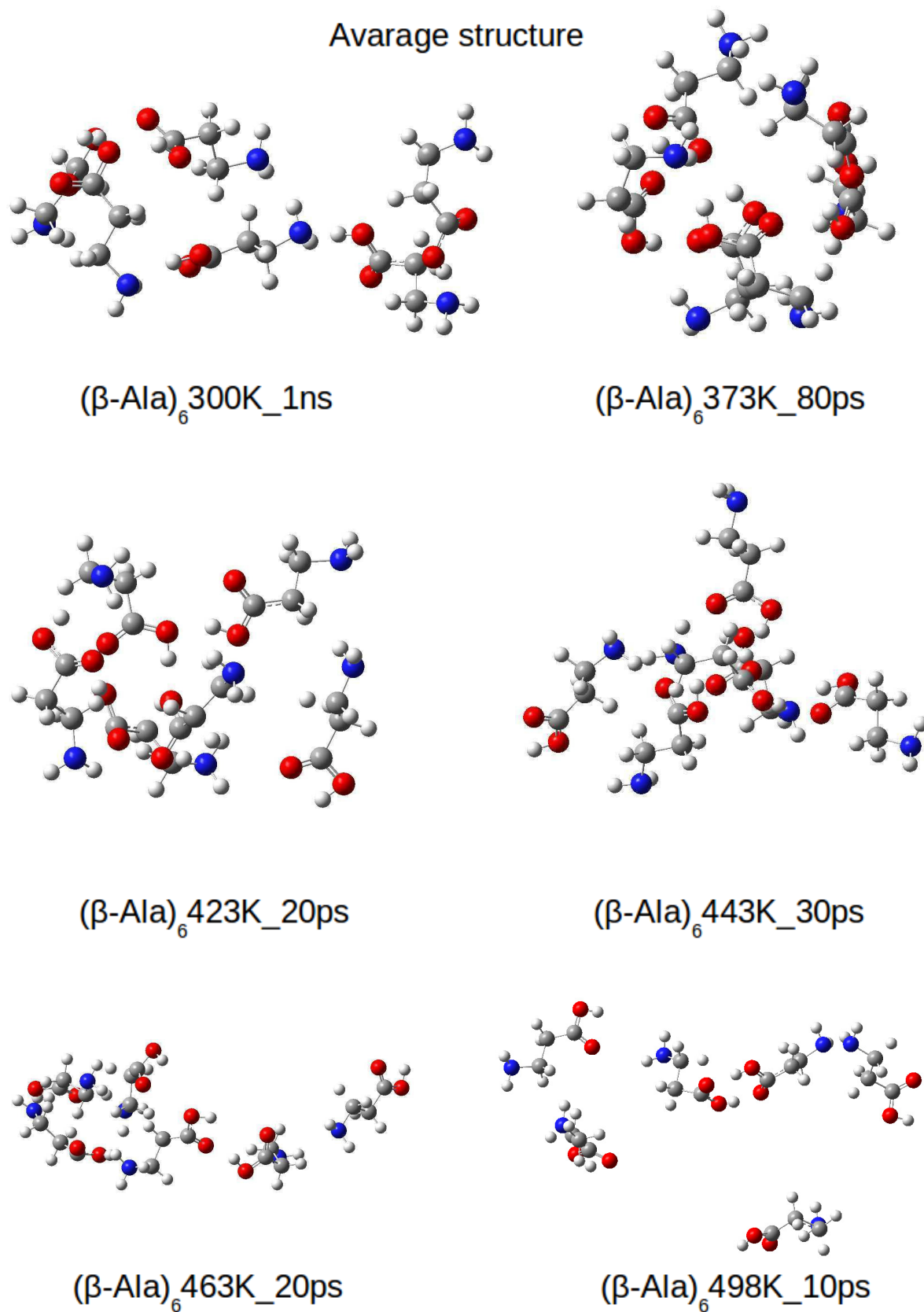
**Figure 7.2:** Average geometries of the six neutral conformers  $(\beta\text{-Ala})_3$  taken from classical molecular dynamics calculations for different temperature: 300K, 423K, 443K, 463K, 498K and optimized geometries for each structure at the M06/6-311++G(d,p) level of theory.



**Figure 7.3:** Average geometries of the six neutral conformers  $(\beta\text{-Ala})_4$  taken from classical molecular dynamics calculations for different temperature: 300K, 423K, 443K, 463K, 498K and optimized geometries for each structure at the M06/6-311++G(d,p) level of theory.

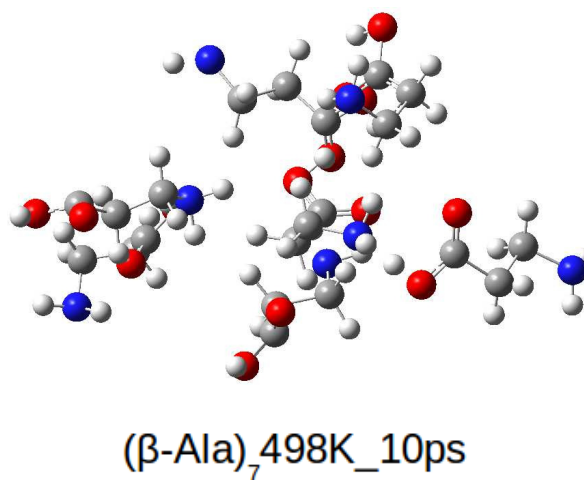
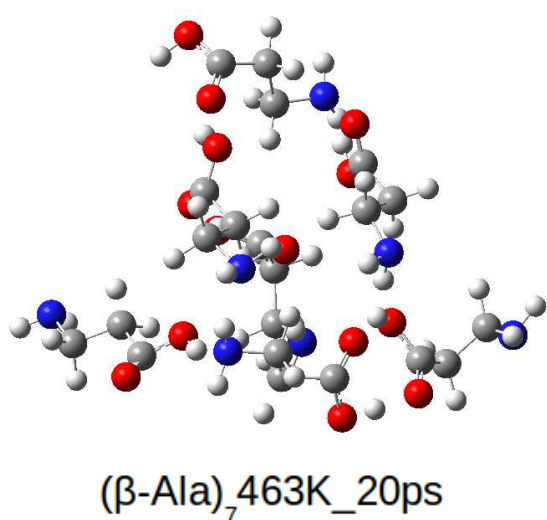
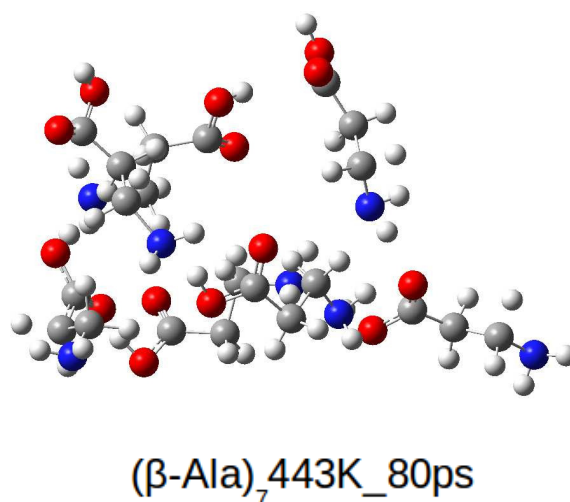
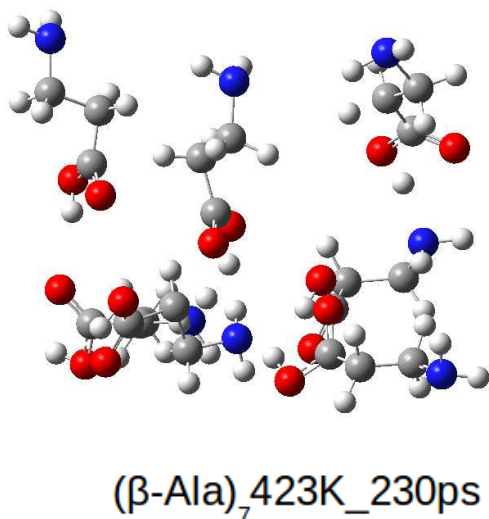
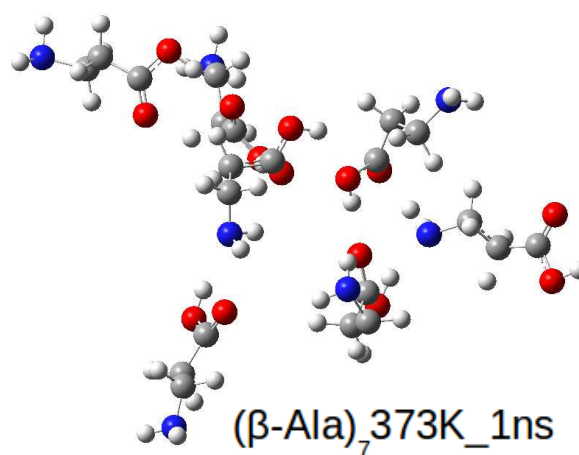
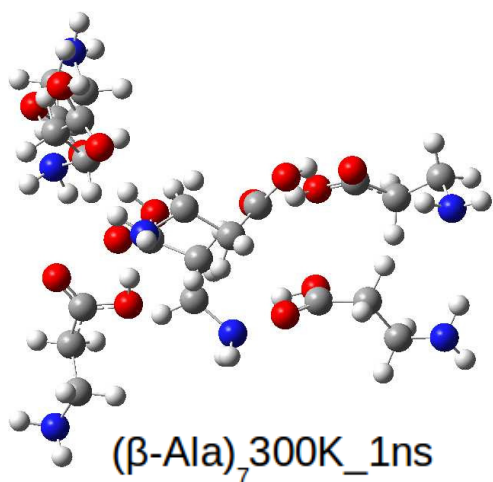


**Figure 7.4:** Average geometries of the six neutral conformers  $(\beta\text{-Ala})_5$  taken from classical molecular dynamics calculations for different temperature: 300K, 423K, 443K, 463K, 498K and optimized geometries for each structure at the M06/6-311++G(d,p) level of theory.

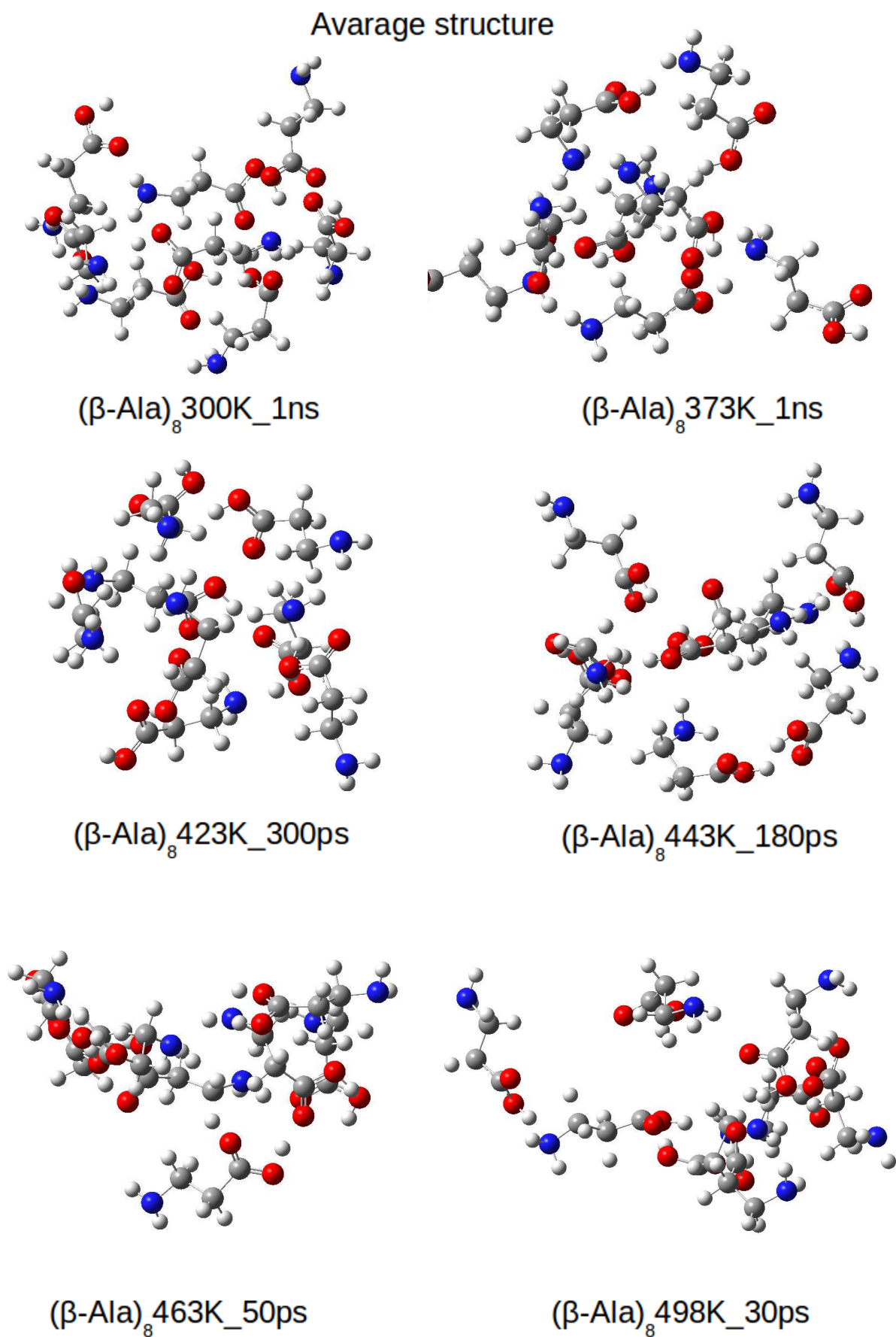


**Figure 7.5:** Average geometries of the six neutral conformers ( $\beta$ -Ala)<sub>6</sub> taken from classical molecular dynamics calculations for different temperature: 300K, 423K, 443K, 463K, 498K.

## Average structure

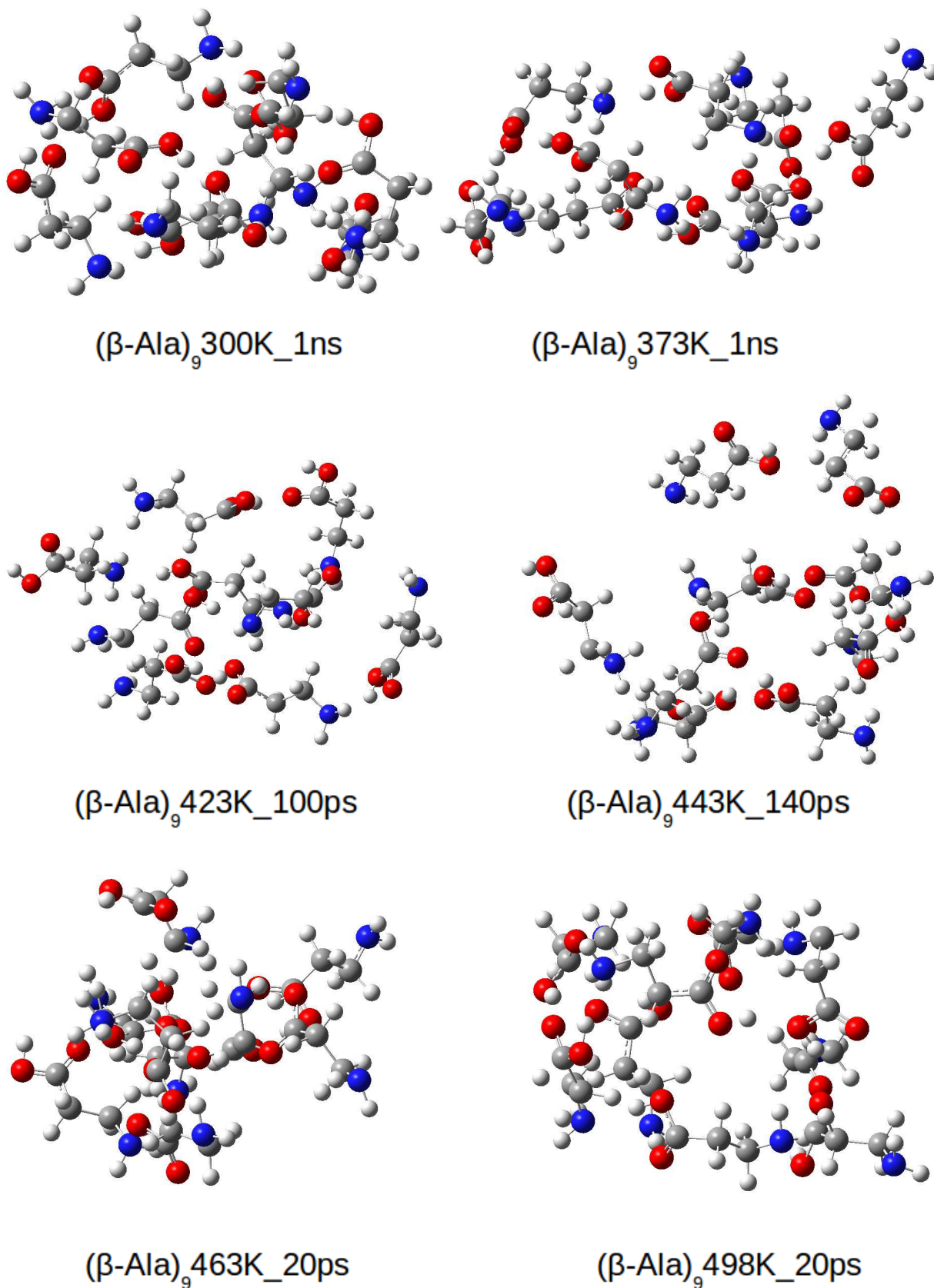


**Figure 7.6:** Average geometries of the six neutral conformers ( $\beta$ -Ala)<sub>7</sub> taken from classical molecular dynamics calculations for different temperature: 300K, 423K, 443K, 463K, 498K.



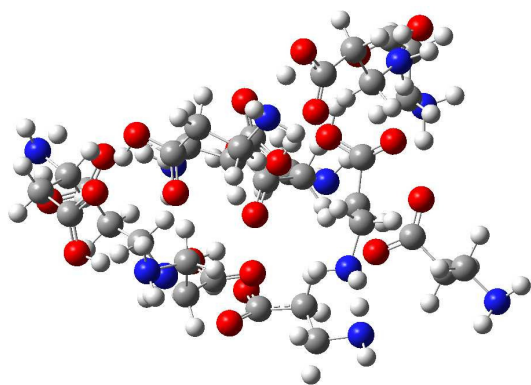
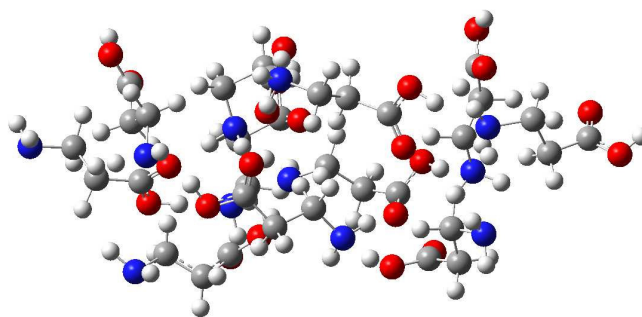
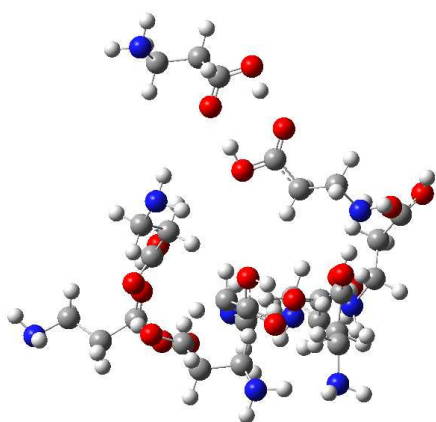
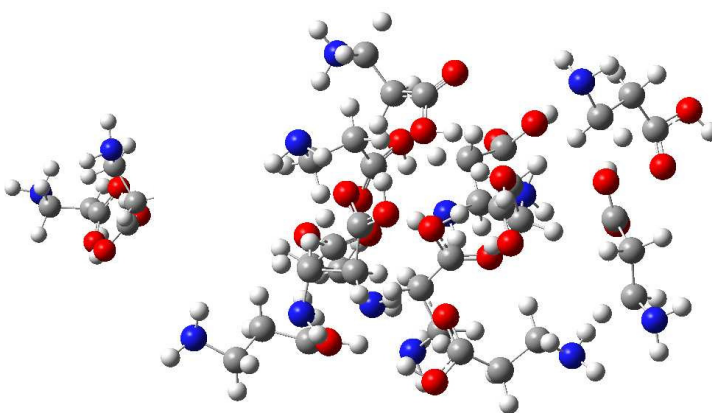
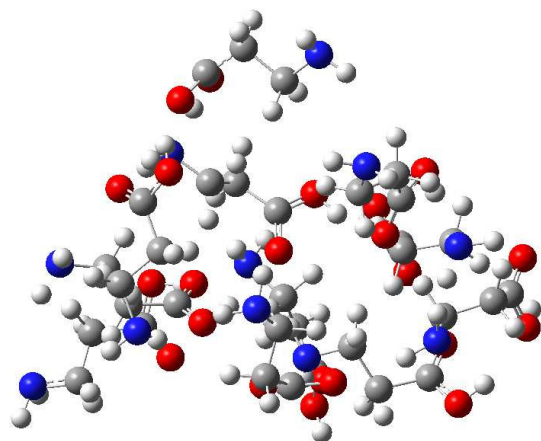
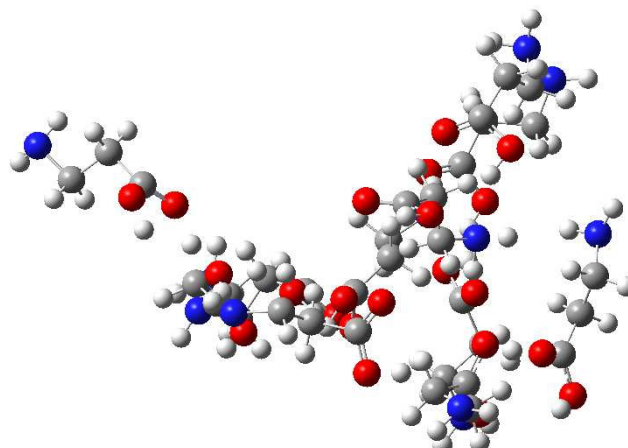
**Figure 7.7:** Average geometries of the six neutral conformers ( $\beta$ -Ala)<sub>8</sub> taken from classical molecular dynamics calculations for different temperature: 300K, 423K, 443K, 463K, 498K.

## Average structure



**Figure 7.8:** Average geometries of the six neutral conformers  $(\beta\text{-Ala})_9$  taken from classical molecular dynamics calculations for different temperature: 300K, 423K, 443K, 463K, 498K.

## Average structure

 $(\beta\text{-Ala})_{10}$  300K\_1ns $(\beta\text{-Ala})_{10}$  373K\_1ns $(\beta\text{-Ala})_{10}$  423K\_250ps $(\beta\text{-Ala})_{10}$  443K\_200ps $(\beta\text{-Ala})_{10}$  463K\_60ps $(\beta\text{-Ala})_{10}$  498K\_60ps

**Figure 7.9:** Average geometries of the six neutral conformers  $(\beta\text{-Ala})_{10}$  taken from classical molecular dynamics calculations for different temperature: 300K, 423K, 443K, 463K, 498K.

## Average structure

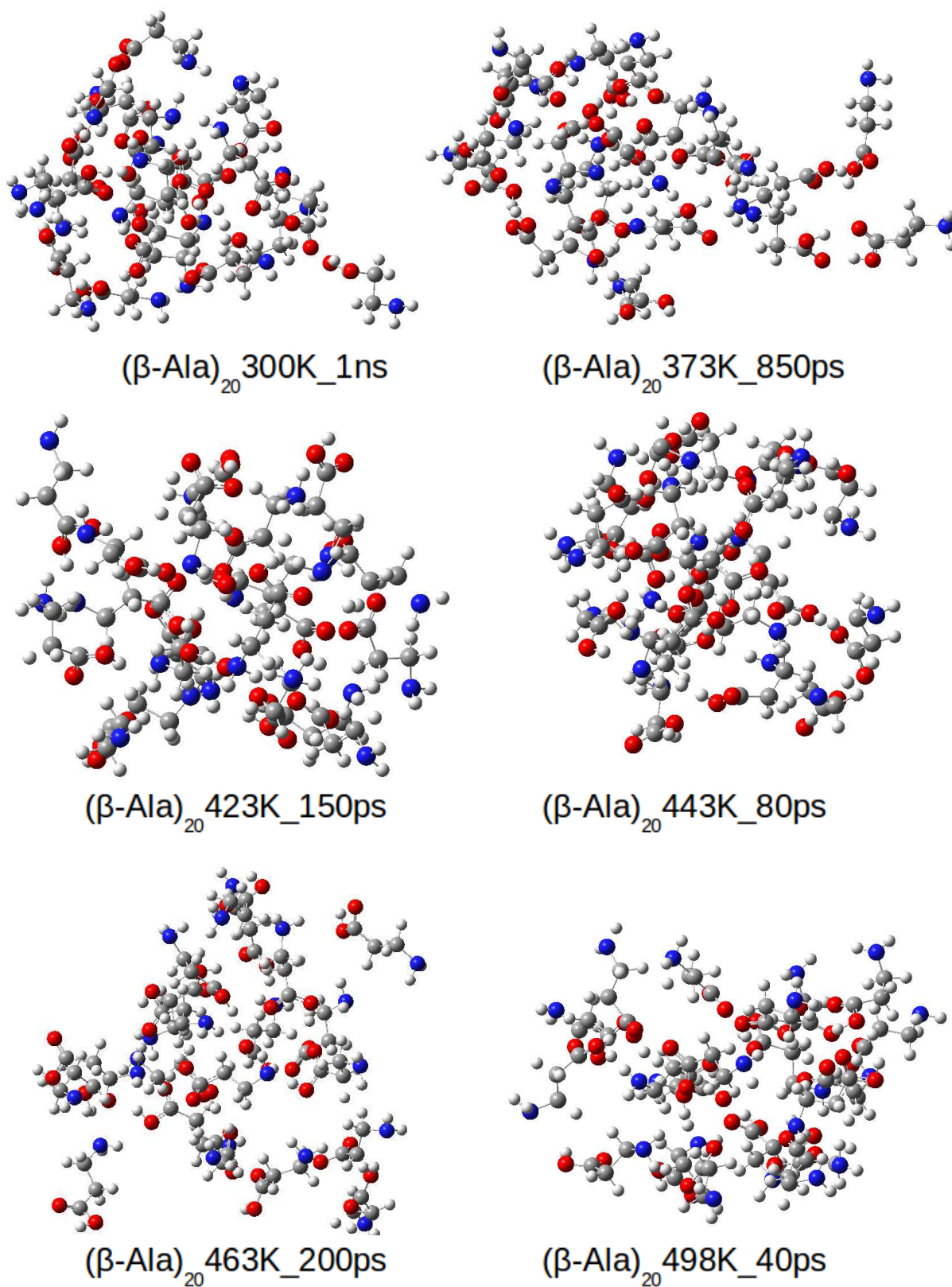


**Figure 7.10:** Average geometries of the six neutral conformers ( $\beta$ -Ala)<sub>20</sub> taken from classical molecular dynamics calculations for different temperature: 300K, 423K, 443K, 463K, 498K.

In figures 7.1 to 7.10 we can notice that for the clusters of  $(\beta\text{-Ala})_n$  with  $2 \leq n \leq 10$  and  $n = 20$  the obtained average geometry extremely depends on the temperature. Moreover, all optimized conformations for  $5 \geq n \geq 2$  are very similar to the averages structures. The contribution of the average structure to the real minimum is noticeable and, in an important degree, the average structure predicts the found minima. Thus, the average structure should present a very similar conformation to the close conformational minimum also for bigger clusters of  $(\beta\text{-Ala})_n$  ( $n \geq 6$ ).  $\beta$ -amino acids built of acyclic residues can form helices<sup>137;145;146</sup> or sheets.<sup>147</sup> Similar structures can be observed for the neutral clusters of  $\beta$ -alanine. For dimers and trimers it is not so common, but for bigger cluster we can see this kind of stabilization effects almost for each conformer for every cluster size. We can observe that until 443K the dominant interaction between the residues are the hydrogen bonds between carboxyl groups –COOH $\cdots$ HOOC–. Different hydrogen bonds are observed at higher temperatures, mainly –OH $\cdots$ N, CH $\cdots$ N and, similar to observed in beta-sheets and helix, =O $\cdots$ HN and CH $\cdots$ O, respectively. Moreover, when the temperature increases the residues are more spread. This is due to the fact that the residues have more internal energy, which can easily breaks the hydrogen bonds and van der Waals interactions. To get deeper insight into the conformational structure of the smaller clusters of  $(\beta\text{-Ala})_n$  with  $2 \leq n \leq 5$  we calculated relative energies, RMSD and BE. The results are presented in the table 7.1 at the two levels of theory employed (B3LYP and M06 with the same basis 6-311++G(d,p)).

Isomer	Level of theory					
	Relative Energy (kcal mol <sup>-1</sup> )		RMSD (Å)		Binding energy (eV)	
	B3LYP	M06	B3LYP	M06	B3LYP	M06
n=2						
$(\beta\text{-Ala})_2$ 300K_200ps	1.79	2.75	0.51	0.48	-0.53	-0.58
$(\beta\text{-Ala})_2$ 373K_80ps	2.49	3.99	0.29	0.28	-0.50	-0.52
$(\beta\text{-Ala})_2$ 423K_60ps	8.98	9.19	1.28	1.27	-0.22	-0.30
$(\beta\text{-Ala})_2$ 443K_15ps	0.00	0.00	2.01	1.99	-0.61	-0.69
$(\beta\text{-Ala})_2$ 463K_42ps	7.48	8.03	1.25	1.15	-0.29	-0.35
$(\beta\text{-Ala})_2$ 498K_60ps	7.45	7.27	1.53	1.43	-0.29	-0.38
n=3						
$(\beta\text{-Ala})_3$ 300K_1ns	1.09	1.44	1.41	1.68	-0.76	-0.86
$(\beta\text{-Ala})_3$ 373K_600ps	0.00	0.00	1.04	1.21	-0.81	-0.92
$(\beta\text{-Ala})_3$ 423K_60ps	0.40	0.40	1.12	1.12	-0.79	-0.90
$(\beta\text{-Ala})_3$ 443K_35ps	10.82	10.87	2.38	2.45	-0.34	-0.45
$(\beta\text{-Ala})_3$ 463K_50ps	3.81	2.68	1.51	1.49	-0.64	-0.81
$(\beta\text{-Ala})_3$ 498K_50ps	11.59	12.02	3.30	3.66	-0.30	-0.40
n=4						
$(\beta\text{-Ala})_4$ 300K_200s	0.00	0.00	1.45	1.59	-1.21	-1.52
$(\beta\text{-Ala})_4$ 373K_28ps	4.16	6.53	0.90	1.26	-1.03	-1.24
$(\beta\text{-Ala})_4$ 423K_10ps	2.00	4.13	1.45	0.99	-1.13	-1.34
$(\beta\text{-Ala})_4$ 443K_80ps	7.79	8.43	1.61	1.66	-0.88	-1.15
$(\beta\text{-Ala})_4$ 463K_50ps	11.31	12.46	3.56	3.49	-0.72	-0.98
$(\beta\text{-Ala})_4$ 498K_30ps	9.54	4.89	2.51	2.38	-0.80	-1.31
n=5						
$(\beta\text{-Ala})_5$ 300K_1ns	0.00	0.00		1.73		
$(\beta\text{-Ala})_5$ 373K_250ps	38.35					
$(\beta\text{-Ala})_5$ 423K_280ps	8.03	3.14		2.10		
$(\beta\text{-Ala})_5$ 443K_200ps						
$(\beta\text{-Ala})_5$ 463K_50ps						
$(\beta\text{-Ala})_5$ 498K_20ps	15.09					

**Table 7.1:** Relative Energies ( $\Delta E$ ) in kcal mol<sup>-1</sup> at different levels of theory in respect to the most stable conformer. RMS of atomic displacement in respect to average structure in Å at different levels of theory. Binding energies in eV at different levels of theory.

We decided to use the M06 functional (see the computational details) and compare some properties of the neutral clusters of the  $(\beta\text{-Ala})_n$ , where  $2 \leq n \leq 5$  with the “magic” B3LYP functional. As we can observe in

the table 7.1, for dimers, when the temperature increases until 443K the stability of the conformer decreases. This is due to the conformational changes in the geometry of the molecule (figure 7.1). We observe breaking of the hydrogen bonds between two carboxyl groups and rotation of one of the molecules with respect to the other. For the  $(\beta\text{-Ala})_2$ 443K\_15ps isomer we observe stabilization through hydrogen bonds again and this conformer becomes the most stable one. This is because the amino groups switch their positions—under and over the plane of the cluster. The optimized geometry for trimers is shown in figure 7.2. The relative energies between isomers are presented in table 7.1. We can notice that for  $T \leq 423K$  there are hydrogen bonds between two carboxyl groups and one amino group and the relative energies are in range of  $\sim 1$  kcal/mol. When the temperature increases we observe the rotation of the residues inside the cluster. For  $T = 443K$  the isomer that we have found predicts a lower number of H bonds making a cluster quite unstable. For higher temperatures the position of the carboxyl and the amino groups is close to each other. That property together with the high stability of  $(\beta\text{-Ala})_3$ 463K\_50ps conformer will allow us to consider the formation of peptide bond after ionization for these conformers. For dimers and trimers both functionals gave the same energy order. Difference between functionals is observed in case of the clusters with  $n = 4$ . Here, we can see that the  $(\beta\text{-Ala})_4$ 498K\_30ps conformer optimized using M06 functional is 5 kcal/mol more stable than at the B3LYP level of theory. In other cases, we can notice that the stability decreases with increasing the temperature.

Root mean square deviation calculations confirmed our previous qualitative observations: the average structures are very close to the real minima. Additionally, the difference increases with the temperature. On the other hand, the geometry optimized at B3LYP and M06 are in all cases very similar.

Binding energy results are correlated with the stability of the clusters. In the table 7.11 we can notice that with the increasing of the cluster size the binding energies drastically decrease, thus increasing the stability of the clusters. We suppose that for big enough clusters the binding energy should become flat or even decrease as a function of cluster size due to the destabilizing effects. This consideration requires other calculations of bigger clusters. Additionally we can see in the figure 7.11 that M06 functional gives BE more negative than B3LYP functional.

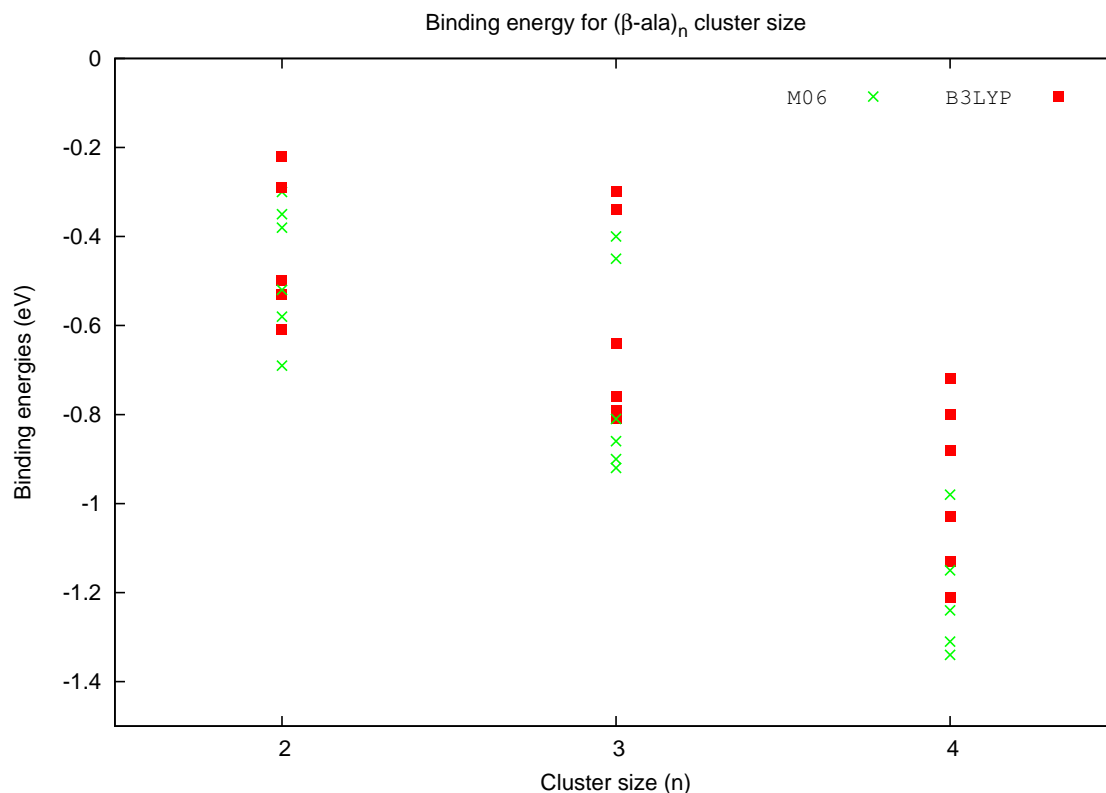


**Figure 7.11:** Binding energies as a function of clusters sizes.

## Hypothesis of peptide bond formation

Clusters of  $\beta$ -alanine can be stabilized in different ways: van der Waals interactions, hydrogen bonds or covalent bonds, which could be formed due the condensation or ionization of one amino acid. The covalent bond linking amino acids is called peptide bond. A schematic contribution of it, as well as hydrogen bonds, to stabilize the cluster of two  $\beta$ -alanine is illustrated below:

- a) the condensation of two  $\beta$ -alanine molecules into a neutral cluster, leading to the formation of a peptide bond;
- b) formation of the neutral cluster of two  $\beta$ -alanine molecules stabilized by hydrogen bonds;
- c) formation of an ionized cluster of two  $\beta$ -alanine molecules with a peptide bond, induced by a highly charged ion ( $O^{3+}$ );
- d) formation of an ionized cluster of two  $\beta$ -alanine molecules, stabilized by hydrogen bonds, induced by highly charged ion ( $O^{3+}$ ).

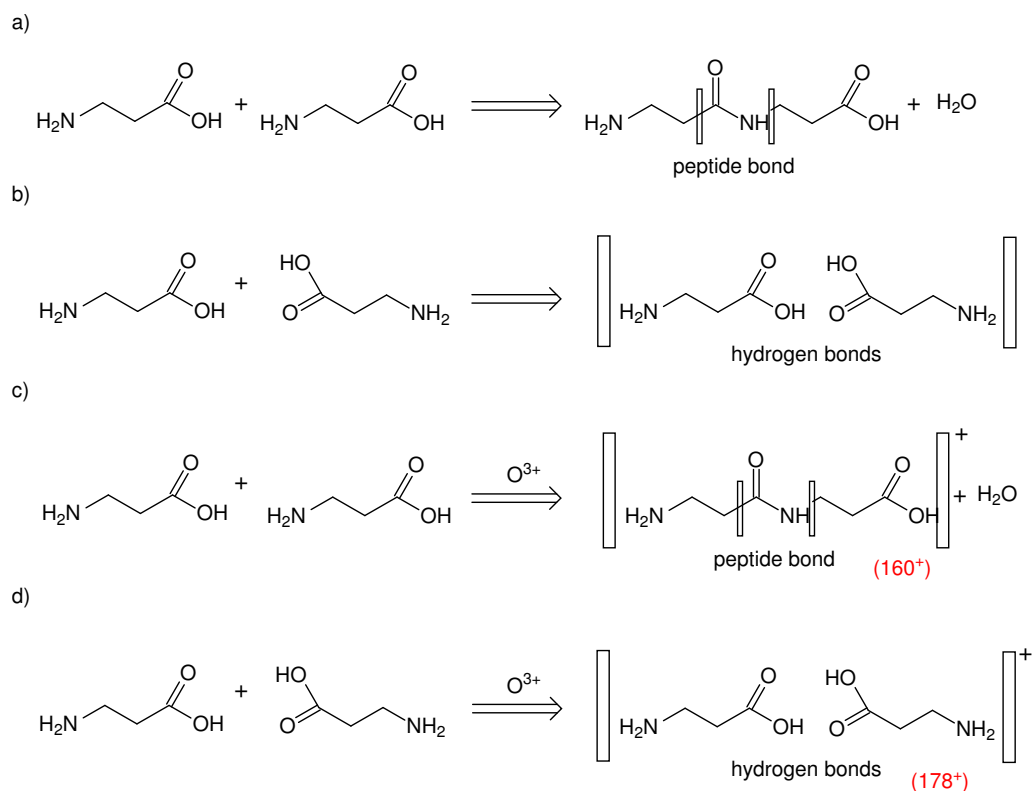


**Figure 7.12:** Schematic hypothetic formation of the peptide bond.

In recent experiments of P. Rousseau et al. (private communication) after ionization of  $\beta$ -alanine clusters in gas phase with high energy  $O^{3+}$  ions, emission of neutral moieties of mass 18 amu is observed. Considering that the mass corresponds to the removal of the neutral water, we expected to observe the formation of a peptide bond. Creating a peptide bond by removing a water molecule in a cluster of amino acids could be associated with hydrophobic and hydrophilic properties of their side chain. Before ionization we have neutral, non-polarized clusters of amino acids. Because they do not bond with polar water, they tend to be keep together and avoid water molecules as much as they can. The core of the clusters therefore tends to be neutral, a hydrophobic core. After the ionization, charged and polar side chains in the cluster become hydrophilic and can loss water and also “drain” out the water molecule from the core of the cluster. Because of that, the geometry of the clusters plays a dominant role in the formation of the peptide bond.

## Part IV

# Conclusions



---

We have investigated the stability, fragmentation dynamics and different de-excitation pathways characterizing the decay of the two simplest lineal amino acids: glycine and  $\beta$ -alanine excited and positively charged in gas phase. We have found many stable charged conformers of both molecules. Besides, the canonical form of the dication for these amino acids does not exist. Ionized dicationic species were found due to the fast (fs time scale) hydrogen migration before suffer Coulomb explosion. We find that these two types of processes occur in competition: charge separating leading to two singly charged fragments and the formation of stable dications that can evaporate neutral particles.

For the glycine molecule, the dominant fragmentation process for the single and double ionization channels is  $C_\alpha$ - $C_{carboxylic}$  bond breaking with the charge located on  $NH_2CH_2^+$  and on  $NH_2CH_2^+/COOH^+$ , respectively. Qualitatively, our theoretical predictions are in good agreement with the mass spectra and coincidence map, recorded after a collision with highly charged ions. In competition with the expected Coulomb explosion, an ultrafast H migration takes place, leading to fragmentation channels with stable dications. The reverse processes may be considered as a new mechanism for the formation of prebiotic molecules in the interstellar media. Moreover, the energy barriers calculated for the fragmentations channels suggest that the energy deposited on the glycine molecule is  $\sim 5$  eV.

In the case of  $\beta$ -alanine we observe competition between direct bond cleavage, isomerization and combined processes. For all these processes the conformers distribution plays a dominant role. Furthermore, the probability of the processes also depends on the excitation energy. In the context of a direct Coulomb explosion the  $C_\alpha$ - $C_{carboxylic}$  bond breaking dominates over the  $C_\alpha$ - $C_\beta$  one. The low probability of the isomerization (around 4%) allows us to draw the conclusion that further emission of neutral moieties leading to stable dicationic species can be a probable reversible process. According to that, the mechanism of producing amino acids in the interstellar space will be possible. Moreover, these results are interesting since amino acids are the essential of life encoding the genetic information and therefore fragmentation of them will affect replication the DNA.

The present study gives not only the general overview of the fragmentation mechanisms but also detailed information about the energy barriers, which have to be overcome to finish the reactions. These processes may occur in other systems and has to be considered to obtain a complete picture of the fragmentation dynamics in complex biomolecular systems.

In this thesis we also presented the flexibility to generate a big number of isomers in clusters of  $\beta$ -alanine as a function of the temperature via a wide range of stereo- and regio-isomers. This enormously expands the structural diversity in the investigation of this kind of systems. Additionally, this demonstrates how many conformers are available to populate at a given temperature.

In the future, we are planning to apply QMMM methods to study clusters with more than five residues. We will also investigate the mechanisms behind the peptide bond formation in clusters of amino acids. Future studies will also aim to the investigation of unimolecular decomposition of more complex systems like solvated clusters of  $\beta$ -alanine using more accurate techniques, as Car-Parinello molecular dynamics (CPMD), to get in depth evaluation of the fragmentation process after ionization.



# Bibliography

- [1] H. R. Pfaendler, J. Gosteli, R. B. Woodward, and G. Rihs. Structure, reactivity, and biological activity of strained bicyclic  $\beta$ -lactams. *Journal of the American Chemical Society*, 103(15):4526–4531, 1981.
- [2] Alcaide B. and Almendros P.  $\beta$ -lactams as versatile synthetic intermediates for the preparation of heterocycles of biological interest. *Current Medicinal Chemistry*, 11(14):1921–1949, 2004.
- [3] P. McCaldon and P. Argos. *Proteins*, 4:99–122, 1988.
- [4] O I Aruoma, M J Laughton, and B Halliwell. Carnosine, homocarnosine and anserine: could they act as antioxidants in vivo? *The Biochemical journal*, 264(3):863–869, 1989.
- [5] Jung Hoon Kang, Kyung Sik Kim, Soo Young Choi, Hyeok Yil Kwon, Moo Ho Won, and Tae-Cheon Kang. Protective effects of carnosine, homocarnosine and anserine against peroxy radical-mediated Cu,Zn-superoxide dismutase modification. *Biochimica et Biophysica Acta (BBA)/General Subjects*, 1570(2):89–96, 2002.
- [6] Choi S.Y., Kwon H.Y., Kwon O.B., and Kang J.H. Hydrogen peroxide-mediated cu, zn-superoxide dismutase fragmentation: protection by carnosine, homocarnosine and anserine. *Biochimica et Biophysica Acta (BBA)/General Subjects*, 1472(3):651–657, 1999.
- [7] Christof Renner, Nadine Zemitzsch, Beate Fuchs, Kathrin D. Geiger, Matthias Hermes, Jan Hengstler, Rolf Gebhardt, JÄErgen Meixensberger, and Frank Gaunitz. Carnosine retards tumor growth in vivo in an NIH3T3-HER2/neu mouse model. *Molecular Cancer*, 9(1):2, 2010.
- [8] R. M. Hobson, B. Saunders, G. Ball, R. C. Harris, and C. Sale. Effects of  $\beta$ -alanine supplementation on exercise performance: a meta-analysis. *Amino Acids*, 43(1):25–37, 2012.
- [9] Guilherme Giannini Artioli, Bruno Gualano, Abbie Smith, Jeffrey Stout, and Jr Lancha, Antonio Herbert. Role of  $\beta$ -alanine supplementation on muscle carnosine and exercise performance. *Medicine and science in sports and exercise*, 42(6):1162–1173, 2010.
- [10] AIS Sports Nutrition.  $\beta$ -alanine, fact sheets:group b supplements, accessed: 04 of june, 2013. [http://www.ausport.gov.au/ais/nutrition/supplements/group\\_b](http://www.ausport.gov.au/ais/nutrition/supplements/group_b), 2009.
- [11] E Juaristi and V. Soloshonok, editors. *Enantioselective Synthesis of  $\beta$ -Amino Acids*. Wiley, 2005.
- [12] P.-O. Sanskog, G. Nilsson, A. Lund, and T. Gilibro. For a pulse radiolysis and esr spectroscopy study on ionized glycine in condensed phase. *J. Phys. Chem.*, 85:2819, 1980.
- [13] Gisbert Depke, Nikolaus Heinrich, and Helmut Schwarz. On the gas phase chemistry of ionized glycine and its enol. a combined experimental and ab initio molecular orbital study. *International Journal of Mass Spectrometry and Ion Processes*, 62:99–117, 1984.
- [14] Audun Sanderud and Einar Sagstuen. Epr and endor studies of single crystals of r-glycine x-ray irradiated at 295 k. *J. Phys. Chem. B*, 102:9353–9361, 1998.

- [15] Sílvia Simon, Mariona Sodupe, and Juan Bertrán. Isomerization versus fragmentation of glycine radical cation in gas phase. *J. Phys. Chem. A*, 106(23):5697–5702, 2002.
- [16] B M Messer, C D Cappa, J D Smith, K R Wilson, M K Gilles, R C Cohen, and R J Saykally. pH dependence of the electronic structure of glycine. *The journal of physical chemistry. B*, 109(11):5375–5382, 2005.
- [17] Santosh Kumar, Amareshwar K. Rai, V.B. Singh, and S.B. Rai. Vibrational spectrum of glycine molecule. *Spectrochimica Acta Part A: Molecular and Biomolecular Spectroscopy*, 61(11-12):2741–2746, 2005.
- [18] J. Bertrán, L. Rodríguez-Santiago, and M. Sodupe. The different nature of bonding in  $\text{Cu}^+$ -glycine and  $\text{Cu}^{2+}$ -glycine. *The Journal of Physical Chemistry B*, 103(12):2310–2317, 1999.
- [19] Michael J. Locke, Richard L. Hunter, and Robert T. McIver. Experimental determination of the acidity and basicity of glycine in the gas phase. *Journal of the American Chemical Society*, 101(1):272–273, 1979.
- [20] Vincenzo Barone, Malgorzata Biczysko, Julien Bloino, and Cristina Puzzarini. Characterization of the elusive conformers of glycine from state-of-the-art structural, thermodynamic, and spectroscopic computations: Theory complements experiment. *Journal of Chemical Theory and Computation*, 9(3):1533–1547, 2013.
- [21] Michelle L. Gordon, Glyn Cooper, Cynthia Morin, Tohru Araki, Cássia C. Turci, Konstantin Kaznatcheev, and Adam P. Hitchcock. Inner-shell excitation spectroscopy of the peptide bond: Comparison of the  $c\ 1s$ ,  $n\ 1s$ , and  $o\ 1s$  spectra of glycine, glycyglycine, and glycyglycylglycine. *The Journal of Physical Chemistry A*, 107(32):6144–6159, 2003.
- [22] L. Rodríguez-Santiago, M. Sodupe, and J. Tortajada. Gas-phase reactivity of  $\text{Ni}^+$  with glycine. *The Journal of Physical Chemistry A*, 105(22):5340–5347, 2001.
- [23] Inés Corral, Otilia Mó, Manuel Yáñez, Jean-Yves Salpin, Jeanine Tortajada, Damian Moran, and Leo Radom. An experimental and theoretical investigation of gas-phase reactions of  $\text{Ca}^{2+}$  with glycine. *Chem. Eur. J.*, 12(26):6787–6796, 2006.
- [24] S. Maclot, M. Capron, R. Maisonnny, A. Ławicki, A. Méry, J. Rangama, J.-Y. Chesnel, S. Bari, R. Hoekstra, T. Schlathölter, B. Manil, L. Adoui, P. Rousseau, and B. A. Huber. Ion-Induced Fragmentation of Amino Acids: Effect of the Environment. *ChemPhysChem*, 12:930–936, 2011.
- [25] Milàn Szori, Balázs Jójárt, Róbert Izsák, Kornél Szori, Imre G Csizmadia, and Béla Viskolcz. Chemical evolution of biomolecule building blocks. can thermodynamics explain the accumulation of glycine in the prebiotic ocean? *Physical chemistry chemical physics*, 13(16):7449–7458, 2011.
- [26] Shan Xi Tian. Conformation effects on the electronic structures of beta-alanine. *The journal of physical chemistry. A*, 110(11):3961–3966, 2006.
- [27] Manuel A. V. Ribeiro da Silva, Maria das Dores M. C. Ribeiro da Silva, Ana Filipa L. O. M. Santos, Maria Victoria Roux, Concepción Foces-Foces, Rafael Notario, Ramón Guzmán-Mejía, and Eusebio Juaristi. Experimental and computational thermochemical study of  $\alpha$ -alanine (DL) and  $\beta$ -alanine. *The journal of physical chemistry. B*, 114(49):16471–16480, 2010.
- [28] M Eugenia Sanz, Alberto Lesarri, M Isabel Pen, Vanesa Vaquero, Vanessa Cortijo, Juan C Lo, and L Alonso. The Shape of Beta-Alanine. *J. Am. Chem. Soc.*, 128:3812–3817, 2006.
- [29] Lidong Zhang, Yang Pan, Huijun Guo, Taichang Zhang, Liusi Sheng, Fei Qi, Po-Kam Lo, and Kai-Chung Lau. Conformation-specific pathways of beta-alanine: a vacuum ultraviolet photoionization and theoretical study. *J. Phys. Chem. A*, 113:5838–5845, 2009.
- [30] Adrià Gil, Sílvia Simon, Luis Rodríguez-Santiago, Juan Bertrán, and Mariona Sodupe. Influence of the Side Chain in the Structure and Fragmentation of Amino Acids Radical Cations. *J. Chem. Theory Comput.*, 3:2210–2220, 2007.

- [31] Adrià Gil, Silvia Simon, Mariona Sodupe, and Juan Bertrán. How the site of ionisation influences side-chain fragmentation in histidine radical cation. *Chemical Physics Letters*, 451:276–281, 2008.
- [32] Sergej Naumov; Igor JanovskĀœ; Wolfgang Knolle; Reiner Mehnert. Radical cation, dimer radical cation and neutral radical of 2,3-dihydropyran - possible initiators of its polymerisation? 204:2099–2104, 2003.
- [33] J L Zweier and P Kuppusamy. In vivo EPR spectroscopy of free radicals in the heart. *Environmental Health Perspectives*, 102(Suppl 10):45–51, 1994.
- [34] M. C. R. Symons. *Chem. Soc. Rev.*, 13:393, 1984.
- [35] Sergej Naumov; Igor JanovskĀœ; Wolfgang Knolle; Reiner Mehnert. Role of distonic dimer radical cations in the radiation-induced polymerisation of vinyl ethers. 236:461–467, 2005.
- [36] Reiner Mehnert; Sergej Naumov; Wolfgang Knolle; Igor JanovskĀœ. Radical formation in electron-irradiated acrylates studied by pulse radiolysis and electron paramagnetic resonance. 201, 2000.
- [37] S. Naumov; I. JanovskĀœ; W. Knolle; R. Mehnert; D.A. Turin. Low-temperature epr and quantum chemical study of lactone radical cations and their transformations. 73:206–212, 2005.
- [38] Kirill B. Nuzhdin; Vladimir I. Feldman; Aleksei V. Kobzarenko. Delocalized methoxyacetone radical cation: structure and reactivity. 18:69–70, 2008.
- [39] Kirill B. Nuzhdin, Vladimir I. Feldman, and Aleksey V. Kobzarenko. Diketone radical cations: Ketonic and enolic forms as revealed by matrix EPR studies and DFT calculations. *The Journal of Physical Chemistry A*, 111(17):3294–3301, 2007.
- [40] Ekaterina S. Shiryayeva; Daniil A. Tyurin; Vladimir I. Feldman. The structure and photochemical transformation of cyclopropylacetylene radical cation as revealed by matrix epr and quantum chemical study. 536, 2012.
- [41] M. Durante and J. S. Loeffler. Charged particles in radiation oncology. *Nat. Rev. Clin. Oncol.*, 7:37–43, 2010.
- [42] M. H. Holzscheiter, N. Bassler, M. Dosanjh, B. S. Sørensen, and J. Overgaard. A community call for a dedicated radiobiological research facility to support particle beam cancer therapy. *Radiother. Oncol.*, 105:1–3, 2012.
- [43] L. Sanche. Low energy electron-driven damage in biomolecules. *The European Physical Journal D - Atomic, Molecular, Optical and Plasma Physics*, 35(2):367–390, 2005.
- [44] D. Schardt, T. Elsässer, and D. Schulz-Ertner. Heavy-ion tumor therapy: Physical and radiobiological benefits. *Rev. Mod. Phys.*, 82:353–425, 2010.
- [45] C V Parast, K K Wong, S A Lewisch, J W Kozarich, J Peisach, and R S Magliozzo. Hydrogen exchange of the glycy radical of pyruvate formate-lyase is catalyzed by cysteine 419. *Biochemistry*, 34(8):2393–2399, 1995.
- [46] Patrick Brunelle and Arvi Rauk. The radical model of alzheimer’s disease: Specific recognition of gly29 and gly33 by met35 in a  $\beta$ -sheet model of  $\alpha\beta$ : An oniom study. *Journal of Alzheimer’s Disease*, 4(4):283–289, 2002.
- [47] E. R. Stadtman. Protein oxidation and aging. *Science*, 257(5074):1220–1224, 1992.
- [48] D. Allan Butterfield and Debra Boyd-Kimball. The critical role of methionine 35 in alzheimer’s amyloid  $\beta$ -peptide induced oxidative stress and neurotoxicity. *Biochimica et Biophysica Acta. Proteins and Proteomics*, 1703(2):149–156, 2005.

- [49] F S Wu, T T Gibbs, and D H Farb. Dual activation of GABAA and glycine receptors by beta-alanine: inverse modulation by progesterone and 5 alpha-pregnan-3 alpha-ol-20-one. *European journal of pharmacology*, 246(3):239–246, 1993.
- [50] Mats Sandberg and Ingemar Jacobson.  $\beta$ -alanine, a possible neurotransmitter in the visual system? *Journal of Neurochemistry*, 37(5):1353–1356, 1981.
- [51] D. Schröder and H. Schwarz. Generation, stability, and reactivity of small, multiply charged ions in the gas phase. *J. Phys. Chem. A*, 103:7385–7394, 1999.
- [52] K. Lammertsma, P. von Ragué Schleyer, and H. Schwarz. Organic dications: Gas phase experiments and theory in concert. *Angew. Chem. Int. Ed.*, 28:1321–1341, 1989.
- [53] P. López-Tarifa, M.-A. Hervé du Penhoat, R. Vuilleumier, M.-P. Gageot, I. Tavernelli, A. Le Padellec, J.-P. Champeaux, M. Alcamí, P. Moretto-Capelle, F. Martín, and M.-F. Politis. Ultrafast nonadiabatic fragmentation dynamics of doubly charged uracil in a gas phase. *Phys. Rev. Lett.*, 107:023202, 2011.
- [54] D. Schröder. Coulomb explosions and stability of multiply charged ions in the gas phase. *Angew. Chem. Int. Ed.*, 43:1329–1331, 2004.
- [55] Evan R. Williams. Proton transfer reactivity of large multiply charged ions. *J. Mass Spectrom.*, 31:831–842, 1996.
- [56] Teng-Yi Huang and Scott A. McLuckey. Gas-phase chemistry of multiply charged bioions in analytical mass spectrometry. *Ann. Rev. Anal. Chem.*, 3:365–385, 2010.
- [57] Scott A. McLuckey and James L. Stephenson. Ion/ion chemistry of high-mass multiply charged ions. *Mass Spect. Rev.*, 17(6):369–407, 1998.
- [58] Diethard Kurt Bohme. Multiply-charged ions and interstellar chemistry. *Phys. Chem. Chem. Phys.*, 13:18253–18263, 2011.
- [59] Jana Roithová and Detlef Schroeder. Bond-forming reactions of molecular dications as a new route to polyaromatic hydrocarbons. *J. Am. Chem. Soc.*, 128(13):4208–4209, 2006.
- [60] Claire L. Ricketts, Detlef Schröder, Christian Alcaraz, and Jana Roithová. Growth of larger hydrocarbons in the ionosphere of titan. *Chem. Eur. J.*, 14(16):4779–4783, 2008.
- [61] Uwe J. Meierhenrich, Guillermo M. Muñoz Caro, Jan Hendrik Bredehöft, Elmar K. Jessberger, and Wolfram H.-P. Thiemann. Identification of diamino acids in the murchison meteorite. *Proceedings of the National Academy of Sciences of the United States of America*, 101(25):9182–9186, 2004.
- [62] Pascale Ehrenfreund, Daniel P. Glavin, Oliver Botta, George Cooper, and Jeffrey L. Bada. Extraterrestrial amino acids in orgueil and ivuna: Tracing the parent body of CI type carbonaceous chondrites. *Proceedings of the National Academy of Sciences*, 98(5):2138–2141, 2001.
- [63] Christopher Chyba and Carl Sagan. Endogenous production, exogenous delivery and impact-shock synthesis of organic molecules: an inventory for the origins of life. *Nature*, 355(6356):125–132, 1992.
- [64] Scott A. Sandford Jason P. Dworkin, David W. Deamer and Louis J. Allamandola. Self-assembling amphiphilic molecules: Synthesis in simulated interstellar precometary ices. *PNAS*, 98:815–819, 2001.
- [65] Jason P.; Sandford Scott A.; Cooper George W.; Allamandola Louis J. Bernstein, Max P.; Dworkin. Racemic amino acids from the ultraviolet photolysis of interstellar ice analogues. *Nature*, 416, 2002.

- [66] U. J.; Schutte W. A.; Barbier B.; Arcones Segovia A.; Rosenbauer H.; Thiemann W. H.-P.; Brack A.; Greenberg J. M. Muñoz Caro, G. M.; Meierhenrich. Amino acids from ultraviolet irradiation of interstellar ice analogues. *Nature*, 416:403–406, 2002.
- [67] Voislav Blagojevic, Simon Petrie, and Diethard K. Bohme. Gas-phase syntheses for interstellar carboxylic and amino acids. *Monthly Notices of the Royal Astronomical Society*, 339(1):L7–L11, 2003.
- [68] Yi-Jehng Kuan, Steven B. Charnley, Hui-Chun Huang, Wei-Ling Tseng, and Zbigniew Kisiel. Interstellar glycine. *Astrophys. J.*, 593(2):848, 2003.
- [69] L. E. Snyder, F. J. Lovas, J. M. Hollis, D. N. Friedel, P. R. Jewell, A. Remijan, V. V. Ilyushin, E. A. Alekseev, and S. F. Dyubko. A rigorous attempt to verify interstellar glycine. *The Astrophysical Journal*, 619(2):914, 2005.
- [70] P. Ehrenfreund, D. P. Glavin, O. Botta, G. Cooper, and J. L. Bada. Extraterrestrial amino acids in Orgueil and Ivuna: Tracing the parent body of CI type carbonaceous chondrites. *Proc. Natl. Acad. Sci. USA*, 98:2138–2141, 2001.
- [71] Carmen Barrientos, Pilar Redondo, Laura Largo, Victor M. Rayón, and Antonio Largo. Gas-phase synthesis of precursors of interstellar glycine: A computational study of the reactions of acetic acid with hydroxylamine and its ionized and protonated derivatives. *Astrophys. J.*, 748(2):99, 2012.
- [72] Albert Rimola, Mariona Sodupe, and Piero Ugliengo. Computational study of interstellar glycine formation occurring at radical surfaces of water-ice dust particles. *The Astrophysical Journal*, 754(1):24, 2012.
- [73] S. Maeda and K. Ohno. Generation mechanisms of amino acids in interstellar space via reactions between closed-shell species: Significance of higher energy isomers in molecular evolution. *The Astrophysical Journal*, 640(2):823, 2006.
- [74] R. G. Parr and Yang W. Density functional theory of atoms and molecules. *Oxford University Press*, 1989.
- [75] M Born and J. R. Oppenheimer. *Ann. Physic*, 84:457, 1928.
- [76] Fock V. *Z. Physic*, 61:126, 1930.
- [77] D. R. Hartree. *Proc. Cambridge Phil. Soc.*, 24:89, 1928.
- [78] C. Møller and Plesset M. S. *Phys. Rev.*, 39:771, 1934.
- [79] P. Hohenberg and W. Kohn. Inhomogeneous electron gas. *Physical Review*, 136(3B):B864–B871, 1964.
- [80] A. D. Becke. Density-functional thermochemistry. iii. the role of exact exchange. *J. Chem. Phys.*, 98:5648–5652, 1993.
- [81] Becke. Density functional exchange energy approximation with correct asymptotic behavior. *Physical review. A*, 38(6):3098–3100, 1988.
- [82] Dario Bressanini, Gabriele Morosi, and Silvia Tarasco. An investigation of nodal structures and the construction of trial wave functions. *The Journal of Chemical Physics*, 123(20):204109–204109–11, November 2005.
- [83] H. Bernhard Schlegel, John M. Millam, Srinivasan S. Iyengar, Gregory A. Voth, Andrew D. Daniels, Gustavo E. Scuseria, and Michael J. Frisch. Ab initio molecular dynamics: Propagating the density matrix with gaussian orbitals. *J. Chem. Phys.*, 114:9758–9763, 2001.
- [84] Stefan Goedecker. Linear scaling electronic structure methods. *Reviews of Modern Physics*, 71(4):1085–1123, 1999.

- [85] Scuseria G. E. Linear scaling density functional calculations with gaussian orbitals. *J. Phys. Chem. A*, 104:4782–4790, 1999.
- [86] Cieplak P. Bayly C. I. Gould I. R. Merz K. M. Jr. Ferguson D. M. Spellmeyer D. C.-Fox T. Caldwell J. W. Cornell, W. D. and P. A. Kollman. A second generation force field for the simulation of proteins, nucleic acids and organic molecules. *J. Am. Chem. Soc.*, 117:5179–5197, 1995.
- [87] & Kollman P. A. Weiner, P. K. Amber: Assisted model building with energy refinement. a general program for modeling molecules and their interactions. *J. Comp. Chem.*, 2:287–303, 1981.
- [88] Kollman P.A. Case D.A. Singh U.C. Ghio C. Alagona G. Profeta S. Jr. Weiner P.K. Weiner, S.J. A new force field for molecular mechanical simulation of nucleic acids and proteins. *J. Am. Chem. Soc.*, 106:765–784, 1984.
- [89] Kollman P. A. Nguyen D. T. Weiner, S. J. and D. A. Case. An all atom force field for simulations of proteins and nucleic acids. *J. Comp. Chem.*, 7:230–252, 1986.
- [90] Junmei Wang, Romain M. Wolf, James W. Caldwell, Peter A. Kollman, and David A. Case. Development and testing of a general amber force field. *Journal of Computational Chemistry*, 25(9):1157–1174, 2004.
- [91] Wendy D. Cornell, Piotr Cieplak, Christopher I. Bayly, and Peter A. Kollmann. Application of RESP charges to calculate conformational energies, hydrogen bond energies, and free energies of solvation. *Journal of the American Chemical Society*, 115(21):9620–9631, 1993.
- [92] Hai Lin and Donald G. Truhlar. QM/MM what have we learned, where are we, and where do we go from here? *Theoretical Chemistry Accounts*, 117(2):185–199, 2007.
- [93] C. Lee, W. Yang, and R. G. Parr. Development of the colle-salvetti correlation-energy formula into a functional of the electron density. *Phys. Rev. B*, 37:785–789, 1988.
- [94] Gerard A. Heal, P. Duane Walker, Michael Ramek, and Paul G. Mezey. Shape-similarity analysis of 20 stable conformations of neutral  $\beta$ -alanine. *Can. J. Chem.*, 74:1660, 1996.
- [95] M. Ramek. *J. Mol. Struct.-THEOCHEM*, 208:301, 1990.
- [96] Michael Ramek and Vincent K. W. Cheng. On the role of polarization functions in SCF calculations of glycine and related systems with intramolecular hydrogen bonding. *International Journal of Quantum Chemistry*, 44(S19):15–26, 1992.
- [97] Michael Ramek; Vincent K. W. Cheng. On the role of polarization functions in scf calculations of glycine and related systems with intramolecular hydrogen bonding. 44, 1992.
- [98] K. Fukui. The path of chemical-reactions - the irc approach. *Acc. Chem. Res.*, 14:363–368, 1981.
- [99] H. B Peng, C.; Schlegel. Combining synchronous transit and quasi-newton methods for finding transition states. *Israeli J. Chem.*, 33:449–54, 1994.
- [100] Chunyang Peng, Philippe Y. Ayala, H. Bernhard Schlegel, and Michael J. Frisch. Using redundant internal coordinates to optimize equilibrium geometries and transition states. *Journal of Computational Chemistry*, 17(1):49–56, 1996.
- [101] Srinivasan S. Iyengar, H. Bernhard Schlegel, John M. Millam, Gregory A. Voth, Gustavo E. Scuseria, and Michael J. Frisch. Ab initio molecular dynamics: Propagating the density matrix with gaussian orbitals. ii. generalizations based on mass-weighting, idempotency, energy conservation and choice of initial conditions. *J. Chem. Phys.*, 115:10291–10302, 2001.

- [102] H. Bernhard Schlegel, Srinivasan S. Iyengar, Xiaosong Li, John M. Millam, Gregory A. Voth, Gustavo E. Scuseria, and Michael J. Frisch. Ab initio molecular dynamics: Propagating the density matrix with gaussian orbitals. iii. comparison with born–oppenheimer dynamics. *J. Chem. Phys.*, 117(19):8694–8704, 2002.
- [103] Srinivasan S. Iyengar, H. Bernhard Schlegel, and Gregory A. Voth. Atom-centered density matrix propagation (admp): Generalizations using bohmian mechanics. *The Journal of Physical Chemistry A*, 107(37):7269–7277, 2003.
- [104] M. J. Frisch, G. W. Trucks, H. B. Schlegel, G. E. Scuseria, M. A. Robb, J. R. Cheeseman, G. Scalmani, V. Barone, B. Mennucci, G. A. Petersson, H. Nakatsuji, M. Caricato, X. Li, H. P. Hratchian, A. F. Izmaylov, J. Bloino, G. Zheng, J. L. Sonnenberg, M. Hada, M. Ehara, K. Toyota, R. Fukuda, J. Hasegawa, M. Ishida, T. Nakajima, Y. Honda, O. Kitao, H. Nakai, T. Vreven, J. A. Montgomery, Jr., J. E. Peralta, F. Ogliaro, M. Bearpark, J. J. Heyd, E. Brothers, K. N. Kudin, V. N. Staroverov, R. Kobayashi, J. Normand, K. Raghavachari, A. Rendell, J. C. Burant, S. S. Iyengar, J. Tomasi, M. Cossi, N. Rega, J. M. Millam, M. Klene, J. E. Knox, J. B. Cross, V. Bakken, C. Adamo, J. Jaramillo, R. Gomperts, R. E. Stratmann, O. Yazyev, A. J. Austin, R. Cammi, C. Pomelli, J. W. Ochterski, R. L. Martin, K. Morokuma, V. G. Zakrzewski, G. A. Voth, P. Salvador, J. J. Dannenberg, S. Dapprich, A. D. Daniels, Ö Farkas, J. B. Foresman, J. V. Ortiz, J. Cioslowski, and D. J. Fox. Gaussian 09 Revision B.01, 2010.
- [105] Douglas A. Gibson; Irina V. Ionova; Emily A. Carter. A comparison of car-parrinello and born-oppenheimer generalized valence bond molecular dynamics. *Chemical Physics Letters*, 240, 1995.
- [106] Wei Zhang, Tingjun Hou, Christian Schafmeister nad Wilson S. Ross, and David A. Case. *Leap and GLeap manual for AmberTools*. 2008.
- [107] R. Maul, F. Ortmann, M. Preuss, K. Hannewald, and F. Bechstedt. DFT studies using supercells and projector-augmented waves for structure, energetics, and dynamics of glycine, alanine, and cysteine. *Journal of Computational Chemistry*, 28:1817–1833, 2007.
- [108] F. J.; Chabalowski C. F.; Frisch M. J. Stephens, P. J.; Devlin. Ab initio calculation of vibrational absorption and circular dichroism spectra using density functional force fields. 98:11623–11627, 1994.
- [109] Jens; Ehrlich Stephan; Krieg Helge Grimme, Stefan; Antony. A consistent and accurate ab initio parametrization of density functional dispersion correction (dft-d) for the 94 elements h-pu. 132, 2010.
- [110] Yan Zhao; Donald G. Truhlar. The m06 suite of density functionals for main group thermochemistry, thermochemical kinetics, noncovalent interactions, excited states, and transition elements: two new functionals and systematic testing of four m06 functionals and 12 other functionals. 119:525–525, 2008.
- [111] Yan Zhao and Donald G. Truhlar. Hybrid meta density functional theory methods for thermochemistry, thermochemical kinetics, and noncovalent interactions: The MPW1B95 and MPWB1K models and comparative assessments for hydrogen bonding and van der waals interactions. *The Journal of Physical Chemistry A*, 108(33):6908–6918, 2004.
- [112] Stefan Grimme. Semiempirical gga-type density functional constructed with a long-range dispersion correction. 27, 2006.
- [113] Rick A. Kendall, Thom H. Dunning, and Robert J. Harrison. Electron affinities of the first-row atoms revisited. systematic basis sets and wave functions. *The Journal of Chemical Physics*, 96(9):6796–6806, 1992.
- [114] Wolfgang Quapp. Chemical reaction paths and calculus of variations. *Theoretical Chemistry Accounts*, 121(5-6):227–237, 2008.
- [115] B. Schlegel. Exploring potential energy surfaces for chemical reactions: An overview of some practical methods. *J. Comput. Chem.*, 24(12):1515–1527, 2003.

- [116] Atilla G. Császár. Conformers of gaseous glycine. *J. Am. Chem. Soc.*, 114:9568–9575, 1992.
- [117] G. Depke, N. Heinrich, and H. Schwarz. On the gas phase chemistry of ionized glycine and its enol. a combined experimental and ab initio molecular orbital study. *Int. J. Mass Spectrom. Ion Processes*, 62:99–117, 1984.
- [118] F Martin and H Zipse. Charge distribution in the water molecule—a comparison of methods. *Journal of computational chemistry*, 26(1):97–105, 2005.
- [119] Benoît Braïda, Philippe C. Hiberty, and Andreas Savin. A systematic failing of current density functionals: Overestimation of two-center three-electron bonding energies. *The Journal of Physical Chemistry A*, 102:7872–7877, 1998.
- [120] Mariona Sodupe, Juan Bertran, Luis Rodríguez-Santiago, and E. J. Baerends. Ground state of the (H<sub>2</sub>O)<sub>2</sub><sup>+</sup> radical cation: DFT versus post-Hartree-Fock methods. *The Journal of Physical Chemistry A*, 103(1):166–170, 1999.
- [121] M. Capron, S. Díaz-Tendero, S. Maclot, A. Domaracka, E. Lattouf, A. Ławicki, R. Maisonnay, J.-Y. Chesnel, A. Méry, J.-C. Pouilly, J. Rangama, L. Adoui, F. Martín, M. Alcamí, P. Rousseau, and B. A. Huber. A multicoincidence study of fragmentation dynamics in collision of  $\gamma$ -aminobutyric acid with low-energy ions. *Chem. Eur. J.*, 18:9321–9332, 2012.
- [122] H.-W. Jochims, M. Schwell, J.-L. Chotin, M. Clemino, F. Dulieu, H. Baumgärtel, and S. Leach. Photoion mass spectrometry of five amino acids in the 6-22 eV photon energy range. *Chem. Phys.*, 298:279–297, 2004.
- [123] S. Bari, F. Alvarado, J. Postma, P. Sobocinski, R. Hoekstra, and T. Schlathölter. Kinetic energy releases of small amino acids upon interaction with keV ions. *Eur. Phys. J. D*, 51:81–87, 2008.
- [124] Kazumi Toriyama and Masaharu Okazaki. Selectively weakened carbon-carbon  $\sigma$ -bond in cation radicals of linear and branched pentanes as studied by electron spin resonance. *The Journal of Physical Chemistry*, 96(17):6986–6991, 1992.
- [125] Okazaki M Toriyama K. Asymmetric distortion of alkane radical cations as studied by epr spectroscopy: The role of pseudo john-teller effects and matrix interaction. *Acta Chem Scand*, 51:167–173, 1997.
- [126] F. Chandezon, H. Lebius, S. Tomita, C. Guet, A. Pesnelle, and B A. Huber. Energy transfer in multi-ionizing ion/cluster collisions. *Phys. Scr.*, T92:168–170, 2001.
- [127] J. Tamuliene, L.G. Romanova, V.S. Vukstich, and A.V. Snegursky. Mechanisms of the electron-impact-induced glycine molecule fragmentation. *Chem. Phys.*, 404(0):36–41, 2012.
- [128] Y. H. Jiang, A. Rudenko, O. Herrwerth, L. Foucar, M. Kurka, K. U. Kühnel, M. Lezius, M. F. Kling, J. van Tilborg, A. Belkacem, K. Ueda, S. Düsterer, R. Treusch, C. D. Schröter, R. Moshhammer, and J. Ullrich. Ultrafast extreme ultraviolet induced isomerization of acetylene cations. *Phys. Rev. Lett.*, 105:263002, 2010.
- [129] Mohamed El-Amine Madjet, Oriol Vendrell, and Robin Santra. Ultrafast dynamics of photoionized acetylene. *Phys. Rev. Lett.*, 107:263002, 2011.
- [130] Ryuji Itakura, Peng Liu, Yusuke Furukawa, Tomoya Okino, Kaoru Yamanouchi, and Hidetoshi Nakano. Two-body coulomb explosion and hydrogen migration in methanol induced by intense 7 and 21 fs laser pulses. *J. Chem. Phys.*, 127(10):104306, 2007.
- [131] Peter Aadal Nielsen, Per-Ola Norrby, Tommy Liljefors, Nadia Rega, and Vincenzo Barone. Quantum mechanical conformational analysis of  $\beta$ -alanine zwitterion in aqueous solution. *Journal of the American Chemical Society*, 122(13):3151–3155, 2000.

- [132] S. Bari, P. Sobocinski, J. Postma, F. Alvarado, R. Hoekstra, V. Bernigaud, B. Manil, J. Rangama, B. Huber, and T. Schlathölder. Fragmentation of  $\alpha$ - and  $\beta$ -alanine molecules by ions at Bragg-peak energies. *J. Chem. Phys.*, 128:074306, 2008.
- [133] J. McGlone Shane and Peter D. Godfrey. Rotational spectrum of neurohormon:  $\beta$ -alanine. *J. Am. Chem. Soc.*, 117:1043–1048, 1995.
- [134] Alex G Harrison. To b or not to b: the ongoing saga of peptide b ions. *Mass spectrometry reviews*, 28(4):640–654, 2009.
- [135] Silvia Simon, Adrià Gil, Mariona Sodupe, and Juan Bertrán. Structure and fragmentation of glycine, alanine, serine and cysteine radical cations. A theoretical study. *J. Mol. Struct.-THEOCHEM*, 727:191–197, 2005.
- [136] P Sobocinski, S Bari, J Postma, F Alvarado, R Hoekstra, B Manil, J Rangama, V Bernigaud, B a Huber, and T Schlathölder. Isomeric effects in ion-induced fragmentation of  $\alpha$ - and  $\beta$ -alanine. *J. Phys.: Conf. Ser.*, 101:012006, 2008.
- [137] J. L. Seebach, D.; Matthews. *Chem. Commun*, 2015, 1997.
- [138] R. P. Cheng, S. H. Gellman, and W. F. DeGrado. *Chem. Rev*, 101:3219, 2001.
- [139] Robert M. Dirks, Milo Lin, Erik Winfree, and Niles A. Pierce. Paradigms for computational nucleic acid design. *Nucleic Acids Research*, 32(4):1392–1403, 2004.
- [140] M. G. Woll, J. D. Fisk, P. R. LePlae, and S. H. Gellman. *J. Am. Chem. Soc.*, 124:12447, 2002.
- [141] D. H. Appella, J. J. Barchi, S. R. Durell, and S. H. Gellman. *J. Am. Chem. Soc.*, 121:2309, 1999.
- [142] Emilie A. Porter, Xifang Wang, Hee-Seung Lee, Bernard Weisblum, and Samuel H. Gellman. Antibiotics: Non-haemolytic  $\beta$ -amino acid oligomers. *Nature*, 404(6778):565–565, 2000.
- [143] David L. Steer, Rebecca A. Lew, Patrick Perlmutter, A. Ian Smith, and Marie-Isabel Aguilar. The use of  $\beta$ -amino acids in the design of protease and peptidase inhibitors. *Letters in Peptide Science*, 8(3-5):241–246, 2001.
- [144] Samuel H. Dado, Gregory P.; Gellman. Intramolecular hydrogen bonding in derivatives of  $\beta$ -alanine and  $\gamma$ -amino butyric acid; model studies for the folding of unnatural polypeptide backbones. *Journal of the American Chemical Society*, 116, 1994.
- [145] Dieter Seebach, Stefan Abele, Thierry Sifferlen, Martin Hänggi, Sibylle Gruner, and Paul Seiler. Preparation and structure of  $\beta$ -peptides consisting of geminally disubstituted  $\beta$ 2,2-and  $\beta$ 3,3-amino acids: A turn motif for  $\beta$ -peptides. *Helvetica Chimica Acta*, 81(12):2218–2243, 1998.
- [146] Benjamin W. Gung, Dong Zou, Apryll M. Stalcup, and Charles E. Cottrell. Characterization of a water-soluble, helical  $\beta$ -peptide. *The Journal of Organic Chemistry*, 64(7):2176–2177, 1999.
- [147] D. Seebach, S. Abele, K. Gademann, and B. Jaun. *Angew. Chem. Int. Ed.*, 38:1595, 1999.